

UNIVERSIDADE FEDERAL DO PARANÁ

GABRIELA GOMES NOGUEIRA SALES

WATER QUALITY MODELING IN A SUBTROPICAL WATER SUPPLY RESERVOIR

CURITIBA

2020

GABRIELA GOMES NOGUEIRA SALES

WATER QUALITY MODELING IN A SUBTROPICAL WATER SUPPLY RESERVOIR

Dissertação apresentada ao Programa de Pós-Graduação
em Engenharia Ambiental, Setor de Tecnologia, Universi-
dade Federal do Paraná, como requisito parcial à obtenção
do título de Mestre em Engenharia Ambiental.

Orientador: Prof. Dr.-Ing. Tobias Bleninger.

Coorientador: Prof. Dr. Michael Männich.

CURITIBA

2020

Catalogação na Fonte: Sistema de Bibliotecas, UFPR
Biblioteca de Ciência e Tecnologia

S163w

Sales, Gabriela Gomes Nogueira

Water quality modeling in a subtropical water supply reservoir [recurso eletrônico] /
Gabriela Gomes Nogueira Sales. – Curitiba, 2020.

Dissertação - Universidade Federal do Paraná, Setor de Tecnologia, Programa de Pós-
Graduação em Engenharia Ambiental, 2020.

Orientador: Tobias Bleninger.

Coorientador: Michael Männich.

1. Reservatórios. 2. Ecologia dos reservatórios. 3. Abastecimento de água. I. Universidade
Federal do Paraná. II. Bleninger, Tobias. III. Männich, Michael. IV. Título.

CDD: 628.1

Bibliotecária: Vanusa Maciel CRB- 9/1928



MINISTÉRIO DA EDUCAÇÃO
SETOR DE TECNOLOGIA
UNIVERSIDADE FEDERAL DO PARANÁ
PRÓ-REITORIA DE PESQUISA E PÓS-GRADUAÇÃO
PROGRAMA DE PÓS-GRADUAÇÃO ENGENHARIA
AMBIENTAL - 40001016075P3

TERMO DE APROVAÇÃO

Os membros da Banca Examinadora designada pelo Colegiado do Programa de Pós-Graduação em ENGENHARIA AMBIENTAL da Universidade Federal do Paraná foram convocados para realizar a arguição da dissertação de Mestrado de **GABRIELA GOMES NOGUEIRA SALES** intitulada: **WATER QUALITY MODELING IN A SUBTROPICAL WATER SUPPLY RESERVOIR**, sob orientação do Prof. Dr. TOBIAS BERNWARD BLENINGER, que após terem inquirido a aluna e realizada a avaliação do trabalho, são de parecer pela sua APROVAÇÃO no rito de defesa.

A outorga do título de mestre está sujeita à homologação pelo colegiado, ao atendimento de todas as indicações e correções solicitadas pela banca e ao pleno atendimento das demandas regimentais do Programa de Pós-Graduação.

Curitiba, 24 de Julho de 2020.

Assinatura Eletrônica

28/07/2020 15:44:05.0

TOBIAS BERNWARD BLENINGER

Presidente da Banca Examinadora (UNIVERSIDADE FEDERAL DO PARANÁ)

Assinatura Eletrônica

28/07/2020 14:38:31.0

JOSÉ RODOLFO SCARATI MARTINS

Avaliador Externo (UNIVERSIDADE DE SÃO PAULO)

Assinatura Eletrônica

28/07/2020 16:18:57.0

CYNARA DE LOURDES DA NÓBREGA CUNHA

Avaliador Interno (UNIVERSIDADE FEDERAL DO PARANÁ)

*Ao meu irmão, Emerson Jango
To my brother, Emerson Jango*

ACKNOWLEDGEMENTS

Important supports were fundamental for the feasibility of this master's dissertation.

Firstly, I am grateful to CAPES (Coordination for the Improvement of Higher Education Personnel - Brazil), for granting my scholarship.

To the MuDak project (Multidisciplinary Data Acquisition as Key for Globally Applicable Water Resource Management), which was essential for the production of quantitative and qualitative information necessary to carry out this research, in addition to the help of many of the project members.

To Sanepar (Sanitation Company of Paraná), for making data available and accessing the Passaúna reservoir, as well as the other institutions that provided materials regarding the study area.

To the PPGEA (Graduate Program in Environmental Engineering), which contributed to my knowledge improvement with its qualified faculty, besides assistance by the Secretariat.

I am especially grateful to my advisors, Tobias Bleninger and Michael Mannich, for guiding me with great enthusiasm in this period, believing in my potential.

I thank my family immensely, especially my parents, Iracema and Émerson, and my brothers, Emerson (Eko) and Paulo, for their unconditional support and motivation. I highlight here Eko, the blue light and basis of the family, who teaches us to be better people every day.

I am grateful to other family members, close friends, and coworkers, who provided me leisure moments and, with that, made lighter this period of so much effort and dedication.

I thank, above all, my husband, Jhonatas Antonelli. I appreciate your understanding and patience in moments of absence and stress due to my studies. Besides your companionship, friendship and for taking care of me with such affection.

Thank you very much!

RESUMO

A gestão adequada de reservatórios perpassa pela compreensão dos complexos e dinâmicos processos que neles ocorrem. O transporte e mistura de grandezas escalares são fortemente influenciados pelo regime térmico do corpo d'água. Modelos hidrodinâmico-ecológico acoplados apresentam-se como uma ferramenta útil, em particular modelos unidimensionais na vertical (1DV), devido à predominância de gradientes verticais na dinâmica de lagos. Além disso, têm como vantagem a possibilidade de estudos de diferentes cenários e longos períodos de simulação, com baixo custo computacional e requisitos mínimos de calibração. O objetivo desse trabalho foi analisar o desempenho do modelo acoplado 1D GLM-AED (*General Lake Model – Aquatic EcoDynamics*) na reprodução de processos físicos, químicos e biológicos de um reservatório subtropical de abastecimento de água (reservatório do Passaúna, Paraná - Brasil). Primeiramente, a modelagem hidrodinâmica foi realizada com o GLM, a fim de simular o balanço hídrico e o comportamento térmico do reservatório. Em seguida, a biblioteca de modelagem AED foi adicionada, ativando os módulos: oxigênio, carbono, nitrogênio, fósforo, matéria orgânica, fitoplâncton e totais. A simulação foi de agosto de 2017 a fevereiro de 2019, sendo adotadas duas configurações, uma com a profundidade total do reservatório (17 m) e outra com a profundidade aproximada da região da captação (12 m), local onde se tinham medições. O período com dados de campo, março de 2018 a fevereiro de 2019, foi utilizado para calibrar o modelo. De modo geral, a simulação para a profundidade total do reservatório apresentou uma melhor performance. Por essa metodologia o modelo conseguiu reproduzir mais adequadamente o balanço hídrico, o que influenciou nos resultados do perfil térmico do corpo d'água. As métricas de erro entre os resultados de temperatura do modelo e os registros dos termistores estão de acordo com valores encontrados na literatura, já que o erro médio absoluto (MAE) ficou abaixo de 1.7 °C e a raiz do erro quadrático médio (RMSE) foi inferior a 2.3 °C. O modelo foi capaz de representar o fenômeno da estratificação, constatado também pelo cálculo de índices físicos, os quais demonstraram uma maior instabilidade no período mais frio, com a ocorrência de mistura entre as camadas. Em relação ao oxigênio dissolvido, o modelo apresentou um padrão de distribuição na coluna d'água bastante homogêneo. A dinâmica foi melhor reproduzida na camada do fundo, a qual exibiu um maior coeficiente de correlação. Contudo, o MAE e RMSE foram menores para a região próxima à superfície, indicando maior concordância dos valores em termos de ordem de grandeza. Quanto às substâncias químicas (nitrogênio e fósforo) e clorofila-a, devido à restrição dos dados medidos, foi priorizado o ajuste da ordem de magnitude. Uma importante análise da qualidade da água do reservatório pôde ser realizada com a classificação do seu estado trófico. Os resultados demonstraram uma predominância de condições mesotróficas do corpo d'água, o que corresponde com outros estudos realizados no reservatório. Constatase que o modelo é qualificado para estudar cenários de gestão, já que apresentou resultados satisfatórios, com resposta a forçantes.

Palavras-chave: Modelagem de reservatórios. Modelo 1D ecológico-hidrodinâmico acoplado. GLM-AED.

ABSTRACT

Appropriate reservoirs management involves understanding the complex and dynamic processes that occur in them. The transport and mixing of scalars are strongly influenced by the waterbody thermal regime. Coupled ecological-hydrodynamic numerical models present as a useful tool, in particular one-dimensional vertical models (1DV), due to vertical gradients predominance in the lake dynamics. In addition, they have the advantage of being able to study different scenarios and perform long-term simulations, with low computational cost and minimum calibration requirements. This work aimed to analyze the performance of GLM-AED (General Lake Model – Aquatic EcoDynamics) 1D coupled model in the reproduction of physical, chemical, and biological processes of a subtropical water supply reservoir (Passaúna reservoir, Paraná - Brazil). Firstly, hydrodynamic modeling was accomplished with GLM, in order to simulate the reservoir water balance and thermal behavior. Then, the AED modeling library was added activating the modules: oxygen, carbon, nitrogen, phosphorus, organic matter, phytoplankton, and totals. The simulation was from August 2017 to February 2019, adopting two configurations, one with the reservoir total depth (17 m) and other with the approximate depth of the intake region (12 m), where measurements were made. Period with field data, March 2018 to February 2019, was used to calibrate the model. In general, the simulation for the reservoir total depth showed a better performance. By this methodology, the model was able to reproduce the water balance more adequately, which influenced the results of the waterbody thermal profile. The error metrics between the temperature model results and the thermistors records are in accordance with values found in literature, since the mean absolute error (MAE) was below 1.7 °C and the root mean square error (RMSE) less than 2.3 °C. The model was able to represent the stratification phenology, also verified by the physical indices calculation, which showed greater instability in the coldest period, with the occurrence of mixing between the layers. Regarding dissolved oxygen, the model showed a very homogeneous distribution pattern in the water column. The dynamics were better reproduced in the bottom layer, which exhibited a higher correlation coefficient. However, MAE and RMSE were lower for the region close to the surface, indicating greater agreement of the values in terms of the order of magnitude. As for chemical substances (nitrogen and phosphorus) and chlorophyll-*a*, due to the restriction of measured data, adjustment of the order of magnitude was prioritized. An important analysis of the reservoir water quality could be performed with the classification of its trophic state. The results showed a predominance of mesotrophic conditions in the waterbody, which corresponds to other studies carried out in the Passaúna reservoir. It appears that the model is qualified to study management scenarios, since it presented satisfactory results, with responses to driving factors.

Keywords: Reservoir modeling. 1D coupled ecological-hydrodynamic model. GLM-AED.

LIST OF FIGURES

2.1	Schematic of a GLM simulation domain, input information (blue text), and key simulated processes (black text). Source: Hipsey et al. (2019)	26
2.2	AED module conceptual model of carbon and nutrient flux pathways and planktonic groups. Source: Hipsey et al. (2013)	30
3.1	Passaúna reservoir location in its sub-basin with the hydrography and the points of the water intake and dam.	32
3.2	Passaúna reservoir bathymetry and main inflows. Source: Adapted from Sotiri (2016)	33
3.3	Temperature and dissolved oxygen (DO) profiles in the Passaúna reservoir between 2005 and 2013. Source: Environmental Institute of Paraná - IAP (2017)	35
4.1	Meteorological data from Tecpar (orange line), Sanepar (green line), and Colônia Dom Pedro (blue bars) stations close to the Passaúna reservoir, from August 2017 to February 2019.	41
4.2	Windrose from the Tecpar station data, from August 2017 to February 2019	41
4.3	Location of the Passaúna reservoir inflows in LARSIM model. Source: MuDak-WRM (2019)	42
4.4	Inflow data of Passaúna reservoir, from Passaúna river (blue line), Ferraria river (green line), and Streams (red line), from August 2017 to February 2019	42
4.5	Outflow series of Passaúna reservoir calculated by members of the MuDak project, from August 2017 to February 2019	42
4.6	Dissolved oxygen (DO) concentration, DO saturation concentration, and water temperature in the Passaúna reservoir inflows (Passaúna river, Ferraria river, and streams), from August 2017 to February 2019	44
4.7	Nitrate (NO_3^-), ammonia (NH_4^+), total nitrogen, phosphate (PO_4^{3-}), total phosphorus, dissolved organic carbon (DOC) and chlorophyll- <i>a</i> data in Passaúna river, from February 2018 to April 2019	44
4.8	Hypsographic curve (elevation-area-volume) of Passaúna reservoir	46
4.9	Flowchart of the model calibration steps	50
4.10	Comparison of initial model results of water quality variables with field data obtained by the MuDak project and Sanepar in Passaúna reservoir, from August 2017 to February 2019	52

4.11	Model results of dissolved and particulate organic phosphorus (DOP and POP), and internal phosphorus of phytoplankton, along with total phosphorus field data obtained by the MuDak project and Sanepar in Passaúna reservoir, from August 2017 to February 2019.	54
5.1	Water level in Passaúna reservoir, from August 2017 to February 2019: measured (red line) and simulated (blue line) water level of the 17 m deep (a) and 12 m deep simulation (c) by GLM-AED, with the mean absolute error (MAE) and root mean square error (RMSE); density scatterplot of the 17 m deep (b) and 12 m deep simulation (d), where each point is colored by the spatial density of nearby points, with Pearson's correlation coefficient (r).	55
5.2	Contour plot of Passaúna reservoir water temperature measured by the thermistor chain at the intake region (a), and simulated by GLM-AED in the configurations of 17 m deep (b) and 12 m deep (c), from March 2018 to February 2019.	57
5.3	Comparison between temperature data measured by thermistors and simulated by GLM-AED model (17 m deep simulation) in the Passaúna reservoir, from March 2018 to February 2019, at depths of 1, 3, 5, 7, 9 and 11 m from the surface, along with the density scatterplot and correlation coefficient value (right side).	58
5.4	Error indices (MAE and RMSE) of simulated Passaúna reservoir water temperature (17 m deep simulation in red line and 12 m deep simulation in blue line) in relation to temperature measurements by thermistors, from March 2018 to February 2019.	59
5.5	Mean absolute error (MAE) from the May to July 2018 period (orange line), and from December 2018 to February 2019 (green line), of the 17 m deep simulation of the Passaúna reservoir.	59
5.6	Physical indices of the Passaúna reservoir calculated with water temperature records measured by thermistors and model data of the 17 m and 12 m deep simulations, from March 2018 to February 2019.	62
5.7	Surface and bottom temperature difference and thermocline depth of the Passaúna reservoir, from the physical indices calculated by records measured and model data of the 17 m and 12 m deep simulations, from March 2018 to February 2019.	63
5.8	Contour plot of Passaúna reservoir dissolved oxygen (DO) in the 17 m deep simulation by GLM-AED, from March 2018 to February 2019.	64
5.9	Comparison Passaúna reservoir dissolved oxygen (DO) between data measured by miniDOT (red line) and simulated by GLM-AED model (blue line; 17 m deep simulation), from April 2018 to February 2019, at depths of 10 m and 0.5 m above bed, along with the density scatterplot and correlation coefficient value (right side).	65

5.10	Comparison Passaúna reservoir dissolved oxygen (DO) between data measured by miniDOT (red line) and simulated by GLM-AED model (blue line; 12 m deep simulation), from April 2018 to February 2019, at depths of 10 m and 0.5 m above bed, along with the density scatterplot and correlation coefficient value (right side).	65
5.11	Contour plot of Passaúna reservoir nitrate (NO_3^-) in the 17 m deep simulation by GLM-AED, from March 2018 to February 2019.	66
5.12	Contour plot of Passaúna reservoir ammonia (NH_4^+) in the 17 m deep simulation by GLM-AED, from March 2018 to February 2019	67
5.13	Contour plot of Passaúna reservoir phosphate (PO_4^{3-}) in the 17 m deep simulation by GLM-AED, from March 2018 to February 2019	67
5.14	Comparison Passaúna reservoir nitrate (NO_3^-), ammonia (NH_4^+) and phosphate (PO_4^{3-}) between data of MuDak laboratory analyzes referring to the intake region and results obtained by the GLM-AED model, along with NO_3^- records by the Opus optical sensor, from March 2018 to February 2019, at surface (up to 1 m deep).	68
5.15	Comparison Passaúna reservoir total nitrogen and phosphorus between data of MuDak and Sanepar laboratory analyzes referring to the intake region and results obtained by the GLM-AED model, from February 2018 to February 2019, at surface (up to 1 m deep).	69
5.16	Contour plot of Passaúna reservoir chlorophyll- <i>a</i> in the 17 m deep simulation by GLM-AED, from March 2018 to February 2019.	70
5.17	Comparison Passaúna reservoir chlorophyll- <i>a</i> between data of MuDak laboratory analyzes referring to the intake region and results obtained by the GLM-AED model, along with Chlorophyll- <i>a</i> records by the NanoFlu optical sensor, from March 2018 to February 2019, at surface (up to 1 m deep).	70
5.18	Trophic level of Passaúna reservoir regarding the concentrations of total phosphorus and chlorophyll- <i>a</i> obtained by GLM-AED model, and the final trophic state index (TSI), calculated according to Lamparelli (2004), from August 2017 to February 2019.	71
A.1	Comparison of the meteorological data from Tecpar and Sanepar monitoring stations close to the Passaúna reservoir, from May 19, 2018, to February 28, 2019.	86
A.2	Density scatterplot of the Tecpar and Sanepar monitoring stations data of air temperature, from May 19, 2018, to February 28, 2019, with Pearson's correlation coefficient (r).	87
A.3	Density scatterplot of the Tecpar and Sanepar monitoring stations data of shortwave radiation, from May 19, 2018, to February 28, 2019, with Pearson's correlation coefficient (r).	87

A.4	Density scatterplot of the Tecpar and Sanepar monitoring stations data of relative humidity, from May 19, 2018, to February 28, 2019, with Pearson's correlation coefficient (r).	88
A.5	Density scatterplot of the Tecpar and Sanepar monitoring stations data of wind speed, from May 19, 2018, to February 28, 2019, with Pearson's correlation coefficient (r).	88

LIST OF TABLES

2.1	Trophic state classification for reservoirs.	23
3.1	Average flow, total nitrogen and total phosphorus loading for the rivers affluent to the Passaúna reservoir.	34
4.1	Correlation coefficient between meteorological data of Tecpar and Sanepar monitoring stations, from May 2018 to February 2019.	40
4.2	Calibrated physical parameters in GLM-AED modeling of the Passaúna reservoir.	49
4.3	Calibrated chemical parameters of Passaúna reservoir modeling with GLM-AED 1D model.	53
4.4	Calibrated phytoplankton parameters in GLM-AED modeling of the Passaúna reservoir.	54
5.1	Studies presenting the calibration MAE and/or RMSE range of water temperature simulations applying 1D models.	61
5.2	Error indices (MAE and RMSE) of physical indices of the Passaúna reservoir between the calculation by records measured and model data of the 17 m and 12 m deep simulations, from March 2018 to February 2019.	61
5.3	Number of days $W < 1$, $W > 1$, $L_N < 1$, $L_N > 1$, $\Delta T < 1^\circ\text{C}$, $\Delta T > 1^\circ\text{C}$, $\Delta T > 2^\circ\text{C}$ and $\Delta T > 3^\circ\text{C}$ of the Passaúna reservoir, from the physical indices calculated by records measured and model data of the 17 m and 12 m deep simulations, from March 2018 to February 2019.	62
5.4	Error indices (MAE and RMSE) for Passaúna reservoir dissolved oxygen (DO) between measurements of the miniDOT and results obtained by GLM-AED model, from April 2018 to February 2019, at depths of 10 m and 0.5 m above bed.	64
5.5	Error indices (MAE and RMSE) for Passaúna reservoir nitrate (NO_3^-) between measurements of the Opus optical sensor and results obtained by the GLM-AED model.	69
5.6	Error indices (MAE and RMSE) for Passaúna reservoir chlorophyll- <i>a</i> between measurements of the NanoFlu optical sensor and results obtained by the GLM-AED model.	70

CONTENTS

1	INTRODUCTION	14
1.1	OBJECTIVES	15
2	WATER QUALITY IN RESERVOIRS	17
2.1	THERMAL STRATIFICATION	18
2.2	EUTROPHICATION	21
2.3	ECOLOGICAL MODELING	23
2.3.1	GLM - Hydrodynamic Module	26
2.3.2	AED - Ecological Module	29
3	STUDY AREA	32
3.1	PREVIOUS STUDIES IN PASSAÚNA RESERVOIR	36
4	MATERIALS AND METHODS	39
4.1	METEOROLOGICAL DATA	39
4.2	HYDROLOGICAL DATA	40
4.3	WATER QUALITY DATA	43
4.4	MODEL SETUP	46
4.4.1	Hydrodynamic Module	46
4.4.2	Ecological Module	48
4.5	POST PROCESSING AND ANALYSIS	51
5	RESULTS AND DISCUSSION	55
5.1	HYDRODYNAMIC MODULE PERFORMANCE	55
5.1.1	Water level	55
5.1.2	Water temperature	56
5.1.3	Physical indices	61
5.2	ECOLOGICAL MODULE PERFORMANCE	63
5.2.1	Oxygen	63
5.2.2	Nutrients (phosphorus and nitrogen)	65
5.2.3	Chlorophyll- <i>a</i>	68
5.2.4	Trophic State Index	70
6	CONCLUSIONS	73
	REFERENCES	76
	APPENDIX A – METEOROLOGICAL DATA COMPARISON	86

1 INTRODUCTION

Reservoirs, also called artificial lakes, are ecosystems formed from the damming of one or more rivers, sometimes flooding large adjacent land areas (Esteves, 2011). These lake environments support extensive ecosystem services such as water supply, flood mitigation, hydropower, as well as aesthetic and cultural benefits, fisheries and biodiversity (Mueller et al., 2016). According to the *Relatório de Segurança de Barragens 2017*, of the National Water Agency - ANA (2018), in Brazil there are currently 24,092 dams registered for various uses, especially irrigation, animal desedentation and aquaculture.

Impacts caused by anthropogenic activities in watersheds, in addition to the indirect pressures from climate change, have led to greater vulnerability of lakes on a global scale (Folke et al., 2004). According to Bhagowati and Ahamad (2019), in the last decades many freshwater lakes turned into highly eutrophied waterbodies. This phenomenon is characterized by the excessive concentration of nutrients in water, basically phosphorus and nitrogen, usually from the discharge of urban, agricultural and industrial effluents. This water enrichment by nutrient causes a large proliferation of aquatic plants, especially algae, causing problems not only for the local biota and the water user, but also for the entire treatment and distribution system (Von Sperling, 1996). Several features of the reservoirs themselves, however, also end up compromising the quality of their water. According to Andreoli and Carneiro (2005), the existing reservoirs in the Curitiba Metropolitan Region (RMC), Paraná state (Brazil), have low average depth, long residence time and extensive surface area, making them susceptible to eutrophication.

The RMC has 45% of its territory considered as Area of Interest of Sources of Public Water Supply (Coordination of the Curitiba Metropolitan Region - COMEC (2017)). Curitiba's Integrated Supply System currently has four reservoirs (Piraquara I and II, Iraí and Passaúna) and one under construction (Miringuava). Specifically, the Passaúna reservoir, object of this study, supplies about 20% of the RMC population, with a useful volume of 48 hm³, a surface area of 9 km², and a mean depth of 6.5 m (SANEPAR, 2013; Carneiro et al., 2016). The choice of study area was within the framework of the MuDak-WRM (2019) project (*Multidisciplinary Data Acquisition as Key for Globally Applicable Water Resource Management*; <https://www.mudak-wrm.kit.edu/>), a partnership between German and Brazilian universities, sanitation and reservoir management companies, and industry partners, in order to study optimized alternatives for water resources management.

The assessment of reservoir water quality is essential to achieve the sustainable balance of its multiple uses, helping to make management decisions (Von Sperling, 1999). For Vinçon-leite and Casenave (2019), management and restoration solutions to control eutrophication must be supported by scientific outcomes, including modelling approaches. Recent dynamic models are very useful tools for obtaining answers to problems, such as how trophic state of a lake will

change if certain amount of nutrient loading is reduced for a certain time period (Bhagowati and Ahamad, 2019). In general, models of lake ecosystems are critical for designing ecosystem control strategies to preserve water quality and achieve economic benefits from the use of natural resources in an aquatic system (Menshutkin et al., 2014).

A trend in the scientific community is the use of one-dimensional (1D) models because they cover a wide range of study areas, due to its computational efficiency and minimum calibration requirements (Bruce et al., 2018; Hipsey et al., 2019). In addition, the use of the 1D structure is justified in many cases given the dominant role of seasonal changes in vertical stratification in lake dynamics, including oxygen, nutrients and metal cycling, and plankton dynamics, besides that horizontal gradients are lower than vertical ones (Hamilton and Schladow, 1997; Gal et al., 2009). Another advantage is the easy linkage with biogeochemical and ecological modeling libraries for complex ecosystem simulations (Hipsey et al., 2019). According to Bueche et al. (2017), the coupling of limnophysical and ecological models is of great importance in the context of global environmental change.

A one-dimensional vertical hydrodynamic open source model adopted in more recent studies (Yao et al., 2014; Read et al., 2014; Fenocchi et al., 2017; Huang et al., 2017; Bueche et al., 2017; Weber et al., 2017; Bruce et al., 2018; Ladwig et al., 2018; Fenocchi et al., 2018) is the General Lake Model - GLM (Hipsey et al. (2019); <http://aed.see.uwa.edu.au/research/models/GLM/>). It was developed in 2012 by the Global Lake Observatory Network (<http://gleon.org/>), a researchers network who aim to understand lakes and reservoirs functioning and how its vary in response to climate and land use change. This model can be coupled with the freely available ecological model library Aquatic Ecdynamics - AED (Hipsey et al. (2013); <http://aed.see.uwa.edu.au/research/models/AED/index.html>) for limnoecological studies (Bucak et al., 2018; Fenocchi et al., 2019; Fadel et al., 2019).

In order to analyze the performance of one-dimensional modeling in reproducing the physical, chemical, and biological processes of a subtropical water supply reservoir (Passaúna reservoir), the GLM-AED 1D coupled model was implemented. Firstly, the hydrodynamic simulation was accomplished with GLM (version 3.0.5), for the purpose to capture lake water balance and thermal stratification dynamic. In sequence, the AED (version 1.3.2) library was added to model both chemical and biological components of the lake ecosystem, activating the following modules: oxygen, carbon, nitrogen, phosphorus, organic matter, phytoplankton, and totals. The modeling period was from August 2017 to February 2019, being chosen to allow comparisons with field data (March 2018 to February 2019), besides being possible to observe the seasonal effects for different seasons of the year.

1.1 OBJECTIVES

The general objective of this work is to apply the GLM-AED 1D coupled model in the Passaúna reservoir simulation to analyze the performance of one-dimensional modeling

in reproducing the physical, chemical, and biological processes of a subtropical water supply reservoir.

The specific objectives are:

- i Compile field and literature data for the hydrodynamic and ecological modules, performing the consistency of the inconsistent or absent information;
- ii Perform the model setup and calibration for the Passaúna reservoir, from March 2018 to February 2019, comparing the model results with accurate observed data from continuous measurements and laboratory analyzes of samples collected in the field;
- iii Evaluate the thermal behavior of the Passaúna reservoir, identifying the stratification periods from field measurement data and model results, besides physical indices calculation;
- iv Analyze the dynamics of some state variables representative of the water quality (oxygen, chlorophyll-*a*, compounds of nitrogen and phosphorus) in the Passaúna reservoir, as well as perform the classification of waterbody trophic state.

2 WATER QUALITY IN RESERVOIRS

The water quality in reservoirs is influenced by several factors, from the conditions of its main inflows, which usually correspond to the greater part of the nutrient loads and sediment, to the physical, chemical and biological interactions that occur in these lacustrine environments. Water characteristics allow the exchange of nutrients and chemical substances between organisms, increasing the dynamics of biogeochemical processes and leading to high rates of primary productivity (Esteves, 2011). The reservoirs morphometric characteristics are also interesting information, especially its depth, length, width, net surface area, drainage area, volume and length of the margins (Porto et al., 1991). A variable able to synthesize some of these characteristics, in a simplified way, is the residence time (or detention), i.e., the period necessary for the reservoir water to be totally renewed, obtained by means of the ratio of the reservoir volume and the mean flow rate (Thomann and Mueller, 1987).

In relation to the horizontal velocities variations in the reservoir, the artificial impoundment of the watercourse cause changes in the hydrodynamic circulation, forming three distinct regions: lotic zone, transition and lentic. The lotic zone, also denominated of river region, is shallow and with strong influence of the tributaries, predominating therefore the advective transport. In the transitional region the depths are higher and the longitudinal flow is reduced, characteristics that are maximized in the lentic zone (reservoir region) (Tundisi and Tundisi, 2008). The formation of these zones is also dependent on the reservoir residence time. In run-of-the-river hydroelectric reservoirs, low detention may not be sufficient for the development of a representative lentic region, making water quality primarily determined by the tributaries. In cases of reservoirs with a high residence time (on the order of years), the lotic and transition zones may be small compared to the formed lentic zone, thus predominating significant effects of biological activities and of sources from the surface or the deeper layers (Fischer et al., 1979).

The biological processes that occur in aquatic systems also condition these to a compartmentalization in different regions: coastal (or riparian), limnetic (or pelagic) and benthic. The coastal strip corresponds to the transition (ecotone) between the terrestrial and lacustrine ecosystems, having several ecological niches and food chains, since they are usually inhabited by aquatic plants, which give the necessary support for the development of several other organisms (Porto et al., 1991). The limnetic range encompasses the innermost central region, where the planktonic community is found, in which the group of invertebrate microorganisms (zooplankton) and algae (phytoplankton - the main primary producers) are highlighted, constituting also viruses, bacteria, protozoa and fungi. The nekton, a community formed mainly by fish, is also present in this area and, unlike plankton, has its own locomotion. Finally, in the deepest layer, the benthic community predominates, formed mainly by bacteria and invertebrate animals. This region is

more characterized by decomposition processes than of organic matter production, which leads to scarcity or non-existence of dissolved oxygen (Esteves, 2011).

Such distribution of the organisms in the aquatic environment is mainly conditioned by the light absorptive capacity inside the waterbody, which section the reservoir in the euphotic (illuminated) and aphotic zone (Porto et al., 1991). The euphotic zone is the water layer capable of maintaining positive values of net primary production, below it, in the afotic zone, prevailing the heterotrophic metabolism. The boundary between these two strata is known as the compensating point of photosynthesis, where the primary production is equal to respiration, and is generally defined as the depth where the radiation intensity corresponds to 1% of the intensity reaching the surface. The determination of the euphotic zone extension is also done by the water transparency, multiplying the value of the Secchi disk depth (Z_{sd}) by a factor, in case of Brazil the most frequently used by the limnologists is 3 (Ishii, 1987). Such depth Z_{sd} is obtained by dipping the white disc, about 20 to 30 centimeters in diameter, into the waterbody by means of a marked rope and verifying the depth of its disappearance (Esteves, 2011). This measure Z_{sd} can also be used for the light extinction coefficient (k) indirect calculation, according the following relation (Poole and Atkins, 1929) as

$$k = \frac{1.7}{Z_{sd}}. \quad (2.1)$$

The progressive solar radiation reduction in the water column with increasing depth can lead to the so-called thermal stratification. This, in turn, can condition the chemical stratification, that is, the non-homogeneous distribution in the water column of the gases, organic, and inorganic compounds (Barbosa et al., 2012). Such processes alter the scalar transport regimes of the waterbody, generating vertical gradients of variables concentrations as dissolved oxygen and nutrients, which can make feasible the eutrophication phenomenon (Esteves, 2011). These processes, intrinsically linked to the water quality of the reservoirs, will be addressed in more detail in the next sections.

2.1 THERMAL STRATIFICATION

Thermal stratification in reservoirs is mainly due to energy balance, this is the combined effects of meteorological forces acting on the water surface, advective and diffusive transport, and inflows. Such phenomenon is facilitated by the thermal expansion properties of water, which creates a stable vertical density gradient owing to heating (or cooling if below 3.98 °C) of surface waters. Nonetheless, the water density and temperature do not vary proportionally; with water temperature increasing, the density differences become growing larger, making the change in density between 4 °C and 5 °C less than between 27 °C and 28 °C. In this way, the stratification patterns of the water column are variable depending on the waterbody location. In tropical regions, is common to occur daily stratification and destratification or stratification during spring,

summer and autumn, and return to the destratification condition in winter (Esteves, 2011). In temperate regions, the stratification phenomenon occurs differently due to the consideration of ice dynamics.

The thermal stratification presence can give rise to three distinct layers: epilimnion, located in the upper region, with a higher luminosity presence and higher concentration of dissolved oxygen; metalimnion, which is the intermediate range, presenting a gradual temperature drop where is located the thermocline (plane that passing at the inflection point of the thermal profile); and hypolimnion, deeper region, with greater stagnation and low luminosity, reaching anoxia in some cases (Von Sperling, 1996). This vertical partitioning of the water column has important implications for the availability of nutrients, light, and microbial substrates, in vertical distribution, migration, and feeding of higher trophic levels like zooplankton and fish, besides controlling the vertical fluxes of dissolved and particulate material (Read et al., 2011).

Some factors, however, act favoring the water column mixing. The wind exerts a turbulent stress action on the water surface, leading to redistribution of heat by the waterbody. The amplitude and vertical dimension of such event is dependent on the wind speed, the location in relation to the reservoir major axis (fetch) and the local topography. Inflows and internal wave processes, i.e., periodic and rhythmic swings of the water mass with intense vertical movement, can interfere in thermal stratification by transferring energy to specific layers. The process known as convective mixing can also erode the stratification. In this case, the water cooling in colder months (on a seasonal scale) or at night (on a daily scale) makes the surface fraction heavier, causing it to sink and thus, destabilize the temperature profile (Tundisi and Tundisi, 2008).

As for the mixing patterns, the reservoirs can be classified as holomictic, with one complete circulation in the water column, meromictic, with only circulation in the upper layer and a lower layer more stable, or yet amictic, without any circulation. The holomictic reservoirs are still different in the circulation's number per year, being able to have only one (monomictic), two (dimictic), several (polymictic) or few circulations (oligomictic). In subtropical reservoirs, there is usually one circulation during the winter, denominating them as warm monomictic (Esteves, 2011).

The characterization of the mixing and stratification processes in reservoirs can be done using physical indices, well established in the literature. These indices can be used to effectively parse out the contributions of convective cooling (decrease in Schmidt Stability), drivers like wind (Wedderburn Number and Lake Number), and destratifying forces that weaken vertical density gradients (decrease in buoyancy frequency) (Read et al., 2011).

The Schmidt Stability (S_T), given in J m^{-2} , represents the resistance to mechanical mixing due to the potential energy inherent in the stratification of the water column, calculated as (Idso, 1973)

$$S_T = \frac{g}{A_s} \int_0^{z_D} (z - z_v) \rho_z A_z \partial z, \quad (2.2)$$

where g (m s^{-2}) is the gravity acceleration, A_s (m^2) is the surface area of the lake, A_z (m^2) is the lake area at the depth z , ρ_z (kg m^{-3}) is the water density at the depth z , z_D (m) is the maximum depth of the lake, and z_v (m) is the depth to the centre of volume of the lake, written as $z_v = \int_0^{z_D} z A_z dz / \int_0^{z_D} A_z dz$.

The Wedderburn Number (W), introduced by Thompson and Imberger (1980), is used to describe potential upwelling events under stratified conditions. This index relates the thrust force to the wind destabilizing force, and can be written as

$$W = \frac{g' z_e^2}{u_*^2 L_s}, \quad (2.3)$$

where $g' = g\Delta\rho/\rho_h$ (m s^{-2}) is the reduced gravity due to the change in density ($\Delta\rho$) between the hypolimnion (ρ_h) and epilimnion (ρ_e), z_e (m) is the depth to the base of the mixed layer, L_s is the lake fetch length and u_* (m s^{-1}) is the water friction velocity due to wind stress. For $W \leq 1$, the deepening of the mixed layer is dominated by the turbulence internal production. In this case, there is a high probability that the thermocline will tilt to the surface at the upwind end of the lake and metalimnetic water will be entrained into the surface mixing layer. Already for $W > 1$, the isotherms inclination due to the wind action is small, thus the mixed layer will deepen slowly and strong thermal stability will occur.

The Lake Number (L_N) describe processes relevant to the internal mixing of lakes induced by wind forcings, being a measure of the potential for mixing across the thermocline. As with W , lower values of L_N represent weak stratification, with potential for mixing. For $L_N > 1$, the stratification is strong and the wind agitates the epilimnion superior portions, so that little mixing in the hypolimnion is expected and little thermocline balance (Imberger and Patterson, 1990). Lake Number is given by

$$L_N = \frac{S_T(z_e + z_h)}{2\rho_h u_*^2 A_s^{1/2} z_v}, \quad (2.4)$$

where z_e and z_h (m) are the depths to the top and bottom of the metalimnion, respectively.

The square of the Brunt-Väisälä Frequency (N^2), given in s^{-1} , quantifies the intensity of local stratification stability of the waterbody (Wuest and Lorke, 2009), and is defined as

$$N^2 = -\frac{g}{\rho_0} \frac{\partial \rho}{\partial z}, \quad (2.5)$$

in which ρ_0 (kg m^{-3}) is the specific mass mean value in the differential interval and z (m) is the coordinate in vertical direction in positive upwards. If $\partial \rho / \partial z < 0$ the stratification is considered stable, otherwise ($\partial \rho / \partial z > 0$) the stratification is unstable.

2.2 EUTROPHICATION

The eutrophication is one of the most challenging environmental problems that the surface waterbodies are facing in present time. It is the enrichment of aquatic ecosystems with nutrients, especially phosphorus and nitrogen, leading to the primary productivity increase, i.e., rate of photosynthesis (Bhagowati and Ahamed, 2019). This ecological process, although it occurs naturally in the waterbodies, has been accelerated by anthropogenic actions in the watersheds. This type of artificial or cultural eutrophication, as it is called, has been observed since the beginning of the twentieth century in industrialized countries (Esteves, 2011; Vinçon-leite and Casenave, 2019).

The main point sources (releases concentrated at a given site) of pollution and, consequently, of nutrients, come from organic discharges of treated and untreated domestic and industrial effluents, from the effluent treatment plants themselves, percolated water from septic tanks and clandestine sewer connections in rainwater networks. The nutrient input is also caused by residues from livestock farming and by fertilizers and agrochemicals from agricultural areas. In this case, the nutrients are transported by surface runoff and depend on the topographic and geological characteristics of the region, as well as the effects of soil erosion and leaching, with the aggravation of diffuse occurrence, making monitoring and control difficult. This situation is associated with precipitation events, which in itself is already considered a significant source of phosphate and nitrogen, especially in regions of intense atmospheric pollution (Andreoli and Carneiro, 2005).

Nutrient concentration imbalance leads to excessive proliferation of primary producers (phytoplankton, aquatic plants, cyanobacteria), reaching uncontrollable outbreaks known as algal bloom. This flowering resulting in high turbidity and anoxic conditions in the waterbody deeper parts, which in turn leads to an internal phosphorus load released by the sediment, amplifying the system eutrophication (Dodds, 2006). The consequent increases of organic matter decomposition causes a significant depletion of oxygen, with the death of aquatic organisms and the release of fetid gases from the bottom sediment, such as hydrogen sulphide and methane (Cunha et al., 2011). There is also a price increase in the water treatment process, since the large amount of algae in the supply reservoirs can cause the filters to become clogged in the stations, as well as impart unpleasant water taste and odor, alter its color, contribute to increase corrosion in the distribution networks, promote the formation of organochlorine compounds and pH raise. One of the major problems, however, involves public health, due to the production by cyanobacteria (a phytoplankton species) of potentially toxic substances, called cyanotoxins, that present risks to human health (Andreoli and Carneiro, 2005).

In this sense, an important waterbody specification is its trophic level, an indicator of the primary production potential, i.e., of the organic matter amount synthesized by autotrophic organisms (algae, macrophytes) and chemotrophic (nitrifying bacteria). Under conditions of low rates of nutrient cycling and renewal of phytoplanktonic biomass (multicellular algae), that is,

reduced primary production, the reservoir is in the oligotrophic state, rising to mesotrophic or eutrophic as these values increase. The eutrophication stage in which the waterbody is present may also have more accurate intermediate classifications, such as ultraoligotrophic, oligomesotrophic, mesoeutrophic, eupolytrophic and hypereutrophic (Von Sperling, 1996; Esteves, 2011). Morphometric, hydrologic, and meteorological factors interrelated also affect the trophic conditions of a waterbody. Shallow lakes, according to Odum (1971), are morphometrically eutrophic even with nutrients low concentrations, since they have a greater water volume receiving solar radiation. Shallow aquatic systems, typically less than 3 m deep, can be defined as standing water bodies, approximately permanent, with the potential to allow light penetration to the bottom. In relation to the reservoir residence time, the organisms density increase is favored the longer the period in which the water is in this environment (Cunha et al., 2011). In brief, for these effects to occur, the favorable temperature and environmental conditions are necessary, high nutrients concentration, slow current velocity, and microbial activity and biodiversity in the waterbody (Li and Liao, 2002).

The trophic state characterization is based on several indicators used together, such as the water transparency degree obtained from the Secchi disk, or the chlorophyll-*a* concentration, a pigment that aggregates the phytoplankton green color, allowing the quantification of its biomass. In nutrients case, phosphorus participates in the aquatic organism's metabolism through the energy storage and the cell membrane structure, whereas nitrogen acts in the proteins formation (Esteves, 2011). Thus, in order to objectively quantify the eutrophication process in lakes and reservoirs, Carlson (1977) proposed the trophic state index (TSI). With simplified equations from the correlations between luminosity in the water column by the Secchi disk, chlorophyll-*a*, and total phosphorus, the TSI was initially developed for the classification of temperate environments. Toledo Jr. et al. (1983) and Toledo Jr. (1990) adapted Carlson (1977) equations for application in tropical and subtropical waterbodies. Later, Lamparelli (2004) updated the equations using only total phosphorus and chlorophyll-*a* data, as shown below

$$TSI(TP) = 10 \left(6 - \frac{1.77 - 0.42 (\ln TP)}{\ln 2} \right) \quad (2.6)$$

$$TSI(Chla) = 10 \left(6 - \frac{0.92 - 0.34 (\ln Chla)}{\ln 2} \right) \quad (2.7)$$

where *TP* is the concentration of total phosphorus and *Chla* of chlorophyll-*a*, both in $\mu\text{g L}^{-1}$ and measured close to the water surface. The final TSI (equation 2.8) results from the simple arithmetic mean of the *TSI(TP)* and *TSI(Chla)*. The limits established for the different trophic classes for reservoirs are described in Table 2.1.

$$TSI = \frac{TSI(TP) + TSI(Chla)}{2} \quad (2.8)$$

In general, the eutrophication process has several consequences for the aquatic ecosystems equilibrium and its different uses, and can be considered a form of pollution (Cunha et al., 2011). In order to eliminate or at least minimize the problems arising from eutrophication, one can adopt strategies grouped in control and corrective measures. Also called prophylactic, the control measures have their action in the hydrographic basin as a whole, aiming to allochthonous loads reduce generated by the urban, agricultural and industrial occupation. On the other hand, the corrective (therapeutic) measures aim to reestablish the eutrophic reservoir equilibrium with the autochthonous loads reduction, that is to say, internal to the environment (Thomann and Mueller, 1987; Von Sperling, 1996).

Table 2.1: Trophic state classification for reservoirs.

Trophic level	Total phosphorus [mg PL ⁻¹]	Chlorophyll-a [µg L ⁻¹]	TSI
Ultraoligotrophic	≤ 0.008	≤ 1.17	≤ 47
Oligotrophic	$0.008 < TP \leq 0.019$	$1.17 < Chl-a \leq 3.24$	$47 < TSI \leq 52$
Mesotrophic	$0.019 < TP \leq 0.052$	$3.24 < Chl-a \leq 11.03$	$52 < TSI \leq 59$
Eutrophic	$0.052 < TP \leq 0.120$	$11.03 < Chl-a \leq 30.55$	$59 < TSI \leq 63$
Supereutrophic	$0.120 < TP \leq 0.233$	$30.55 < Chl-a \leq 69.05$	$63 < TSI \leq 67$
Hypereutrophic	> 0.233	> 69.05	> 67

Source: Adapted from Lamparelli (2004).

2.3 ECOLOGICAL MODELING

The mathematical modeling use is increasingly recurrent in studies and projects related to water resources, since it allows an overview of the processes dynamics in these systems. In addition to providing insights to field data of present conditions, models have the potential to forecast the effects of future changes and the necessary remediation measures, through the simulation of different management scenarios (Bruce et al., 2006; Trolle et al., 2012). Coupled ecological-hydrodynamic models are important instruments to improve the understanding of ecological processes in complex aquatic ecosystems (Fadel et al., 2019). Over the years, studies have used ecological lake models for purposes such as combatting eutrophication, developing mitigation strategies (such as external load reduction and biomanipulation), and predicting the climate change impacts on lake ecosystems (Bucak et al., 2018).

Dynamic models represent the processes involved in the environmental by means of a set of appropriate differential equations and boundary conditions, whose solution is obtained by numerical methods. Thus, the models allow integrating spatially dispersed information, interpreting measurements made at sampling points, interpolating information to regions where data are not available, and make predictions through scenarios. Obtaining quality information through these tools stems, however, from the modeler's understanding of the essence of the interest phenomena, as well as the fundamentals of the modeling process, limitations and potentialities of the model used (Rosman, 2019).

Because they are approximations of reality, it is indispensable to carry out the calibration and validation steps of the model, also analyzing the errors and sensitivity to input data (variable or coefficient). The calibration aims to obtain a good adjust between the estimated (calculated by the model) and observed (measured) data, through the variation of the model parameters (coefficients). The validation corresponds to the evaluation of the model fit submitted to a different set of experimental data. When there are no measurement records, however, typical coefficient values based on the literature are used (Von Sperling, 2014).

The choice of the model spatial dimension occurs in function on the study object, the detail level required, and the computational availability (depending on the simulated time interval). Zero dimension models have limited use for cases where can be assumed that substance concentration is uniform within the control volume. One-dimensional models simulate the processes considering one dimension in space, longitudinal or vertical. 1DH models are applicable to study variations along the reservoir axis, while 1DV are often used to analyze vertical thermal and chemical stratification. 2D (two-dimensional) models simulate the phenomena disregarding variations in one of the directions, can be two-dimensional in plan (2DH) or in profile (2DV). 2DH models consider the longitudinal and transverse directions, being used to visualize the velocities and concentrations in shallow waterbodies. 2DV, mediated laterally, are useful when in addition to vertical stratification, there is longitudinal variation due to the reservoir length. Models that represent ecosystem spatial heterogeneity in the three dimensions (3D), although they emerged in the early 2000s, began to be more applied as of 2010 with increasing computational power and in situ measurements (Vinçon-leite and Casenave, 2019).

Often, lake managers and reservoir operators prefer models having a simpler application, as they are more agile for a specific function and more suited to parameter identification and scenario-testing workflows (Bruce et al., 2018). Thus, the modeling community of lacustrine systems has often relied on one-dimensional models (1D), due the dominant role of seasonal changes in vertical stratification in lake and reservoir dynamics. Another advantage is the easily linked with biogeochemical and ecological modeling libraries for complex ecosystem simulations (Hipsey et al., 2019).

According to Menshutkin et al. (2014), some 1D models usually used for lake ecosystems are SALMO-HR, DYRESM-MYL2, PCLake and PROTECH. The version 1D of the SALMO model reproduces seasonal temperature variations, stratification, and turbulence. The DYRESM model takes into account the vertical gradients of lake water characteristics and allows the coupling with the CAEDYM model for water quality studies. The PCLake is designed for describing eutrophication processes in nonstratified shallow lakes in the macrophytes presence, accounting the biomass dynamics of diatoms, green, and blue-green algae, as well as zooplankton and zoobenthos. The PROTECH model is intended especially for studying the phytoplankton community dynamics, can account for ten different phytoplankton groups.

Another one-dimensional model, adopted in more recent studies and chosen to be used in this work, is the General Lake Model - GLM (Hipsey et al. (2019); <http://aed.see.uwa.edu>.

[au/research/models/GLM/](http://research/models/GLM/)), an open-source hydrodynamic model. It was developed in 2012 by the Global Lake Ecological Observatory Network (<http://gleon.org/>), a researchers network who aim to understand lakes and reservoirs functioning and how its vary in response to climate and land use change. This model can be coupled with the freely available ecological model library Aquatic Ecodynamics - AED (Hipsey et al. (2013); <http://aed.see.uwa.edu.au/research/models/AED/index.html>) for limnoecological studies.

The GLM was applied by Read et al. (2014), in which 2368 temperate lakes were simulated over three decades, revealing weak coherence in stratification phenology. Yao et al. (2014) compared the performance modelling water temperature and ice dynamics of four models (Hostetler, Minlake, Simple Ice Model or SIM and GLM), using 16 years of field data from Harp Lake (Ontario, Canada). Huang et al. (2017) used the GLM to simulate water temperature changes in Nam Co, the second largest lake on the central Tibetan Plateau (China), for the period 1979 – 2012. Fenocchi et al. (2017) modeling a deep subalpine lake (Lake Maggiore, Northern Italy/Southern Switzerland) with GLM between 1998 and 2014, to analyze the influence of inflows on the thermodynamic structure. Bueche et al. (2017) used the GLM to simulate water temperatures and ice cover of a medium-sized lake (Lake Ammersee, Germany).

Weber et al. (2017) simulated the Grosse Dhuenn Reservoir (Germany) with GLM, seeking to optimize withdrawal from drinking water reservoir to reduce downstream temperature pollution and reservoir hypoxia. Bruce et al. (2018) did a multi-lake comparative analysis of the GLM with the stress-testing evaluation for 32 lakes across a global observatory network. Bucak et al. (2018) modeled with SWAT, PCLake and GLM-AED the effects of climatic and land use changes on phytoplankton and water quality of the largest freshwater lake of the Mediterranean basin (Lake Beyşehir). Fenocchi et al. (2018) studied the possible mixing regime evolution of Lake Maggiore under climate change in the 2016 – 2085 period, through numerical simulations performed with GLM. Fenocchi et al. (2019) calibrated and validated the GLM-AED2 for the Lake Maggiore for an overall 16.75 year, focusing on the reproduction of both deep-water chemistry and phytoplankton biomass and succession.

Silva et al. (2015) used the GLM to model the Pampulha lagoon, located in Belo Horizonte (Minas Gerais, Brazil), in order to evaluate the effects on the thermal structure and cyanobacteria dynamic by urban stormwater runoff. Barbosa et al. (2015) performed a sensitivity analysis and calibration optimization of the GLM model at Paranoá Lake (Brasília-DF, Brazil), between March 2007 and March 2009. Belico et al. (2017) also studied the Pampulha lagoon applying the GLM-AED eco-hydrodynamic model, focused on the investigation of the rainy events impacts on the reservoir dynamic, through monthly and time monitoring data (2011 – 2015). Soares et al. (2019) used the GLM to evaluate the water scarcity impacts in the southeastern region of Brazil, simulating the Serra Azul reservoir (MG) during the period from 2009 to 2016.

2.3.1 GLM - Hydrodynamic Module

The General Lake Model – GLM (Hipsey et al. (2019); <http://aed.see.uwa.edu.au/research/models/GLM/>) is a one-dimensional hydrodynamic model designed to simulate the water balance and the vertical stratification of lacustrine systems. The model computes the temperature, salinity and density gradients in vertical profiles, considering the effect of inflows and outflows, mixing, heat exchange, including the ice cover on surface heating. The Figure 2.1 shows a schematic of a GLM simulation domain.

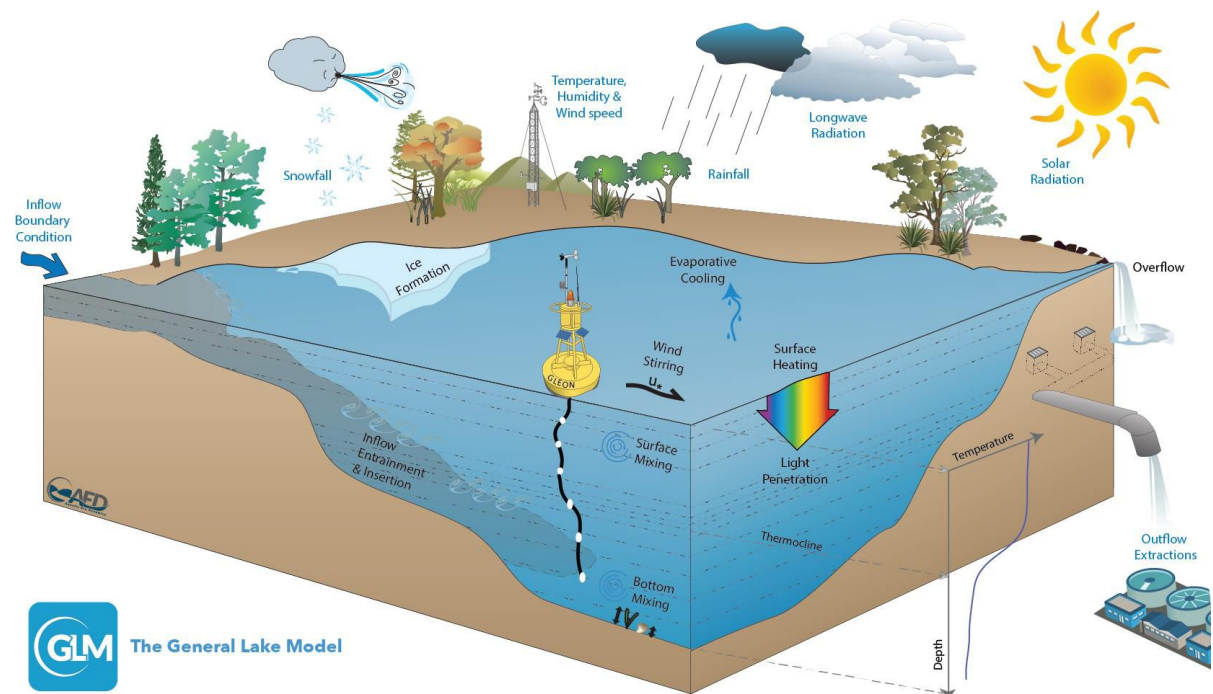


Figure 2.1: Schematic of a GLM simulation domain, input information (blue text), and key simulated processes (black text).

Source: Hipsey et al. (2019).

A flexible Lagrangian layer structure (Imberger et al., 1978; Imberger and Patterson, 1981) is adopted by the GLM. This layer scheme allows the layers thickness change dynamically by contraction and expansion, in addition to regulating the layer's number throughout the simulation to maintain homogeneous properties within the same layer. Because it does not require the calculation of vertical velocities, this layer structure considerably decreases computational processing time (Fernandes, 2018). The layers volume is determined by interpolation based on the site-specific hypsographic curve (Hipsey et al., 2019).

The mixing dynamics for the surface mixed layer (surface mixing) is based on estimating the amount of turbulent energy available. The balance between the available energy and the energy required for mixing to occur provides the surface mixed layer deepening rate. The available kinetic energy is calculated due to contributions from wind stirring, convective overturn, shear production between layers, and Kelvin–Helmholtz billowing.

Mixing below the thermocline in lakes, in the deeper hypolimnion, is modelled using a characteristic vertical diffusivity, which is the sum of the molecular diffusivity for scalars and the turbulent diffusivity. In GLM there is the possibility of choosing non-diffusivity, a constant vertical diffusivity over the water depth below the surface mixed layer, or a derivation by Weinstock (1981). The last option is described as being suitable for regions displaying weak or strong stratification, whereby diffusivity increases with dissipation and decreases with heightened stratification.

The water balance in the model includes user-defined fluxes, which may be surface mass fluxes (evaporation, rainfall, and snowfall), inflows (surface or submerged inflows, and local run-off from the surrounding exposed lakebed area), and outflows (withdrawals, overflow, and seepage). The calculation of the net water flux over the entire lake is summarized according to the following equation

$$\frac{dV_S}{dt} = A_S \frac{dh_S}{dt} + \sum_I^{N_{INF}} Q_{inf} - \sum_O^{N_{OUTF}} Q_{outf} - Q_{seepage} - Q_{ovfl}, \quad (2.9)$$

where V_S is the total lake volume, t is time, A_S is the lake surface area, h_S represents the changes in the surface layer height, and the remaining terms (Q_{inf} , Q_{outf} , $Q_{seepage}$, and Q_{ovfl}) correspond the inflows and outflows.

The general heat budget equation (2.10) for the uppermost layer consider the balance of shortwave (ϕ_{SW}) and longwave (ϕ_{LW}) radiation fluxes and sensible (ϕ_H) and evaporative (ϕ_E) heat fluxes (all W m^{-2}). Being c_w the specific heat capacity of water, T_s the surface temperature, and z_s and ρ_s the depth and density of the surface layer, respectively.

$$c_w \rho_s z_s \frac{dT_s}{dt} = \phi_{SW_s} - \phi_E + \phi_H + \phi_{LW_{in}} - \phi_{LW_{out}}. \quad (2.10)$$

If the solar radiation data are not available, the GLM compute surface irradiance from a theoretical approximation based on the Bird Clear Sky Model (BCSM) (Bird, 1984) modified for cloud cover. Longwave radiation can be provided as a net flux, an incoming flux, or, if there are no data, then it may be calculated by the model internally from the cloud cover fraction and air temperature. Still, if the cloud data are also not available, the model will compare the measured and theoretical clear-sky solar irradiance (estimated by the BCSM) to approximate the cloud cover fraction.

The penetration depth of shortwave radiation into the lake is wavelength specific and depends on the water clarity via the light extinction coefficient, K_W (m^{-1}). One of the options in GLM is assumes that the photosynthetically active radiation (PAR) fraction of the incoming light is the most penetrative and follows the Beer-Lambert law, where K_W may be set by the user as constant, read in from a time series file, or linked with the water quality model. The other

possibility is adopts a more complete light absorption algorithm that integrates the attenuated light intensity across the bandwidth spectrum.

The model accounts for the surface fluxes of sensible heat and latent heat using commonly adopted bulk aerodynamic formulae. The water column thermal budget may also be affected by heating or cooling from the soil–sediment below. For each layer, the rate of temperature change depends on the temperature gradient and the relative area of the layer volume in contact with bottom sediment.

Inflows have a prescribed composition (temperature, salinity, and scalars), except local runoff, which is assumed to be at air temperature with zero salinity. The river inflows flow through the water column until reaching a layer of the same density, i.e., neutral buoyancy. Then, a new layer is created, with thickness dependent on the inflow volume. Submerged inflows are inserted at the user-specified depth, with zero entrainment, may being mixed with adjacent layers (above or below) depending on the density difference and layer thickness criteria.

The inflow entrainment coefficient, E_{inf} , is computed based on the bottom drag being experienced by the inflowing water, $C_{D_{inf}}$, and the water stability, characterized by the Richardson number, Ri_{inf} . The calculation (equation 2.11) use the approximation given in Imberger and Patterson (1981), as written in Ayala et al. (2014) as

$$E_{inf} = 1.6 \frac{C_{D_{inf}}^{3/2}}{Ri_{inf}}. \quad (2.11)$$

The inflow Richardson number (Ri_{inf}), in turn, is based on the drag coefficient by assuming the velocity and Froude number typically small, and considering the channel geometry (Imberger and Patterson, 1981)

$$Ri_{inf} = \frac{C_{D_{inf}} \left(1 + 0.21 \sqrt{C_{D_{inf}}} \sin \alpha_{inf} \right)}{\sin \alpha_{inf} \tan \Phi_{inf}}, \quad (2.12)$$

where α_{inf} is the stream half-angle assuming an approximate triangular cross section, and Φ_{inf} is the angle of the slope of the inflow thalweg relative to horizontal in the region where it meets the waterbody.

As for the outflows, four options can be included, being withdrawals from a specified depth, adaptive offtake, vertical groundwater seepage, and river outflow-overflow from the surface of the lake. For the first case, the model assumes an algorithm in which the thickness of the withdrawal envelope is dependent on the internal Froude (Fr) and Grashof (Gr) numbers and the parameter R (Fischer et al., 1979; Imberger and Patterson, 1981)

$$Fr = \frac{f_{outf} Q_{outf_x}}{N_{outf} W_{outf} L_{outf}^2} \quad (2.13)$$

$$Gr = \frac{N_{outf}^2 A_{outf}^2}{D_{outf}^2} \quad (2.14)$$

$$R = FrGr^{1/3} \quad (2.15)$$

where W_{outf} , L_{outf} , and A_{outf} are the width, length, and area of the lake at the outlet elevation, N_{outf}^2 is the Brunt-Väisälä frequency, and D_{outf}^2 is the vertical diffusivity averaged over the layers corresponding to the withdrawal thickness, δ_{outf} . The thickness of the withdrawal layer is calculated depending on the value of R (Fischer et al., 1979) such that

$$\delta_{outf} = \begin{cases} 2L_{outf}Gr^{-1/6} & R \leq 1 \\ 2L_{outf}Fr^{1/2} & R > 1 \end{cases} \quad (2.16)$$

The approach for adaptive offtake or selective withdrawal is used for accommodating flexible reservoir withdrawal regimes and their effects on the thermal structure within a reservoir. Seepage of water from the lake can be configured assumed constant or dependent on the overlying lake head, being constrained within the model to ensure no more than 90% of the layer can be reduced in any one time step. In case of the lake volume exceeds the maximum volume, the excess water is assumed to leave the domain as an overflow. The overflow rate is then computed as the sum of the flow over the weir crest and the volume of water exceeding the volume of the domain.

2.3.2 AED - Ecological Module

The Aquatic Ecodynamics (Hipsey et al. (2013); <http://aed.see.uwa.edu.au/research/models/AED/index.html>) is an open-source modeling library for aquatic ecodynamics simulations, with intent to encompassing a diverse range of approaches to the applications, can be linked to numerous physical models, including GLM. This library consists of numerous modules that are designed as individual components, which can be enabled and configured to custom aquatic ecosystem conceptualizations, either simple or complex. When coupled with the hydrodynamic driver, the modules allow for a comprehensive simulation of processes that govern the transportation and fate of water quality attributes.

In general, model components consider the cycling of carbon, nitrogen, phosphorus and silica, as well as components such as dissolved oxygen, organic matter (dissolved and particulate), relevant fluxes at the air-water and sediment-water interface, besides are able to simulate organisms including different functional groups of phytoplankton and zooplankton. Other modules describing pathogens, aqueous geochemistry, bivalves, among others, may also be configured. A general summary of the key modules is presented in Figure 2.2.

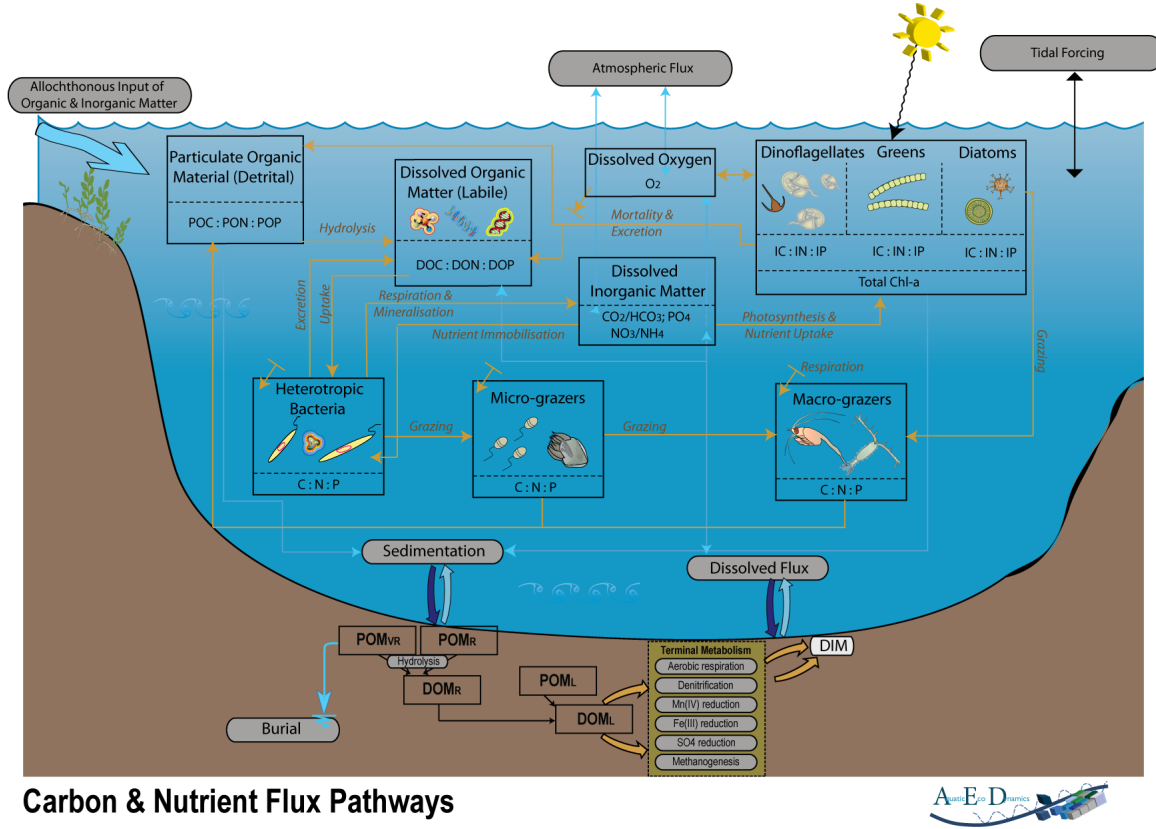


Figure 2.2: AED module conceptual model of carbon and nutrient flux pathways and planktonic groups.
Source: Hipsey et al. (2013).

In relation to the incident shortwave radiation, it is provided by the hydrodynamic driver, where it is used for surface thermodynamics calculations. The light extinction coefficient can be dynamically adjusted according to the concentrations of algae, inorganic and detrital particulates, and dissolved organic carbon in the water column. The simulation of most elements occurs through balance equations that have a similar structure. As an example, the rate of change of dissolved oxygen is presented as

$$\frac{dO_2}{dt} = \pm f_{atm}^{O_2} \pm f_{sed}^{O_2} - \frac{f_{miner}^{DOC}}{\chi_{C:O_2}^{miner}} - \frac{f_{nitrif}}{\chi_{N:O_2}^{nitrif}} + \sum_a^{N_{PHY}} \left(\frac{f_{uptake}^{PHYC_a}}{\chi_{C:O_2}^{PHY}} \right) - \sum_a^{N_{PHY}} \left(\frac{f_{resp}^{PHYC_a}}{\chi_{C:O_2}^{PHY}} \right) - \sum_z \left(\frac{f_{resp}^{ZOO_z}}{\chi_{C:O_2}^{ZOO}} \right) \quad (2.17)$$

Where $f_{atm}^{O_2}$ represents atmospheric exchange; $f_{sed}^{O_2}$ is sediment oxygen demand; $\frac{f_{miner}^{DOC}}{\chi_{C:O_2}^{miner}}$ and $\frac{f_{nitrif}}{\chi_{N:O_2}^{nitrif}}$ are the microbial consumption during the mineralization and nitrification processes, respectively, of organic matter; $\sum_a^{N_{PHY}} \left(\frac{f_{uptake}^{PHYC_a}}{\chi_{C:O_2}^{PHY}} \right)$ is the oxygen production by photosynthesis; $\sum_a^{N_{PHY}} \left(\frac{f_{resp}^{PHYC_a}}{\chi_{C:O_2}^{PHY}} \right)$ and $\sum_z \left(\frac{f_{resp}^{ZOO_z}}{\chi_{C:O_2}^{ZOO}} \right)$ are oxygen consumption by phytoplankton and zooplankton respiration. The sediment oxygen demand flux implemented varies as a function of the overlying water temperature and dissolved oxygen levels. Microbial activity facilitates the breakdown of organic carbon and a stoichiometrically equivalent amount of oxygen is removed. The nitrification process also requires oxygen, depending also of the half-saturation constant for the effect of

oxygen limitation. Photosynthetic oxygen production and respiratory oxygen consumption is summed over the number of simulated phytoplankton groups.

Both the inorganic and organic, and dissolved and particulate forms of carbon, nitrogen and phosphorus are modeled explicitly along the degradation pathway of particulate organic matter to dissolved organic matter and then to dissolved inorganic matter. The decomposition and mineralization processes are temperature dependent and under anaerobic conditions are able to slow down. The nitrogen cycle account the additional processes of denitrification, nitrification and molecular nitrogen fixation. Already the phosphorus cycle also includes adsorption and desorption of phosphate onto suspend solids. The silica cycle comprehend the processes of biological uptake of dissolved form by diatoms, dissolved sediment fluxes and diatom mortality.

The phytoplankton simulation can be performed for several groups and its mass balance is calculated considering nutrient and carbon absorption and losses by excretion, natural mortality, respiration, sedimentation and assimilation by zooplankton. The maximum potential growth rate at 20 °C is multiplied by the limiting factors of luminosity and nutrients. The level of light limitation can be modeled considering whether or not the photoinhibition condition. Under optimum temperature conditions, the maximum productivity of phytoplankton occurs; above this temperature, the productivity reduces until it becomes zero at the maximum temperature supported; and below the standard temperature, productivity follows the Arrhenius equation.

Nutrients absorption can be estimated by considering a constant nutrient to carbon ratio conversion or by taking into account dynamic intracellular stores. For static absorption model, the value of the ratio and a half-saturation constant for the absorption must be determined. For dynamic absorption model, a maximum absorption rate must be determined and the minimum and maximum concentrations in which the carbon and nutrient ratio will vary. Phytoplankton will only absorb phosphorus in its soluble form (dissolved inorganic phosphorus), but for nitrogen it is possible to determine a preference factor between nitrate, ammoniac nitrogen and the potentially labile fraction of dissolved organic nitrogen.

Biomass losses by excretion, natural mortality and respiration are modeled using a single coefficient such as "respiration rate". The metabolic losses related to the organic fractions of phosphorus and nitrogen (particulates and dissolved) are obtained proportionally to the ratios P:C and N:C respectively, multiplied by the mortality and excretion rates that occurred in the time step. The AED also allows setting conditions of limitation for salinity, which if present will influence the respiration rate.

Net zooplankton growth is calculated as a balance between food assimilation and losses from respiration, excretion, predation and mortality. Food assimilation takes into account the maximum potential rate of grazing, assimilation efficiency and temperature and food limitation functions. A constant internal nutrient ratio is assumed for simplicity, and since the various input and output fluxes have variable C:N:P ratios, the excretion of nutrients is dynamically adjusted each timestep. More details about the mass balances and biogeochemical algorithms of the model are found in Hipsey et al. (2013).

3 STUDY AREA

Passaúna reservoir was formed in 1990 by damming the Passaúna river. It is located (Figure 3.1) in the south-west zone of the Curitiba Metropolitan Region (RMC), Paraná state in south Brazil, between the parallels $25^{\circ}26'$ – $25^{\circ}32'$ South and the meridians $49^{\circ}23'$ – $49^{\circ}21'$ West. Its catchment, of about 200 km^2 , is part of the Upper Iguaçu watershed (Dias, 1997; Sauniti et al., 2004). The reservoir is used primarily for public water supply to around 20% of the RMC population, about half a million inhabitants, with a regularized intake flow of $2 \text{ m}^3 \text{ s}^{-1}$ by Sanitation Company of Paraná (SANEPAR, 2013).

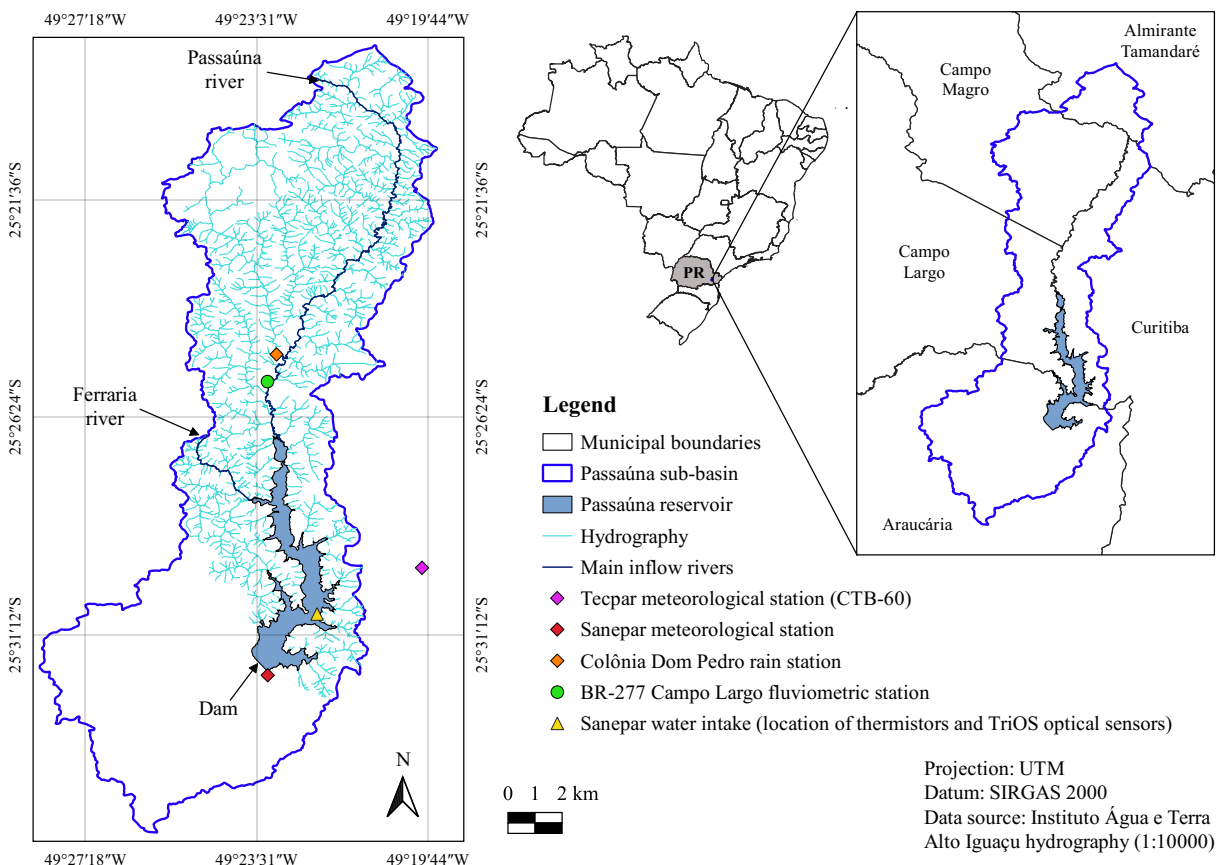


Figure 3.1: Passaúna reservoir location in its sub-basin with the hydrography and the points of the water intake and dam.

Considered the second largest reservoir of the RMC, the Passaúna has 48 hm^3 of useful volume and 59 hm^3 of total volume (SANEPAR, 2013). The reservoir surface area is approximately 9 km^2 , the maximum and mean depths are 16 m and 6.5 m, respectively. The spillway crest elevation is 887.2 m and the estimated residence time is of 292 days (Carneiro et al., 2016). The reservoir's bathymetry, obtained by Sotiri (2016) with echo-sounding measurements, is presented in Figure 3.2, where the main tributaries are identified.

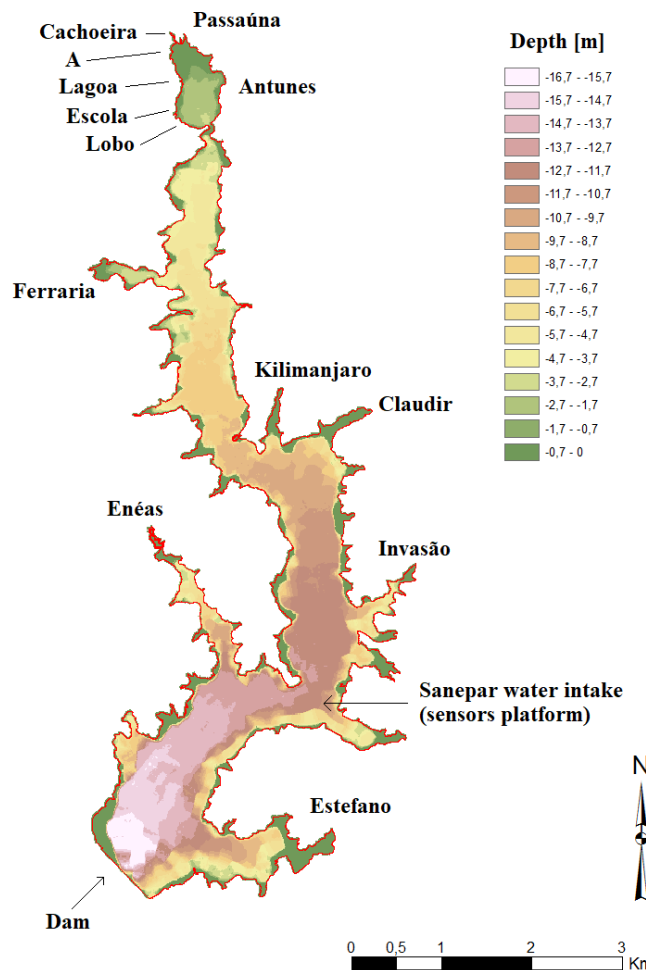


Figure 3.2: Passaúna reservoir bathymetry and main inflows.
Source: Adapted from Sotiri (2016).

In terms of inflow, the largest contribution comes from Passaúna river, representing 65.6% of the reservoir main tributaries, since its drainage area is also significant, about 83 km². The other tributaries are described in Table 3.1, along with the results obtained by Veiga and Dziedzic (2010) for total annual nitrogen and phosphorus load. It is possible to note the large contribution, besides the Passaúna river (93.904 kg year⁻¹ of total nitrogen and 5.789 kg year⁻¹ of total phosphorus), of the Invasão river in comparison to the others. In addition, approximately 69.7% of the sub-basin area contributes for runoff to the reservoir (Marcon, 2018).

The Table 3.1 also shows the land use and occupation predominant in the region, where it is noted a mixture of urban and rural activities. According to Andreoli et al. (2003) and Carneiro et al. (2016), the watershed of Passaúna reservoir includes paper and fertilizer industries, building companies, slaughter houses, mining, cemeteries and a closed controlled dump site, in addition to farming (mostly corn, beans and potato). The region suffers from anthropogenic actions since the 1980s, with the occurrence of irregular riverbank occupations, the presence of industries and agricultural areas without adequate management methods (Xavier, 2005). Rauen et al. (2018) point out there are underdeveloped areas in the watershed where unregulated sewage

contamination reportedly occurs due to septic tank effluents and irregular disposal onto the drainage network. However, investments are being made to improve sewage collection, pumping and treatment sin the Upper Iguaçu watershed (Castro et al., 2017).

Table 3.1: Average flow, total nitrogen and total phosphorus loading for the rivers affluent to the Passaúna reservoir.

River	Drainage área [km ²]	Average flow [m ³ s ⁻¹]	Main land use	Nitrogen mass flow [kg year ⁻¹]	Phosphorus mass flow [kg year ⁻¹]
Passaúna	82.73	1.36	Urban / agriculture	93,904	5,789
Ferraria	11.07	0.18	Agriculture	7,396	861
Cachoeira	10.82	0.18	Urban / agriculture	19,157	2,038
Estefano	5.90	0.09	Forest / agriculture	1,794	143
Antunes	4.01	0.07	Forest / agriculture	1,905	71
A	3.14	0.05	Agriculture	1,635	162
Enéas	2.53	0.04	Agriculture	999	49
Claudir	2.04	0.03	Urban / agriculture	108	23
Kilimanjaro	1.16	0.02	Forest / agriculture	601	18
Lobo	0.94	0.01	Urban / agriculture	768	18
Lagoa	0.67	0.01	Agriculture	784	112
Invasão	0.60	0.01	Urban / agriculture	8,060	772
Escola	0.42	0.01	Urban / agriculture	284	108

Source: Adapted from Veiga and Dziedzic (2010).

The land use in the sub-basin also entails in the increment of sediment entering into the reservoir. Sauniti et al. (2004), in a study about Passaúna reservoir sedimentation, verified rates of sedimentation between 0.66 and 3.04 cm per year for the period analyzed (1990 to 2002). The results showed layers of sedimentation in different regions within the reservoir, with thicknesses varying from 8.0 cm to 36.5 cm. Sotiri (2016) analyzed bottom sediment samples of Passaúna reservoir, verifying that the predominant composition is of fine grain. The author has also obtained a sediment thickness map, where it was observed values thickness higher in the deepest part near the dam, up to 1.3 m. In this sense, the State Environmental Protection Area (*Área de Proteção Ambiental - APA*) of Passaúna represents an important instrument of control and limit land use on the watershed and, hence, of protection the reservoir water quality. This APA was established in 1991 followed by Ecological Economic Zoning in 2001, covering 16.000 ha of the reservoir drainage area, from the sources of the Passaúna River to the reservoir dam (Tamanini, 2008).

According to Environmental Institute of Paraná (*Instituto Ambiental do Paraná - IAP* (2017)), the reservoir is classified as warm monomictic, presenting mixed water column during the winter and thermal stratification in the warmer months. Figure 3.3 shows the temperature and dissolved oxygen (DO) profiles measured by the IAP at the Dam Station (25°31'7.7"S and 49°23'2.03"W), the lentic, wide and deep region of the reservoir, from 2005 to 2013. It is possible to observe a oxygen depletion in the deeper layers, leading to anoxia, and high values in the surface, due to the reaeration process and, possibly, the phytoplankton production in the euphotic zone.

IAP (2017) monitoring results demonstrated that the reservoir has oligotrophic characteristics, but sometimes was classified as mesotrophic. Overall, it showed good water transparency

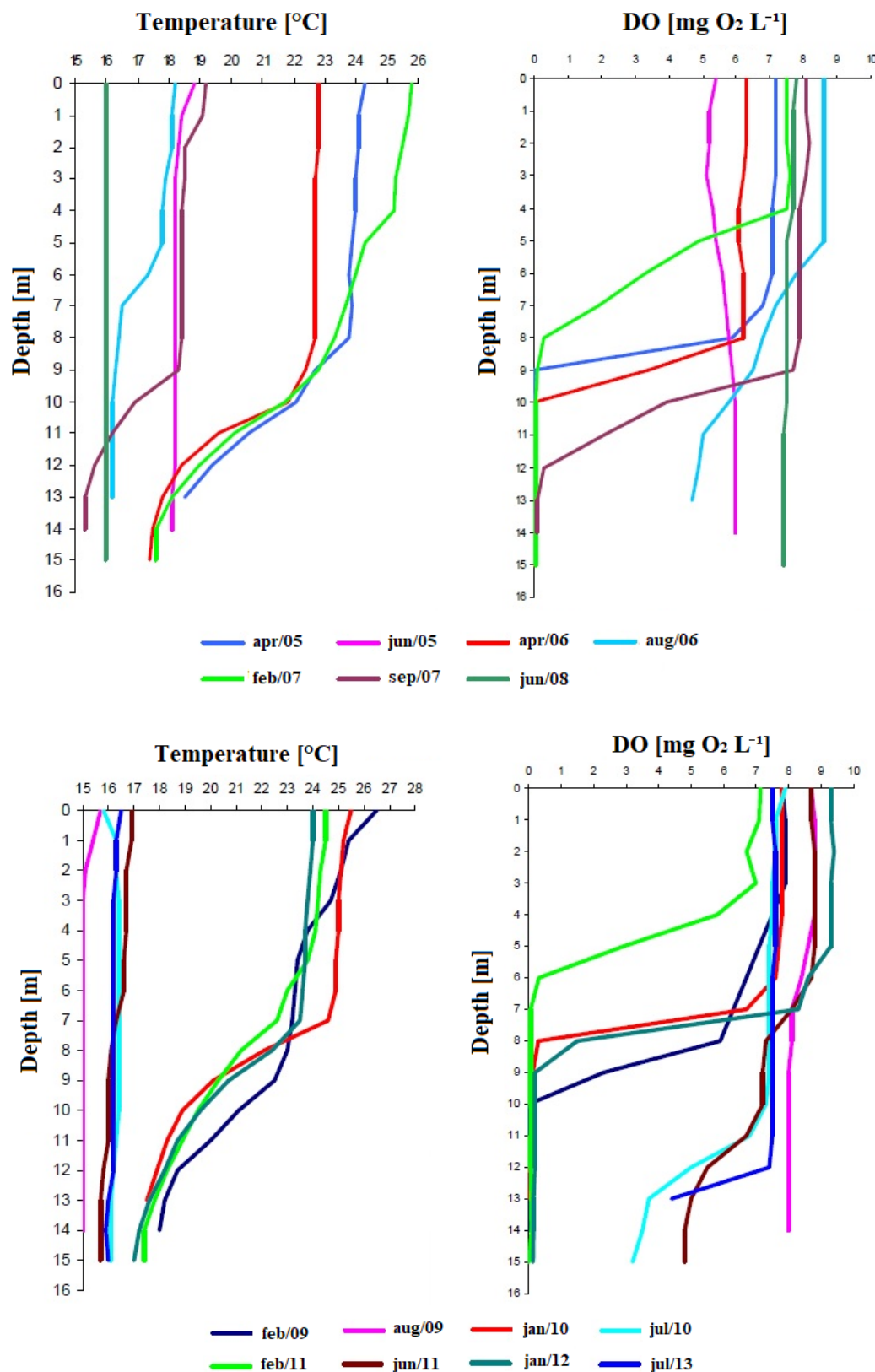


Figure 3.3: Temperature and dissolved oxygen (DO) profiles in the Passaúna reservoir between 2005 and 2013.
Source: Environmental Institute of Paraná - IAP (2017).

conditions, low to moderate nutrient concentrations (nitrogen and phosphorus) and low levels of organic matter. The pH values remained within the limits established by current legislation (between 6 and 9) for almost the entire study period (1999 to 2013). In relation to the phytoplankton, a small concentration of cyanobacteria cells (blue algae) was detected during the monitored period, with values below $10\,000\text{ cells mL}^{-1}$, and the most frequent species were not considered potentially toxic. Also, the predominant classification was presenting as moderately degraded, within limits considered acceptable to be used as source of supply.

Dias (1997) had already classified the Passaúna reservoir as a warm monomictic lake, observing that the thermal stratification is accompanied by chemical stratification and that, during this period, there is a strong oxygen depletion due to autochthonous loads from the flooded vegetation in the reservoir formation. It also found that the high residence time and the low depths minimize the purification capacity of the pollutant loads coming from the drainage basin, with negative consequences for the water quality. However, the reservoir dendritic configuration favors the central body protection against these loads, considering that the flooded littoral areas accumulate the organic matter and absorb nutrients, mainly by the macrophytes existing in these places.

In a recent study, Rauen et al. (2018) evaluated the state of reservoir water quality and temporal trend of chronic anthropogenic impacts, using indicators and indexes in an integrated physical-chemical-biological approach. They reported that, for most samples, the reservoir water quality was mostly good, with a moderate improvement detected for the 2004 – 2014 period. In terms of macroinvertebrate diversity, the reservoir was found to be moderately impacted, probably caused by domestic and agricultural effluent pollution impacts. The trophic state oscillated between mesotrophic and oligotrophic. Thereby, it is important control the potentially detrimental activities within the basin to reduce impact risks and to help promoting water security in the region.

3.1 PREVIOUS STUDIES IN PASSAÚNA RESERVOIR

The construction of the Passaúna reservoir for the public supply purpose led to the realization, by the IAP in Brazil Germany Technical Cooperation Agreement, of the *Estudo de Caso do Reservatório do Passaúna*. The technical reports (SUREHMA, 1990 and 1991 apud Dias, 1997) were prepared by a multidisciplinary team, focusing on the integrated study of the Passaúna watershed. Subsequently, Dias (1997) carried out a survey of macro-scale information in the basin, in addition to performing the reservoir limnological study and its main tributary rivers. Smaha and Gobbi (2003) developed and implemented a one-dimensional model to simulate reservoir eutrophication, with emphasis on the chlorophyll-*a* concentration. It was possible to conclude that chlorophyll-*a* concentrations were high, given the load of the tributaries.

Xavier (2005) evaluated the influence of land use and occupation, and geomorphological characteristics on the reservoir water quality. Indicated that the contributing rivers are quite

impacted, and that the Passaúna reservoir can be classified as mesotrophic. Veiga and Dziedzic (2010) estimated the reservoir nutrient loads using the FLUX software, based on measured data and considering the predominant soil use for the export coefficient calculation. Salgado and Rauen (2014) made the physical characterization of the reservoir sediments by determining the grain sizes distribution and density. Siqueira (2014) sought to estimate the reservoir sediment input, creating different scenarios as a function of the sediment rating curve, reaching a variation of 0.104 hm³ and 0.155 hm³ of mean volume.

Costa et al. (2015) made a diagnosis of the reservoir water quality including its risk of eutrophication, based on a historical series of data and new measurements. The results showed that the reservoir had a good water quality and that, in 84% of the data, the reservoir trophic state oscillated between oligotrophic and mesotrophic, detecting the risk of eutrophy in only 8% of the samples. Carneiro et al. (2016) studied the water balance and phosphorus balance in the Passaúna reservoir for the years 2010 to 2012, evaluating the exchange of this nutrient between the water-sediment interface. The phosphorus loads in the reservoir were predominantly derived from the region tributaries, and there was also an increase in the contribution through groundwater inputs. Furthermore, it was observed that, on average, 30% of the phosphorus entering the reservoir is retained in the sediments and if this charge returns to the water, it may lead to the depletion of the dissolved oxygen.

Godoy (2017) sought to evaluate the water quality dynamics in the Passaúna reservoir, along with the characterization of organic matter. The results showed tendencies of higher concentration of autochthonous material in the lacustrine region while the pedogenic material was strongly found in the tributaries and in the reservoir. Also, total phosphorus values were observed above that allowed by the legislation in some sites of the reservoir, even in different climatic and hydrological conditions. Rauen et al. (2018), as already commented, also carried out an evaluation of the quality of the water of the reservoir, but based on historical data using Water Quality Index (WQI) and Trophic State Index (TSI), as well as novel macroinvertebrate data for Shannon-Weaver Index (H'). They also evaluated the level of compliance of water quality parameters with Brazilian regulatory standards.

Polli (2018) performed the modeling of heat transport in three reservoirs, including Passaúna, where the focus was to identify if there are horizontal temperature gradients. The Passaúna results confirmed that the water from inflow was colder than the reservoir. The main temperature differences occurred in depth, with gradients from shallower water to the deepest point. In addition, thermocline depth varied from shallower to deeper water. The author also verified similarity in the results of the physical indices calculated from 1D model data and the measurement values. It concluded, therefore, that it is possible to identify periods of mixing and stratification with simple models, like one-dimensional, and low-time processing.

A recent research program carried out in the reservoir (2015 – 2018) was the SeWaMa (*Innovative Approaches for Future Sediment and Water Management in Brazil*) within the NoPa call (Novas Parcerias, funded by CAPES and DAAD), a partnership between German and

Brazilian universities and sanitation and reservoir management companies. The project involved researchers from different areas studying sedimentation in reservoirs (Zarebska, 2016; Sotiri, 2016), water quality aspects, land use, GHG production and emission (Marcon et al., 2017; Marcon, 2018; Marcon et al., 2019), and suspended solids (Wosiacki, 2017).

Currently, the reservoir is a study environment of MuDak-WRM (2019) (*Multidisciplinary Data Acquisition as Key for a Globally Applicable Water Resource Management*; <https://www.mudak-wrm.kit.edu/>), a Brazil-Germany cooperation too, with the aim of studying optimized alternatives for water resources management. Some of the published works of this project are Kern et al. (2018a,b), Wagner et al. (2018), Krumm et al. (2019), Krumm and Haag (2019a,b), Wagner et al. (2019), Fuchs et al. (2019), Sotiri et al. (2019), and Kern and Schenk (2019).

4 MATERIALS AND METHODS

The GLM-AED (General Lake Model – Aquatic EcoDynamics) 1D coupled model was used in Passaúna reservoir simulation, in order to analyze the performance of one-dimensional modeling in reproducing the physical, chemical, and biological processes of a subtropical water supply reservoir. Firstly, the hydrodynamic simulation was accomplished with GLM (version 3.0.5), for the purpose to capture lake water balance and thermal stratification dynamic. In sequence, the AED (version 1.3.2) library was added to model both chemical and biological components of the lake ecosystem, activating the following modules: oxygen, carbon, nitrogen, phosphorus, organic matter, phytoplankton, and totals.

The modeling period was from August 2017 to February 2019, being chosen to allow comparisons with field data (March 2018 to February 2019), besides being possible to observe the seasonal effects for different seasons of the year. The beginning of the modeling, August 2017, was chosen because it is one of the year months in which the reservoir water column is mixed, due to the colder temperatures, allowing the model to “warm-up” faster. Start the simulation in a period when the waterbody is not thermally stratified also helps to reduce the effects of uncertainties in initial conditions (Soares et al., 2019). Another weighted aspect was the reservoir depth defined in the model. It was decided to carry out two simulations with different depths. In the first, was opted for the reservoir total depth, approximately 17 m. In the other, was used the depth in the intake region, about 12 m, as it is the place where the field measurements, used in the comparison of the modeled results, were made.

GLM-AED model requires a hypsographic curve; an initial profile of temperature and salinity in the water column; hourly meteorological time-series data for surface forcing; daily time series of inflow, its temperature, salinity, and scalars (water quality variables); and daily outflow. Next, such data used in the modeling will be presented. Then, will be described the model setup and the calibration step. Finally, post-processing and analysis.

4.1 METEOROLOGICAL DATA

The meteorological dataset used for the work development was obtained from three monitoring stations. Shortwave radiation, air temperature, relative humidity, and wind speed data, from August 1st to May 18th, 2018, were achieved by the CTB-60 solarimetric station of the Paraná Institute of Technology (Tecpar), located 4 km from reservoir water withdrawal. The remainder of these meteorological data, until February 28, 2019, were made available by the Paraná Sanitation Company (Sanepar), with the records of the station installed by them near the reservoir. This configuration was due the fact that Sanepar only has started to be operated on May 14, 2018, with gaps in the first records, however. In relation to Tecpar data, failures were also observed in October (days 1 to 11) and November 2017 (days 7 to 13), and May 2018, from

the 12th. The missing data was completed by filling the first half of the period with data from the same amount of previous days, while the second half considered the subsequent days. In order to justify the data compatibility from the two stations, the correlation coefficient was calculated for the period from May 2018 to February 2019 (Table 4.1), in which both stations had data available. It is observed that, according to the literature, the result for all variables presented a correlation considered strong, that is, above 0.7 (Cohen, 1988; Dancey and Reidy, 2006). In the Appendix A are the graphs referring to this data.

Table 4.1: Correlation coefficient between meteorological data of Tecpar and Sanepar monitoring stations, from May 2018 to February 2019.

Air temperature	Shortwave radiation	Relative humidity	Wind speed
0.94	0.89	0.90	0.73

The climate of the region is humid subtropical, with an average annual temperature of 17 °C, without a well defined dry season and a rainfall index of around 1.500 mm annually (Araucária, 2003). Precipitation data were obtained from Colônia Dom Pedro station (code 02549080), located in Campo Largo (latitude 25°25'01"S and longitude 49°23'05"W) and operated by National Water Agency (ANA). The data were on a daily scale and, to be inserted in the model, were passed to hourly resolution dividing the daily value in 24 hours. The other data previously cited, which were at a higher resolution (Tecpar data every 1 minute and Sanepar data every 10 minutes), were converted to mean hourly data.

Figure 4.1 shows the data used in the modeling, where the average air temperature in the studied period is 19 °C, reaching a maximum of 34 °C at the end of January 2019 and a minimum of 1.7 °C in July 2018. The relative air humidity presented a mean of 79%, remaining most of the time (62%) above this value. During the simulated months, an accumulation of 2878 mm of rainfall was recorded: 807.7 mm in 2017 (August to December), 1571.7 mm in the year 2018, and 498.4 mm in January and February 2019. Regarding the intensity of the wind, the average speed was 1.9 m s⁻¹, with the predominant wind direction being east, southeast, and northeast, as shown in Figure 4.2.

4.2 HYDROLOGICAL DATA

The hydrological data upstream of the reservoir were provided by MuDak-WRM (2019) research project partners, with the calibration of the LARSIM (Large Area Runoff Simulation Model) rainfall-runoff model. The LARSIM model was used to describe continuous runoff processes in Passaúna watershed and its river network, dividing the area of the contributing basin into 64 elements (Figure 4.3). Therefore, were used data from the BR-277 Campo Largo fluvimetric station (code 65021800), located on the Passaúna river about 2.4 km from the reservoir entrance (latitude 25°25'37"S and longitude 49°23'17"W), and operated by National Water Agency (ANA).

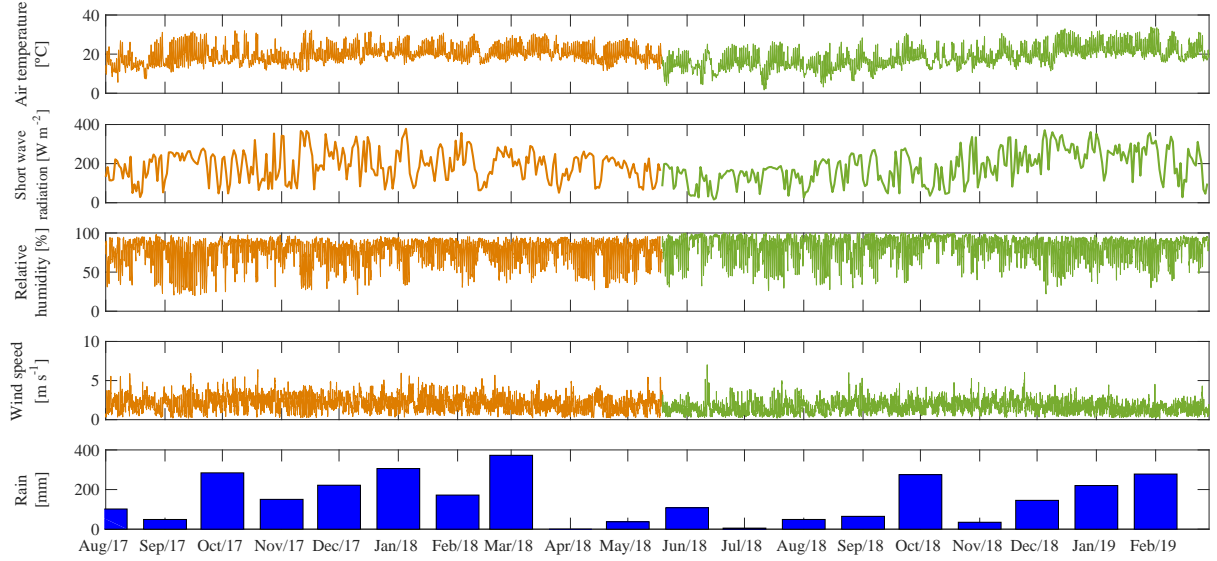


Figure 4.1: Meteorological data from Tecpar (orange line), Sanepar (green line), and Colônia Dom Pedro (blue bars) stations close to the Passaúna reservoir, from August 2017 to February 2019.

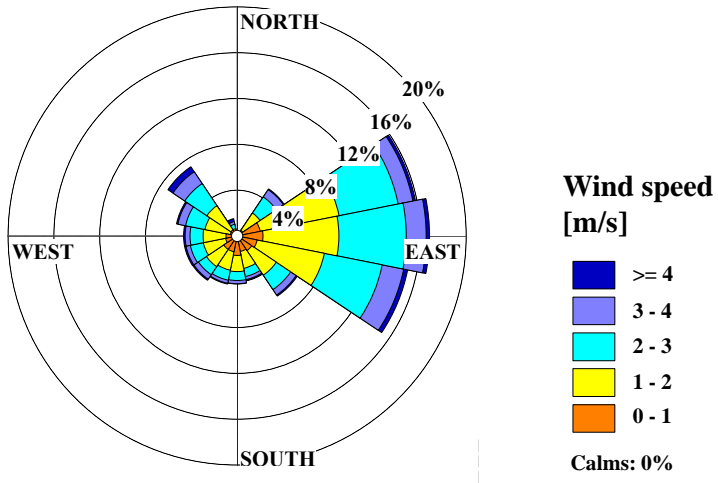


Figure 4.2: Windrose from the Tecpar station data, from August 2017 to February 2019.

From the LARSIM model data, three input inflow files for the GLM-AED were elaborated, divided into: Passaúna river, with data from the 154 station; Ferraria river, with data from 195 station; other streams, with the sum of the flows of the remaining stations. In Figure 4.4 is exhibited the mentioned data, where it is observed an average input contribution of $2.0 \text{ m}^3 \text{ s}^{-1}$ from the Passaúna river, $0.1 \text{ m}^3 \text{ s}^{-1}$ from the Ferraria river, $0.4 \text{ m}^3 \text{ s}^{-1}$ from other streams, and an average of the total flow of $2.5 \text{ m}^3 \text{ s}^{-1}$. The maximum flow rate was $10.9 \text{ m}^3 \text{ s}^{-1}$ from the Passaúna river and the minimum was $0.03 \text{ m}^3 \text{ s}^{-1}$ from the Ferraria river.

The outflows from the Sanepar withdrawal, the spillway, and bottom outlet of the reservoir, provided by the Sanitation Company, were corrected by members of the MuDak project, to be used in the modeling. The reason for the data adjustment was inconsistencies in the water balance, with the lack of water in the reservoir. This fact may have been caused by inaccuracies in outflow measurements, the option considered, or even errors in the Passaúna water level

measurements. The new outflow series, shown in the Figure 4.5, has an average flow equal to $2.5 \text{ m}^3 \text{ s}^{-1}$, half the average value of Sanepar's data; the maximum was $11.9 \text{ m}^3 \text{ s}^{-1}$ and the minimum equal to zero.

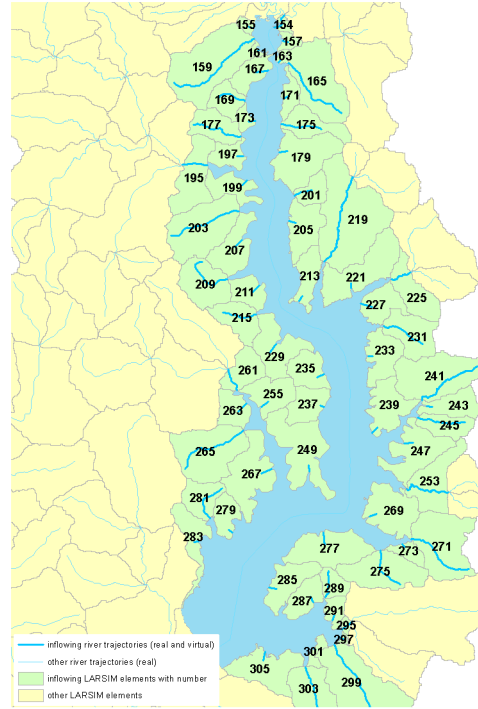


Figure 4.3: Location of the Passaúna reservoir inflows in LARSIM model.
Source: MuDak-WRM (2019).

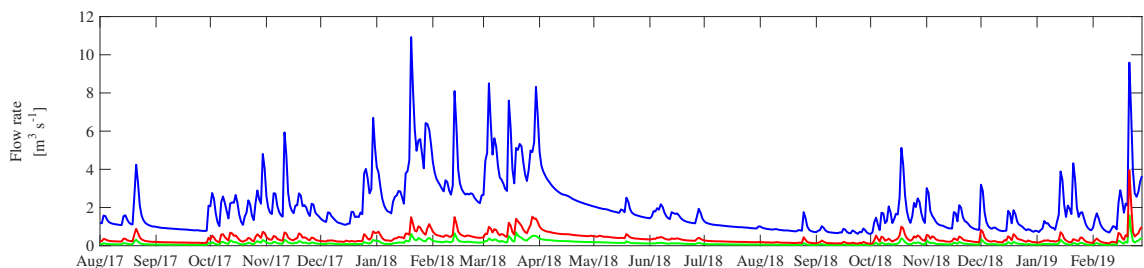


Figure 4.4: Inflow data of Passaúna reservoir, from Passaúna river (blue line), Ferraria river (green line), and Streams (red line), from August 2017 to February 2019.

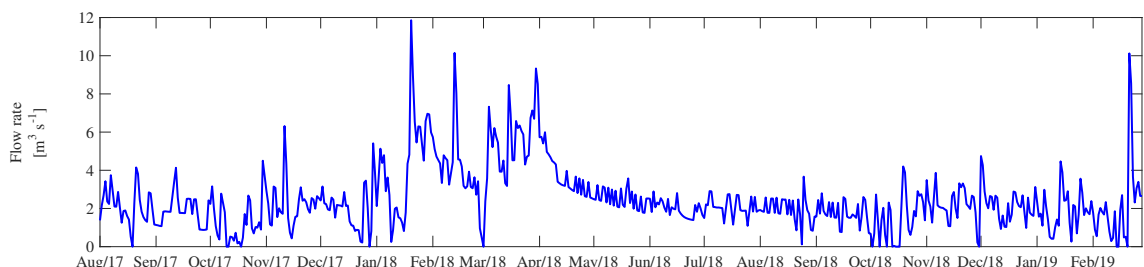


Figure 4.5: Outflow series of Passaúna reservoir calculated by members of the MuDak project, from August 2017 to February 2019.

4.3 WATER QUALITY DATA

In the model, inflows have a prescribed composition: temperature, salinity, and other dissolved substances. Temperature data upstream of the reservoir was obtained by MuDak-WRM (2019) research project partners, along with the inflow data of LARSIM model. Thus, in the Passaúna river input file, were inserted temperature values from the 154 station; in the Ferraria river, the 195 station data; and for the other streams, the temperature average of the remaining stations were calculated. The values of dissolved oxygen (DO) were obtained with the records, every 5 minutes, of a miniDOT Oxygen Logger (Precision Measurement Engineering brand) installed in the Passaúna river, also within the scope of the MuDak-WRM. The measurements took place from March 2018, to fill the data of the previous period (August 2017 to February 2018) the values of the corresponding months of the year 2018 were copied.

In Figure 4.6 the two mentioned parameters (temperature and DO) are shown, noting that the DO values (first graph) were entered equally in the three inflow files. The other graphs show the temperature values at each specified inlet and the respective oxygen saturation concentration. It is verified that the Passaúna river temperature ranged from 13.1 °C to 24.2 °C, with an average value of 18.6 °C. The values for the Ferraria river were 23.0 °C of maximum, 12.7 °C of minimum and an average of 18.0 °C, and for the other streams equal to 23.4 °C, 11.5 °C and 18.5 °C, respectively. The DO presented an average of 5.8 mg O₂ L⁻¹, reaching a maximum of 7.7 mg O₂ L⁻¹ and a sharp decline of 1.4 mg O₂ L⁻¹ in July 2018. The oxygen saturation concentration values for the three inflows were very similar, with an average of 9.4±0.1 mg O₂ L⁻¹.

The other water quality parameters provided in the inputs were phytoplankton concentration, dissolved inorganic carbon (DIC), pH, ammonia (NH₄⁺), nitrate (NO₃⁻), phosphate (PO₄³⁻), in addition to the particulate and dissolved fractions of the organic components of carbon (POC and DOC), nitrogen (PON and DON), and phosphorus (POP and DOP). For this purpose, were used data from laboratory analyzes of samples collected in the field, on a few days between February 2018 and April 2019, within the scope of the MuDak project. Figure 4.7 shows concentration values of NH₄⁺, NO₃⁻, PO₄³⁻, nitrogen and phosphorus total, dissolved organic carbon (DOC) and chlorophyll-a, in a reservoir inflow point (Passaúna river). At some dates, the laboratory analyzes did not reach conclusive results. The May 2018 and April 2019 phosphate samples showed very low values, less than the limit of detection (LD) or limit of quantification (LQ). In the chlorophyll-a case, due to an error in the equipment that performs the sample readings, the results for the months of October, November, and December 2018 were not processed.

According to Resolution nº 04/2013, of the Committee of the Alto Iguaçu Basin and Upper Ribeira Affluents (COALIAR., 2013), the Passaúna river is classified into two classes, according to National Environmental Council (CONAMA., 2005) Resolution 357/2005. From its source to the Sanepar dam it is class 2; from the dam to its mouth is categorized as class 3. The place where sampling was performed is therefore considered class 2. It is observed that nitrate concentrations are below the permitted maximum limit (10.0 mg N L⁻¹) by legislation. The

maximum value of total ammonia nitrogen depends on the water pH, according to the resolution. The highest measured ammonia concentration was 0.5 mg N L^{-1} , in February 2019. This value, stricter limit in the entire pH range, corresponds to the maximum allowed by legislation when the pH is above 8.5. In some pH measurements in the Passaúna river, carried out by two sensors (Horiba and Aquaread) between August 2018 and February 2019, a maximum value of 7.79 was verified.

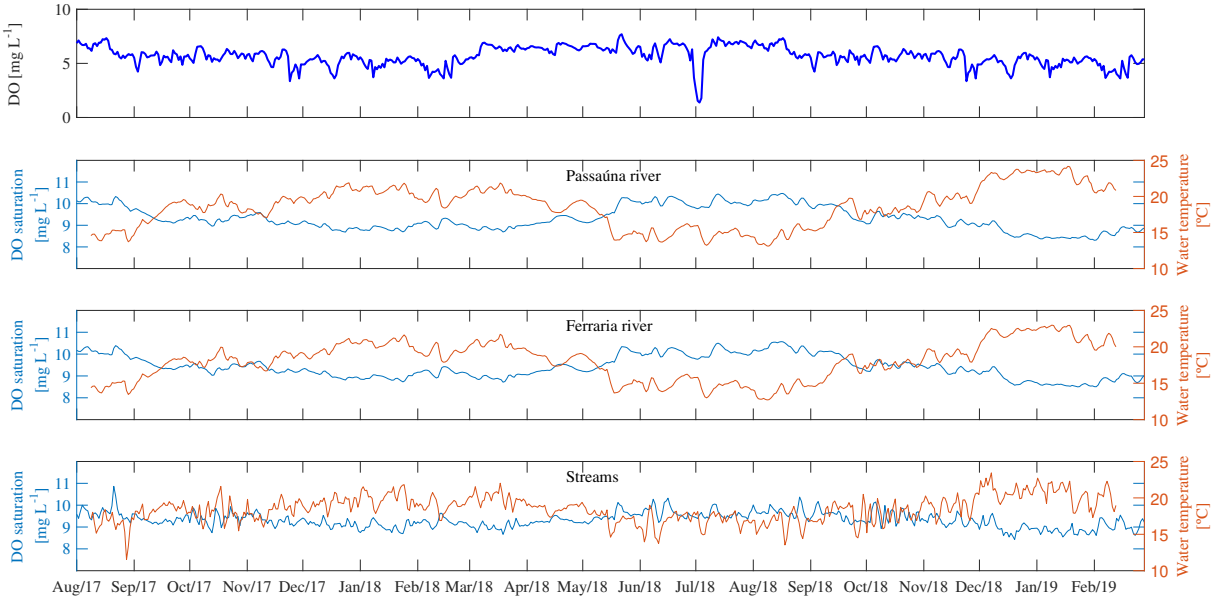


Figure 4.6: Dissolved oxygen (DO) concentration, DO saturation concentration, and water temperature in the Passaúna reservoir inflows (Passaúna river, Ferraria river, and streams), from August 2017 to February 2019.

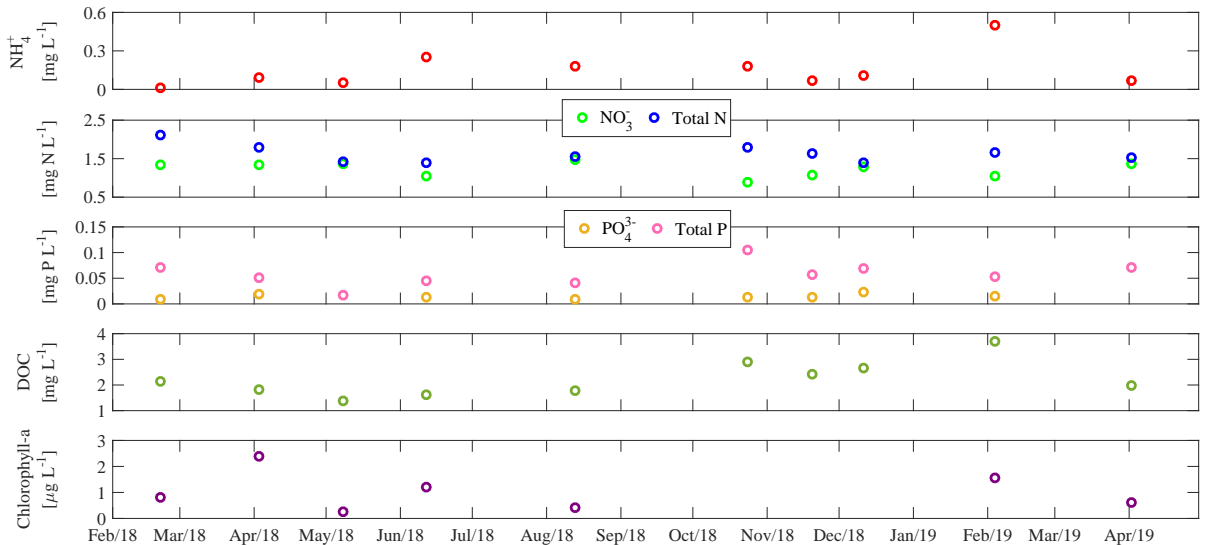


Figure 4.7: Nitrate (NO_3^-), ammonia (NH_4^+), total nitrogen, phosphate (PO_4^{3-}), total phosphorus, dissolved organic carbon (DOC) and chlorophyll-a data in Passaúna river, from February 2018 to April 2019.

Regarding phosphorus, the resolution establishes limits only for the total fraction, with the maximum allowed equal to 0.03 mg P L^{-1} for lentic environments, and 0.05 mg P L^{-1} for

direct tributaries of the lentic environment. It can be seen, thus, that in most of the monitored period, concentrations were above this limit, reaching 0.11 mg PL^{-1} in October 2018. In terms of chlorophyll-*a*, the laboratory analyzes results showed values below the maximum allowed for class 2 ($30 \mu\text{g L}^{-1}$) and even for class 1 ($10 \mu\text{g L}^{-1}$). As for DO, the CONAMA Resolution determines that in any class 2 freshwater sample the concentration cannot be less than $5.0 \text{ mg O}_2 \text{ L}^{-1}$. Nevertheless, in the data recorded by the miniDOT sensor in the Passaúna river, values occurred below this limit.

As the field campaigns mentioned were not carried out in all months of the simulated period, interpolations and extrapolations were made with the laboratory analysis data to obtain a complete time series of model forcing input. Firstly, the load at each inflow was calculated, from concentration (laboratory procedure) and flow (LARSIM model) measured on the day. In the months when there were no sample collections in the reservoir, the load was calculated by averaging the values obtained on the previous and subsequent dates. Then, the concentrations in each river were recalculated, using the average monthly flow in the months without measured data. As the measurements took place only from February 2018, the data from the previous period, since August 2017, were inserted by repeating the values of the respective month of the year 2018. Furthermore, the water quality data were kept constant throughout each month for inserted into the model inflows files. In the pH case, a constant value of 7.4 was inserted for the entire simulation period, based on the average of some measurements at the inflow point, in 2018 and 2019. The constant value was chosen because there were only a few days of measurement (five) and the variation in the values was 0.31 (standard deviation). Regarding dissolved inorganic carbon, as there was no information, a constant value (1 mg L^{-1}) was used.

The values of particulate organic carbon (POC) were inserted equally to measurements of dissolved (DOC). The same procedure occurred for nitrogen and phosphorus organic, and in the case of nitrogen, the organic portion was calculated by subtracting the ammonia and nitrate concentrations from the total nitrogen. For phosphorus, the calculation was also made by the difference of the inorganic portion, that is, the phosphate, of the total. The fractions proportion of particulate and dissolved organic matter in the model input file was then changed in the calibration step, reaching a result of 70% corresponding to the particulate portion and 30% dissolved. Moreover, phytoplankton concentration data were provided at the reservoir inlets. Such values were achieved from chlorophyll-*a* data of the field samples analysis, using the carbon to chlorophyll ratio equal 50 mg C/mg Chla for the conversion, based on the range of 40 to 90 mg C/mg Chla by AED manual (Hipsey et al., 2013). The extrapolation procedure for the months in which there were no measurements was the same previously mentioned for the other variables, based on the load calculation.

4.4 MODEL SETUP

4.4.1 Hydrodynamic Module

The configuration of the GLM-AED model started with the organization of the input files. The time series of meteorological data (air temperature, radiation, wind speed, relative humidity and precipitation) were converted to mean hourly data. The reservoir hydrological data (inflows and outflows), as well as the prescribed composition of the inflows (temperature, salinity, and scalars), were inserted with daily temporal resolution. As there was no data available of longwave radiation and cloud cover at the chosen weather stations, the `rad_mode` setting 3 was defined. In this way, the model first estimates the cloud cover fraction, comparing the solar irradiance measured and the potential clear-sky, approximated by the model Bird Clear Sky Model (BCSM) (Bird, 1984). It then calculates the longwave radiation from the air temperature and cloud cover fraction determined.

The hypsographic curve (elevation-area-volume) of the Passaúna reservoir (Figure 4.8) was obtained from multibeam sonar measurements made by MuDak-WRM (2019) project partners. The initial elevation is 869.64 masl, rising to 887.3 masl in the area corresponding to approximately 8.5 km^2 . For the simulation with 12 m depth configuration, the elevation of the bottom-most point of the reservoir has been changed to 875.3 masl. Regarding the initial depth of the reservoir, in the simulation of the total lake depth, 17.41 m was defined, based on the water elevation (887.05 masl) on August 1, 2018, when the simulation starts. In the simulation considering the intake facility region, 12.0 m was established because it was the average value found in the CTD (conductivity, temperature and depth) probe depth record, at this location.

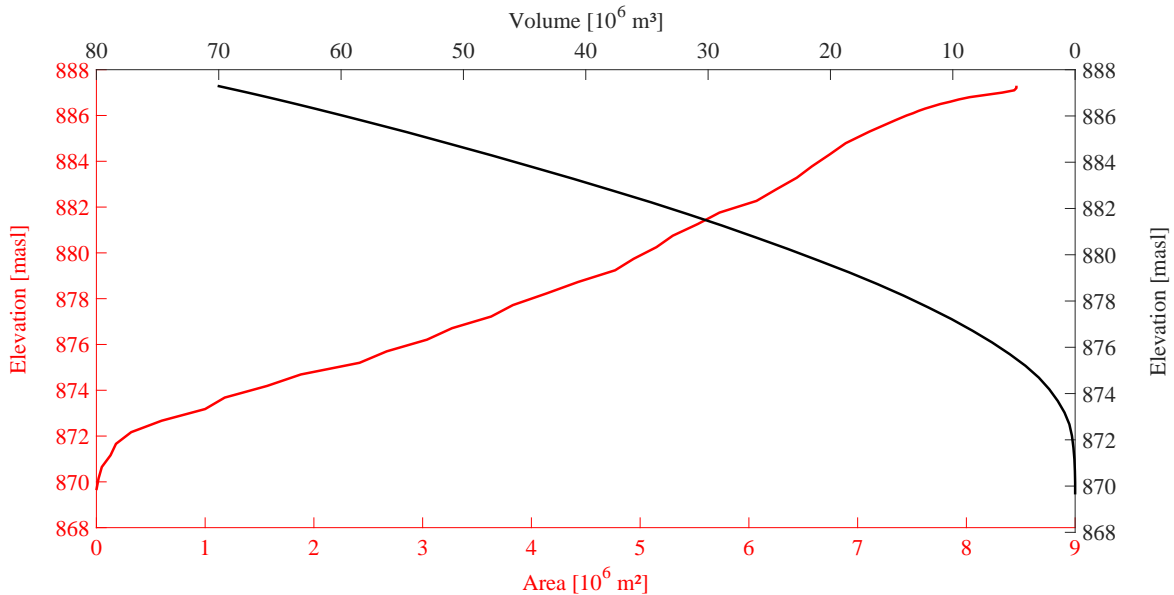


Figure 4.8: Hypsographic curve (elevation-area-volume) of Passaúna reservoir.

The initial condition of null salinity was assumed, as well as for the tributaries, because study site is a freshwater ecosystem and thus the effect of the salt concentration on water density being negligible compared to that of temperature. The initial temperature profile was established as 16 °C constant throughout the depth. This value was based on the average water temperature measured in the reservoir in August 2018. The measurements, between March 2018 and February 2019, were made by thermistors installed near the Sanepar intake, fixed to a rope with weight on the bottom and a buoy submerged on the surface, at depths of 1 m to 11 m relative to the water surface, since the maximum depth in this reservoir region is around 12 m. The Minilog-II-T produced by Vemco have an accuracy of ±0.1 °C and a resolution of 0.01 °C, with temperature recording every 1 minute.

Manual trial-and-error calibration was adopted, based on the graphical comparison of modeled and observed water level and temperature, aiming to minimize their discrepancies with the quantification of the errors. The level measurement data used were those of Sanepar. For the temperature comparison, the thermistors records, previously mentioned, were used. It is noteworthy that the temperature model results used were of layers as from the surface, since the most superficial layer was the thermistors reference, as they were attached to a buoy submerged on the surface. Model performance was assessed by Pearson's correlation coefficient (r), the mean absolute error (MAE) and root mean square error (RMSE). Equations 4.1, 4.2 and 4.3 presents the r , MAE and RMSE calculation, respectively. The N is the number of observations, O_i and P_i , the “ith” observed and model predicted data, \bar{O} and \bar{P} are the mean data.

$$r = \frac{\sum_{i=1}^N (O_i - \bar{O})(P_i - \bar{P})}{\sqrt{\sum_{i=1}^N (O_i - \bar{O})^2 \sum_{i=1}^N (P_i - \bar{P})^2}} \quad (4.1)$$

$$MAE = \frac{1}{N} \sum_{i=1}^N |P_i - O_i| \quad (4.2)$$

$$RMSE = \sqrt{\frac{1}{N} \sum_{i=1}^N (P_i - O_i)^2} \quad (4.3)$$

The light attenuation coefficient defined (0.67 m^{-1}) was the average of the values calculated according to Poole and Atkins (1929), using Secchi disk depths measured at the reservoir intake point. Such measurements were performed between April and December 2018, ranging from 1.95 m to 3.05 m. The minimum and maximum thicknesses of the model layers were set to 0.1 m and 0.5 m, respectively, in order to lead to the highest accuracy in preliminary simulations. Another modified parameter was the river inflow slope, defined as 0.5°. Its adjustment is necessary to correct the magnitude of momentum and entrainment associated with

plunging inflows (Bruce et al., 2018). For the remaining parameters, including those relating to mixing efficiency, surface heat exchange, among others, were kept the default values (Hipsey et al., 2019). The Table 4.2 summarizes the calibration parameters of the model. Simulation was conducted with an 1 h time step, and the state variables output were processed in the same resolution.

4.4.2 Ecological Module

The model ecological component runs with the same hourly time step of the hydrodynamic one and, as mentioned earlier, the activated AED library modules were oxygen, carbon, nitrogen, phosphorus, organic matter, phytoplankton, and totals. The initial oxygen concentration was set to $7.0 \text{ mg O}_2 \text{ L}^{-1}$, an average value of measurement results on August 1, 2018, by a sensor close to the water surface. This miniDOT Oxygen Logger was installed in the Passaúna reservoir near the Sanepar intake, in two depths (10 m and 0.5 m above bed), taking measurements from April 2018 to February 2019.

The initial condition for ammonia (0.07 mg N L^{-1}) was defined by the average of the concentrations measured at the intake point, in August 2018, by the laboratory analyzes of the field samples. The same procedure occurred for DOC (2.31 mg C L^{-1}), with the same value being attributed to POC. In the case of DON and PON, both equal to 0.12 mg N L^{-1} , the calculation of total nitrogen minus the inorganic portion (ammonia and nitrate) was performed. For nitrate (0.20 mg N L^{-1}), phosphate ($0.001 \text{ mg P L}^{-1}$), POP ($0.006 \text{ mg P L}^{-1}$) and DOP (0.01 mg P L^{-1}), the initial values were adjusted in the model calibration. For DIC, the same concentration of inflows (1.0 mg C L^{-1}) was maintained, and pH (7.59) was assigned the value measured by a Horiba sensor at the reservoir intake point, in August 2018.

The data recorded by the Oxygen Loggers installed in the reservoir, mentioned above, were used to calibrate the ecological module, comparing them with the modeled DO results. As for the other chemical variables, the calibration of the relevant modules was also performed by evaluating the discrepancies between observed and simulated data. Thus, were used data from the analysis of samples collected in the field in the reservoir intake point, obtained under the MuDak project, as well as total nitrogen and phosphorus data measured by Sanepar. For nitrate and chlorophyll-*a* there are also records obtained by the Opus and NanoFlu optical sensors from TriOS (<https://www.trios.de/en/>). These sensors were installed on a platform on the water's surface, next to the Sanepar withdrawal, and has been in operation since early March 2018, measuring data every 15 minutes at a depth of approximately 135 cm. The Opus is a spectral sensor for the online measurement of nitrogen and carbon compounds, with a measurement range of $0 \text{ a } 10 \text{ mg L}^{-1}$ and an accuracy of $\pm(5\% + 0.01)$. NanoFlu fluorometers are instruments used to determine dyes and pigments (such as cyanobacteria, chlorophyll-*a* or colored dissolved organic matter), by measuring fluorescence emission in a range of 0 to 200 mg L^{-1} and with an accuracy of $\pm 5\%$.

Table 4.2: Calibrated physical parameters in GLM-AED modeling of the Passaúna reservoir.

Parameter	Description	Value	Unity	Reference
<i>Model structure</i>				
N_{max}	Maximum layers number	500	-	Hipsey et al. (2019)
ΔV_{min}	Minimum layer volume	0.025	m^3	Hipsey et al. (2019)
Δz_{min}	Minimum layer thickness	0.1	m	Manual calibration
Δz_{max}	Maximum layer thickness	0.5	m	Manual calibration
<i>Mixing</i>				
C_K	Mixing efficiency - convective overturn	0.2	-	Wu (1973)
C_W	Mixing efficiency - wind stirring	0.23	-	Yeates and Imberger (2003)
C_T	Mixing efficiency - unsteady turbulence (acceleration)	0.51	-	Sherman et al. (1978)
C_S	Mixing efficiency - shear production	0.3	-	Spigel et al. (1986)
C_{KH}	Mixing efficiency - Kelvin-Helmholtz turbulent billows	0.3	-	Sherman et al. (1978)
C_{HYP}	Mixing efficiency - hypolimnetic turbulence	0.5	-	Weinstock (1981)
<i>Light</i>				
K_w	Light extinction coefficient	0.67	m^{-1}	Field data
<i>Meteorology</i>				
f_{SW}	Scaling factor to adjust the shortwave radiation data	1.0	-	Hipsey et al. (2019)
f_{RH}	Scaling factor to adjust the relative humidity data	1.0	-	Hipsey et al. (2019)
f_{AT}	Scaling factor to adjust the air temperature data	1.0	-	Hipsey et al. (2019)
f_R	Scaling factor to adjust the rainfall data	1.0	-	Hipsey et al. (2019)
f_U	Scaling factor to adjust the wind speed data	1.0	-	Hipsey et al. (2019)
C_H	Bulk aerodynamic coefficient for sensible heat transfer	0.0013	-	Bueche et al. (2017)
C_E	Bulk aerodynamic coefficient for latent heat transfer	0.0013	-	Bruce et al. (2018)
C_D	Bulk aerodynamic coefficient for transfer of momentum	0.0013	-	Fischer et al. (1979)
<i>Inflow</i>				
f_{inf}	Scaling factor to adjust the provided input data	1.0	-	Hipsey et al. (2019)
α_{inf}	Stream half-angle	82.4°	Degrees	Field data
Φ_{inf}	Bottom slope angle	0.5°	Degrees	Manual calibration
$C_{D_{inf}}$	Stream-bed drag coefficient	0.016	-	Hipsey et al. (2019)
<i>Outflow</i>				
f_{outf}	Scaling factor to adjust the outflow data	1.0	-	Hipsey et al. (2019)

The calibration approach had different focuses depending on each variable. In oxygen case, as it was available continuous field data in several water depths, was tried to adjust its dynamics and magnitude. The importance of this is because the DO exerts great influence on the processes of the other water quality parameters, such as nitrification, organic matter mineralization, among others, in addition to being essential for the survival of aquatic organisms. As for chemical substances, due to the restriction of measured data, it was prioritized to adjust the order of magnitude. Even for parameters with continuous sensor records, little correlation was found in comparison to laboratory analyzes, that is, without enough information to represent the dynamics of the variables in the reservoir.

Figure 4.9 shows the flowchart of the calibration steps. In the configuration file referring to the chemical parameters (oxygen, nitrogen, phosphorus, and organic matter), the average of the range values described in the AED manual (Hipsey et al., 2013) was initially inserted. In the phytoplankton module, it was chosen to model only 1 group that would represent the set of photosynthetic microorganisms present in the reservoir, leaving the default values in the configuration file, at the beginning. After a first test simulation (Figure 4.10), it was observed the

need to change the internal concentration dynamics of phytoplankton nitrogen and phosphorus to a fixed value, adjusting such concentrations.

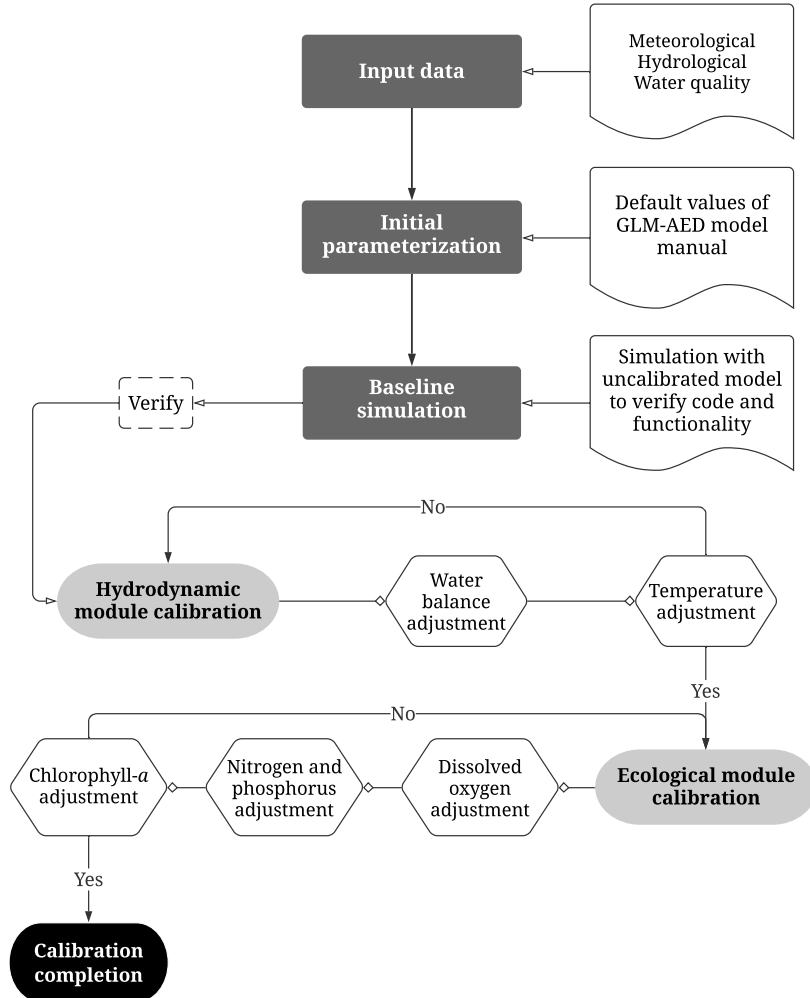


Figure 4.9: Flowchart of the model calibration steps.

In order to refine the nitrate results, it was necessary to define a very low nitrification rate compared to the literature range, 0.01 to 0.2 (Fenocchi et al., 2019). Simultaneously, the denitrification rate was increased, as the model values were overestimated. To adjust the total phosphorus, the contribution of each component was separately observed (Figure 4.11), verifying that the DOP represented the largest portion and was responsible for the high values, above the measurements. The organic fractions in the inflow files were then modified, leaving 70% for the particulate form and 30% for the dissolved. Subsequently, the decomposition of particulate organic matter (POM) to dissolved was reduced, the sedimentation rate of POM was increased, as well as the initial condition of DOP and POP. Then, the goal was to adjust the chlorophyll-*a* results, changing the phytoplankton growth rate and the carbon to chlorophyll ratio. Finally, the fraction of metabolic loss that is true respiration was reduced with the view to regulate the surface

DO concentration. Tables 4.3 and 4.4 summarize the model calibration parameters relating to chemical variables and phytoplankton, respectively.

4.5 POST PROCESSING AND ANALYSIS

For the purpose of verifying the stability and intensity of reservoir stratification, some physical indices were calculated (Schmidt Stability, Wedderburn Number, Lake Number, and Brunt-Väisälä Frequency). To do so was used Lake Analyzer, an open-source software developed by Read et al. (2011) for the determination of mixing and stratification indices in lakes and reservoirs. The indices were estimated for both GLM-AED outputs (configurations of 17 m and 12 m deep) and observed thermistor data. The comparison of thermocline depth calculations was included in the analysis as it is a simple, widely-used metric of mixed layer depth.

Regarding reservoir water quality, sought to evaluate the temporal variability, over the simulated period, of waterbody trophic levels in relation to model results of total phosphorus concentrations, chlorophyll-*a*, and the final index calculation (equation 2.8), as established by Lamparelli (2004) (Table 2.1). In the trophic state index, the results corresponding to phosphorus demonstrate the reservoir eutrophication potential, since this nutrient acts as the causative agent of the process. The assessment related to chlorophyll-*a*, in turn, should be understood as a measure of waterbody response to the causative agent, indicating the algae growth level. Thus, the average index includes the cause and effect of the process CETESB (2018).

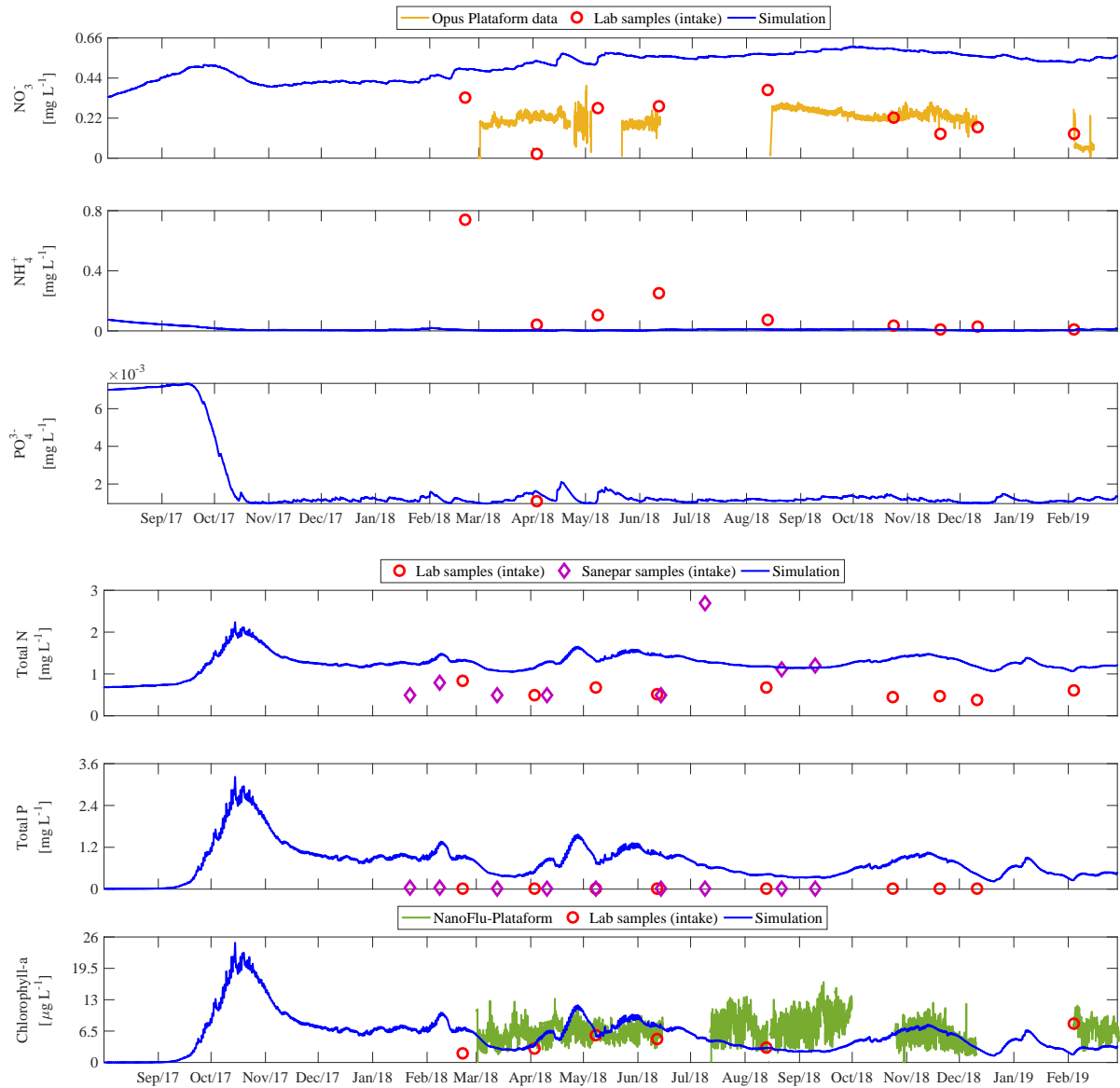


Figure 4.10: Comparison of initial model results of water quality variables with field data obtained by the MuDak project and Sanepar in Passaúna reservoir, from August 2017 to February 2019.

Table 4.3: Calibrated chemical parameters of Passaúna reservoir modeling with GLM-AED 1D model.

Parameter	Description	Value	Unity	Reference
<i>Oxygen</i>				
<i>oxy_initial</i>	Initial DO concentration	218.75	mmol O ₂ m ⁻³	Field data
<i>Fsed_oxy</i>	Sediment DO	-22	mmol O ₂ m ⁻² day ⁻¹	Hipsey et al. (2013)
<i>Ksed_oxy</i>	Half-saturation concentration of oxygen sediment flux	15.6	mmol m ⁻³	Hipsey et al. (2013)
<i>theta_sed_oxy</i>	Arrhenius temperature multiplier for sediment oxygen flux	1.08	-	Hipsey et al. (2013)
<i>oxy_min</i>	Minimum DO concentration	0	mmol O ₂ m ⁻³	Field data
<i>oxy_max</i>	Maximum DO concentration	340	mmol O ₂ m ⁻³	Field data
<i>Carbon</i>				
<i>dic_initial</i>	Initial DIC concentration	83.259	mmol C m ⁻³	Field data
<i>Fsed_dic</i>	Sediment DIC flux	3	mmol C m ⁻² day ⁻¹	Hipsey et al. (2013)
<i>Ksed_dic</i>	Half-saturation oxygen concentration controlling DIC flux	20	mmol m ⁻³	Hipsey et al. (2013)
<i>theta_sed_dic</i>	Arrhenius temperature multiplier for sediment DIC flux	1.08	-	Hipsey et al. (2013)
<i>pH_initial</i>	Initial pH value	7.59	-	Field data
<i>Nitrogen</i>				
<i>amm_initial</i>	Initial NH ₄ ⁺ concentration	5.349	mmol N m ⁻³	Field data
<i>nit_initial</i>	Initial NO ₃ ⁻ concentration	14.285	mmol N m ⁻³	Field data
<i>Rnitrif</i>	Maximum reaction rate of nitrification at 20 °C	0.001	day ⁻¹	Manual calibration
<i>Rdenit</i>	Maximum reaction rate of denitrification at 20 °C	0.1	day ⁻¹	Manual calibration
<i>Knitrif</i>	Half-saturation oxygen concentration for nitrification	78.1	mmol O ₂ m ⁻³	Hipsey et al. (2013)
<i>Kdenit</i>	Half-saturation oxygen concentration for denitrification	14.05	mmol O ₂ m ⁻³	Hipsey et al. (2013)
<i>theta_nitrif</i>	Arrhenius temperature multiplier for nitrification	1.08	-	Hipsey et al. (2013)
<i>theta_denit</i>	Arrhenius temperature multiplier for denitrification	1.05	-	Hipsey et al. (2013)
<i>Fsed_amm</i>	Sediment NH ₄ ⁺ flux	3.885	mmol N m ⁻² day ⁻¹	Hipsey et al. (2013)
<i>Fsed_nit</i>	Sediment NO ₃ ⁻ flux	-14.27	mmol N m ⁻² day ⁻¹	Hipsey et al. (2013)
<i>Ksed_amm</i>	Half-saturation oxygen concentration controlling NH ₄ ⁺ flux	8.58	mmol m ⁻³	Hipsey et al. (2013)
<i>Ksed_nit</i>	Half-saturation oxygen concentration controlling NO ₃ ⁻ flux	8.87	mmol m ⁻³	Hipsey et al. (2013)
<i>theta_sed_amm</i>	Arrhenius temperature multiplier for sediment NH ₄ ⁺ flux	1.08	-	Hipsey et al. (2013)
<i>theta_sed_nit</i>	Arrhenius temperature multiplier for sediment NO ₃ ⁻ flux	1.08	-	Hipsey et al. (2013)
<i>Phosphorus</i>				
<i>frp_initial</i>	Initial PO ₄ ³⁻ concentration	0.036	mmol P m ⁻³	Field data
<i>Fsed_frp</i>	Sediment PO ₄ ³⁻ flux	0.102	mmol P m ⁻² day ⁻¹	Hipsey et al. (2013)
<i>Ksed_frp</i>	Half-saturation oxygen concentration controlling PO ₄ ³⁻ flux	15.6	mmol m ⁻³	Hipsey et al. (2013)
<i>theta_sed_frp</i>	Arrhenius temperature multiplier for sediment PO ₄ ³⁻ flux	1.08	-	Hipsey et al. (2013)
<i>Organic matter</i>				
<i>poc_initial</i>	Initial POC concentration	192.0579	mmol C m ⁻³	Field data
<i>doc_initial</i>	Initial DOC concentration	192.0579	mmol C m ⁻³	Field data
<i>pon_initial</i>	Initial PON concentration	8.3409	mmol N m ⁻³	Field data
<i>don_initial</i>	Initial DON concentration	8.3409	mmol N m ⁻³	Field data
<i>pop_initial</i>	Initial POP concentration	0.2	mmol P m ⁻³	Field data
<i>dop_initial</i>	Initial DOP concentration	0.3228	mmol P m ⁻³	Field data
<i>Rpoc_hydrol</i>	Breakdown rate of POC at 20 °C	0.04	day ⁻¹	Hipsey et al. (2013)
<i>Rdoc_minerl</i>	Mineralisation rate of DOC at 20 °C	0.0265	day ⁻¹	Hipsey et al. (2013)
<i>Rpon_hydrol</i>	Breakdown rate of PON at 20 °C	0.0075	day ⁻¹	Hipsey et al. (2013)
<i>Rdon_minerl</i>	Mineralisation rate of DON at 20 °C	0.0265	day ⁻¹	Hipsey et al. (2013)
<i>Rpop_hydrol</i>	Breakdown rate of POP at 20 °C	0.001	day ⁻¹	Manual calibration
<i>Rdop_minerl</i>	Mineralisation rate of DOP at 20 °C	0.03	day ⁻¹	
<i>theta_hydrol</i>	Arrhenius temperature multiplier for POM breakdown	1.08	-	Hipsey et al. (2013)
<i>theta_minerl</i>	Arrhenius temperature multiplier for DOM mineralisation	1.08	-	Hipsey et al. (2013)
<i>Kpom_hydrol</i>	Half-saturation oxygen concentration for POM breakdown	62.5	mmol O ₂ m ⁻³	Hipsey et al. (2013)
<i>Kdom_minerl</i>	Half-saturation oxygen concentration for DOM mineralisation	62.5	mmol O ₂ m ⁻³	Hipsey et al. (2013)
<i>KeDOM</i>	Light extinction coefficient due to DOM contribution	0.000005	-	Hipsey et al. (2013)
<i>KePOM</i>	Light extinction coefficient due to POM contribution	0.00096	-	Hipsey et al. (2013)
<i>w_pom</i>	Settling rate of POM	-0.35	m day ⁻¹	Manual calibration
<i>Fsed_doc</i>	Sediment DOC flux	2.0	mmol m ⁻² day ⁻¹	Hipsey et al. (2013)
<i>Fsed_don</i>	Sediment DON flux	0.32	mmol m ⁻² day ⁻¹	Hipsey et al. (2013)
<i>Fsed_dop</i>	Sediment DOP flux	0.03	mmol m ⁻² day ⁻¹	Hipsey et al. (2013)
<i>Ksed_dom</i>	Half-saturation oxygen concentration controlling DOM flux	100	mmol m ⁻³	Hipsey et al. (2013)
<i>theta_sed_dom</i>	Arrhenius temperature multiplier for sediment DOM flux	1.08	-	Hipsey et al. (2013)

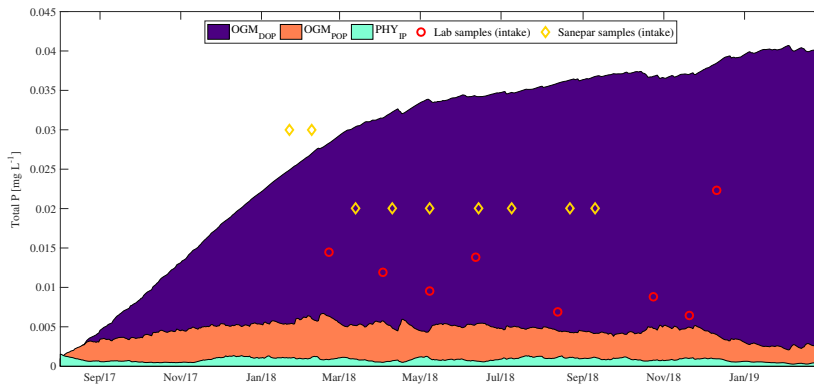


Figure 4.11: Model results of dissolved and particulate organic phosphorus (DOP and POP), and internal phosphorus of phytoplankton, along with total phosphorus field data obtained by the MuDak project and Sanepar in Passaúna reservoir, from August 2017 to February 2019.

Table 4.4: Calibrated phytoplankton parameters in GLM-AED modeling of the Passaúna reservoir.

Parameter	Description	Value	Unity	Reference
<i>General</i>				
<i>p_initial</i>	Initial phytoplankton concentration	10	mmol C m ⁻³	Manual calibration
<i>w_p</i>	Sedimentation rate	0.1	m day ⁻¹	Manual calibration
<i>Xcc</i>	Carbon to chlorophyll ratio	20	mg C/mg Chla	Manual calibration
<i>Growth</i>				
<i>R_growth</i>	Phytoplankton maximum growth rate at 20 °C	2.5	day ⁻¹	Manual calibration
<i>theta_growth</i>	Arrhenius temperature scaling for growth function	1.06	-	Hipsey et al. (2013)
<i>T_std</i>	Standard temperature	15	°C	Manual calibration
<i>T_opt</i>	Optimum temperature	20	°C	Manual calibration
<i>T_max</i>	Maximum temperature	35	°C	Manual calibration
<i>Light</i>				
<i>I_K</i>	Half saturation constant for light limitation of growth	25	micro E m ⁻² s ⁻¹	Hipsey et al. (2013)
<i>KePHY</i>	Specific attenuation coefficient	0.001	mmol C m ⁻³ m ⁻¹	Manual calibration
<i>Respiration</i>				
<i>f_pr</i>	Fraction of primary production lost to exudation	0.005	-	Hipsey et al. (2013)
<i>R_resp</i>	Phytoplankton respiration/metabolic loss rate at 20 °C	0.03	day ⁻¹	Manual calibration
<i>theta_resp</i>	Arrhenius temperature scaling factor for respiration	1.05	-	Hipsey et al. (2013)
<i>k_fres</i>	Fraction of metabolic loss that is true respiration	0.001	-	Manual calibration
<i>k_fdom</i>	Fraction of metabolic loss that is DOM	0.005	-	Manual calibration
<i>Nitrogen</i>				
<i>K_N</i>	Half-saturation concentration of nitrogen	10	mmol N m ⁻³	Manual calibration
<i>X_ncon</i>	Constant internal nitrogen concentration	0.55	mmol N/mmol C	Manual calibration
<i>Phosphorus</i>				
<i>K_P</i>	Half-saturation concentration of phosphorus	0.15	mmol P m ⁻³	Hipsey et al. (2013)
<i>X_pcon</i>	Constant internal phosphorus concentration	0.005	mmol P/mmol C	Manual calibration

5 RESULTS AND DISCUSSION

5.1 HYDRODYNAMIC MODULE PERFORMANCE

5.1.1 Water level

The reservoir water level behavior was best represented in the simulation with the total depth (17 m). In this case, mean absolute error (MAE) was 0.11 m, and root mean square error (RMSE) equal to 0.16 m, as shown in Figure 5.1 (a). For the 12 m simulation, the MAE and RMSE were 4.2 and 3.25 times higher, respectively (Figure 5.1 (c)). Besides, in Figure 5.1 (b, d) are plotted the density scatterplot of the observed and calculated values. It is observed that in the periods when the reservoir is at the highest level (from January to April 2018) the figure shows high probability nuclei (red color), that is, there was a greater agreement between the model results and measurements in the same place. The calculation of the correlation coefficient also demonstrates that the 17 m simulation presented better water level results since the r was 0.95 m. For the 12 m simulation, the value was 0.91 m, indicating a 4.4% lower correlation.

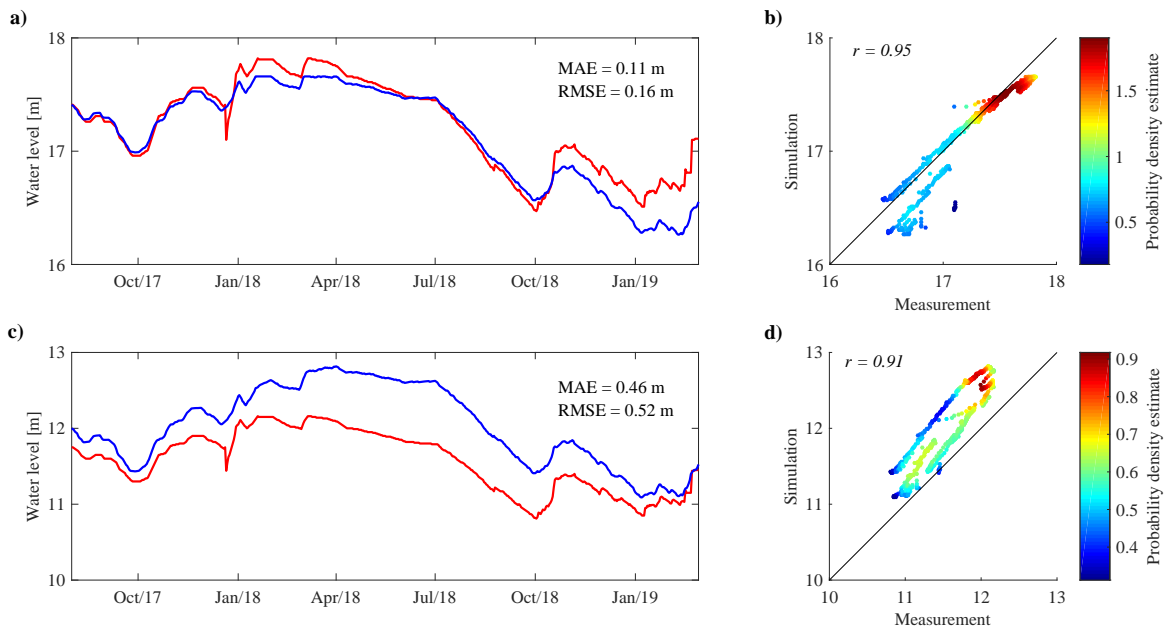


Figure 5.1: Water level in Passaúna reservoir, from August 2017 to February 2019: measured (red line) and simulated (blue line) water level of the 17 m deep (a) and 12 m deep simulation (c) by GLM-AED, with the mean absolute error (MAE) and root mean square error (RMSE); density scatterplot of the 17 m deep (b) and 12 m deep simulation (d), where each point is colored by the spatial density of nearby points, with Pearson's correlation coefficient (r).

It is also verified that the discrepancies in the modeled and observed data reflect errors, predominantly, in the magnitude of the water level, with the biggest differences in the 17 m simulation occurring between January and February 2019. In these months, the model underestimated the reservoir level, reaching a difference of 0.62 m. As for the 12 m simulation,

the model overestimated the level throughout the simulated period, with the biggest difference (0.83 m) at the end of June 2018. Such tendencies to overestimate or underestimate the water level are also represented in the previous correlation graph, where negative and positive bias is observed in the first simulation and only positive in the second, 12 m. Regarding the dynamics of water level variation, in both simulations, the model managed to reproduce in a very similar way to field measurement, i.e., got the phases of rising and falling level right. The maximum elevation of the measured water level was 887.46 masl (17.82 m and 12.16 m) between January and February 2018, reaching a fall to 886.11 masl (16.47 m and 10.81 m) in late September and early October 2018.

5.1.2 Water temperature

The GLM simulations (17 m and 12 m deep) of the thermal structure evolution of the Passaúna reservoir is illustrated in Figure 5.2 (b and c, respectively), along with the contour graph of the lake temperature measured by the thermistors (a). It is noted that the model was able to represent the waterbody thermal dynamics in a similar way to the measurements, considering the period of the thermistors records (March 2018 to February 2019) and the location where they were (12 m deep). However, in the layers closest to the surface, the modeled values were overestimated, reaching a temperature of around 35 °C, while the thermistors measured a maximum value of 29 °C. But, in general, the model managed to reproduce the stratification phenology. In the coldest period, between June and August 2018, the reservoir is mixed, with an average water temperature of 17.0 °C, which was also verified in the measurements. In the other months, the water column is stratified due to the heating of the higher layers.

Figure 5.3 shows the comparison of temperature values measured by thermistors and those obtained by the model, in the 17 m deep simulation, for six depths (1, 3, 5, 7, 9 and 11 m from the surface), along with the density scatterplot and correlation coefficient value. The most evident discrepancy between modeling and observations occurred in the late year 2018 and early 2019, with the model overestimating the temperature close to the surface, as already commented. It is noted that the model started to lose quality in the temperature results due to the uncertainties in the water balance input information, since problems were detected in both in the same period. It is also noticed that the higher layers dynamics in the epilimnion responds to the forcing, that is, to the heat exchanges on the surface. This fact can be confirmed by the value of the correlation coefficient (0.98), the best result among the depths. However, in the deeper layers, from 7 m approximately, the temperature was underestimated, as can also be seen in the negative bias of the density scatterplots. The reason may be associated with the model's difficulty in simulating heat transfer to deep layers. Fenocchi et al. (2017, 2018) point out that 1D models, in general, reproduce the deep mixing in an approximate way.

Was chose to present the graphs only for the 17 m simulation, as the results for the 12 m deep were similar, as can be seen in Figure 5.4, in which the MAE and RMSE are plotted along the reservoir depth for both configurations. The biggest errors occurred for the most superficial

layers, due to the detachment of the modeled results in relation to those observed. The MAE reached a maximum of 1.69°C for the simulation of 17 m deep (red line) and 1.47°C for the 12 m (blue line). The maximum values of the RMSE were 2.28°C and 2.08°C , respectively. The temperature discrepancies reduced between 4 and 6 m and, in the case of the 17 m simulation, for the reservoir bottom layer. The smallest mean absolute errors were 0.66°C for the 17 m depth simulation and 0.62°C for the 12 m; the lowest RMSE was 0.81°C for both.

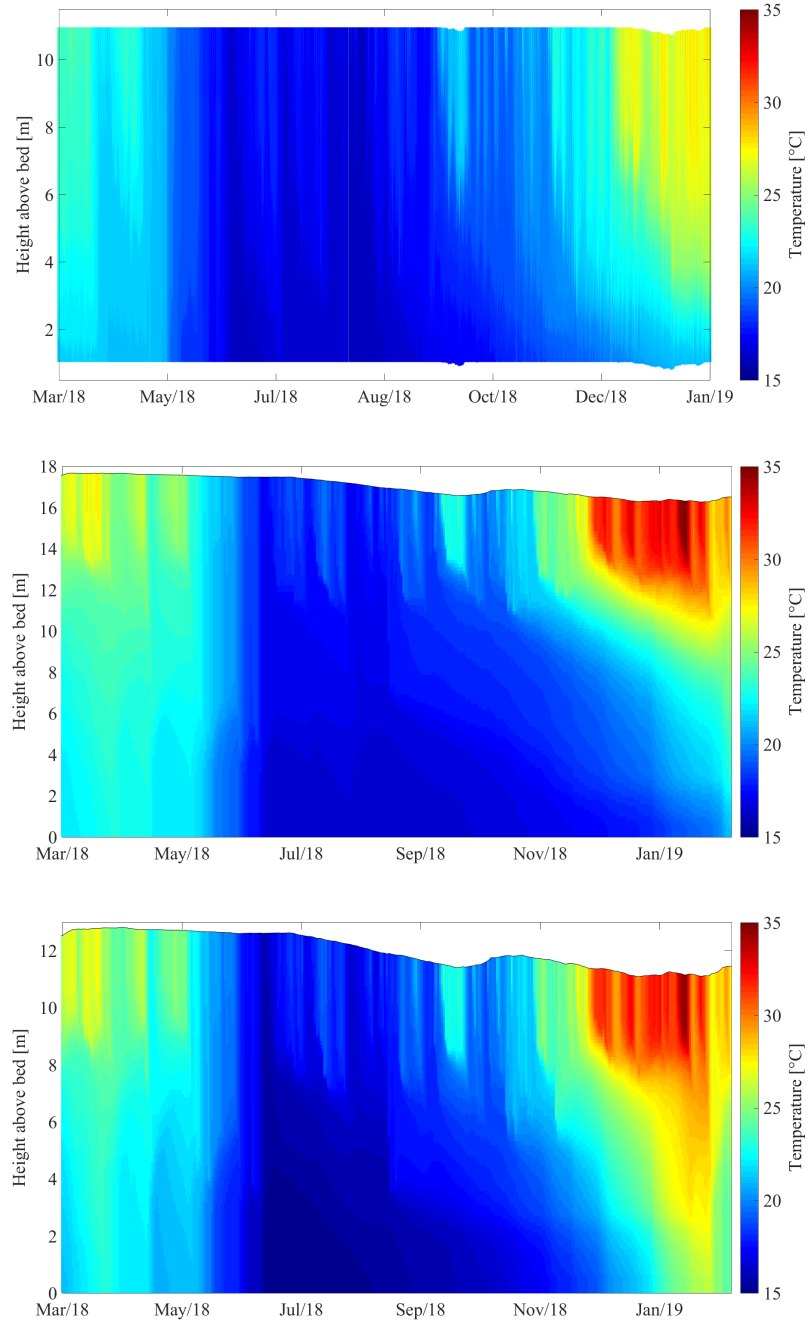


Figure 5.2: Contour plot of Passaúna reservoir water temperature measured by the thermistor chain at the intake region (a), and simulated by GLM-AED in the configurations of 17 m deep (b) and 12 m deep (c), from March 2018 to February 2019.

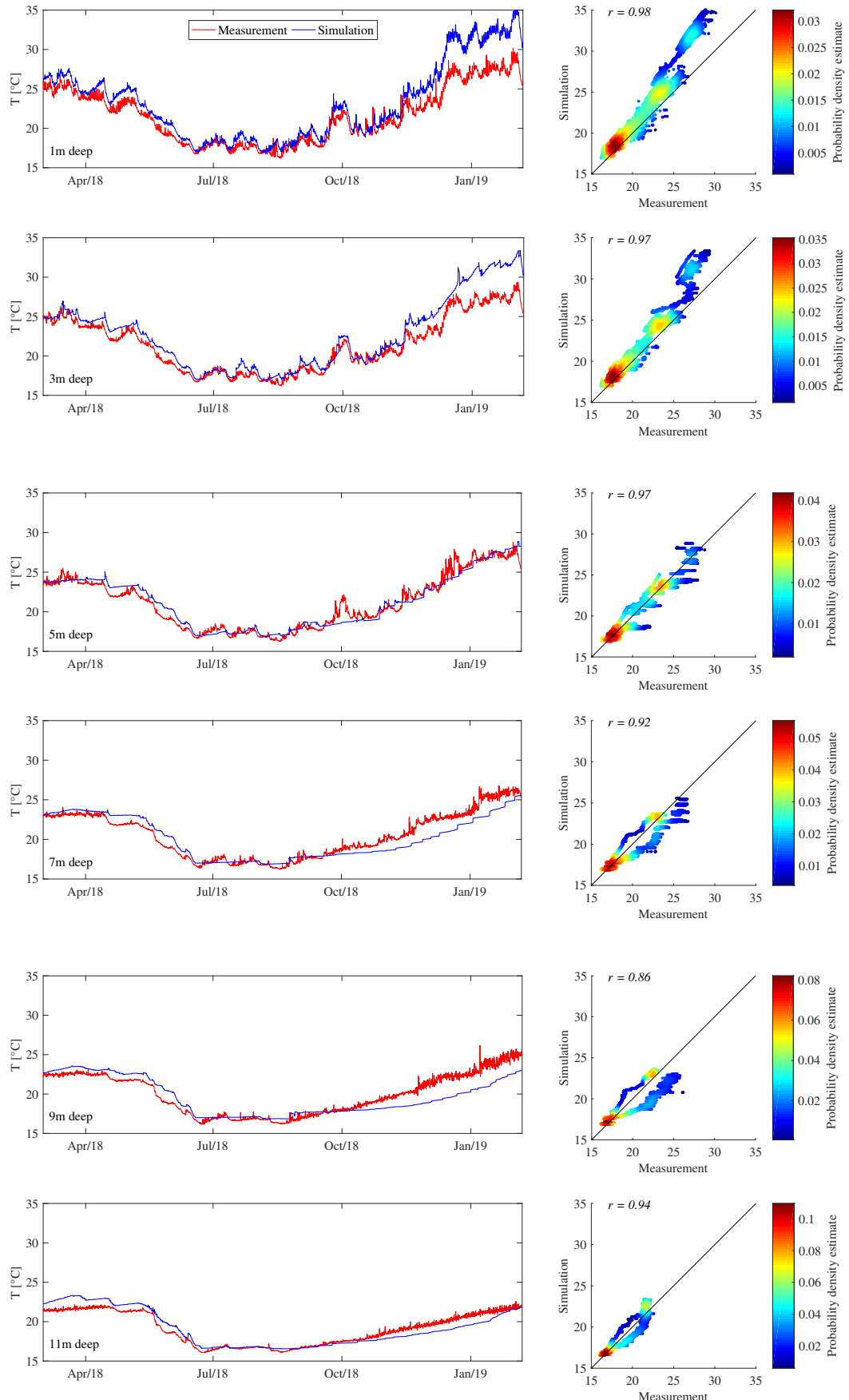


Figure 5.3: Comparison between temperature data measured by thermistors and simulated by GLM-AED model (17 m deep simulation) in the Passaúna reservoir, from March 2018 to February 2019, at depths of 1, 3, 5, 7, 9 and 11 m from the surface, along with the density scatterplot and correlation coefficient value (right side).

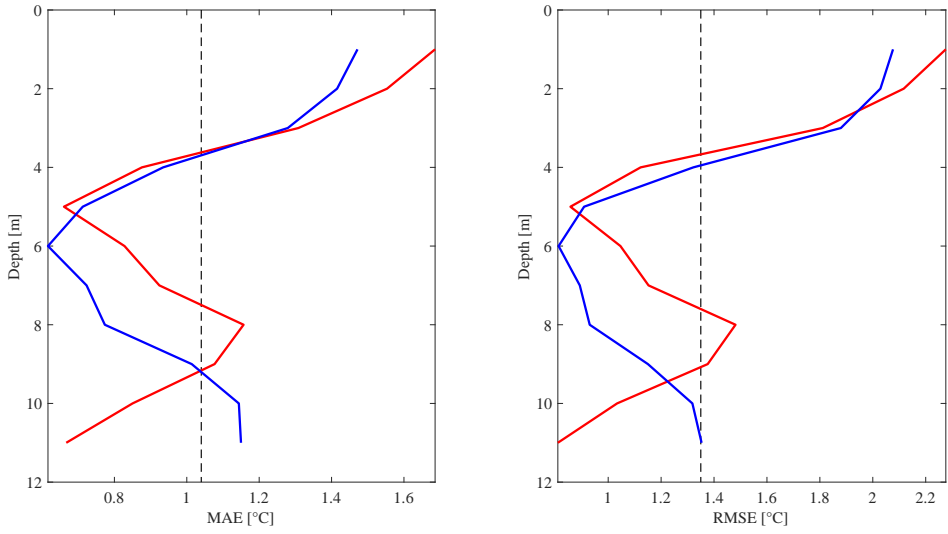


Figure 5.4: Error indices (MAE and RMSE) of simulated Passaúna reservoir water temperature (17 m deep simulation in red line and 12 m deep simulation in blue line) in relation to temperature measurements by thermistors, from March 2018 to February 2019.

However, in Figure 5.3 it was also possible to verify that the high probability nuclei are concentrated in the lowest temperatures, emphasizing that the model is able to represent the cooling period more adequately. Therefore, the mean absolute error, of the 17 m simulation, was plotted in Figure 5.5 for the coldest period (yellow line), from May to July 2018, and for the summer (green line), from December 2018 to February 2019. It is evident, in this way, that the errors in the simulation occur, predominantly, in the warm-up period. In this time interval, in which the flow increases and the model starts to err the water balance a lot, the error amplitude was from $0.71\text{ }^{\circ}\text{C}$ to $4.47\text{ }^{\circ}\text{C}$. In the dry period, the error variation was only $0.32\text{ }^{\circ}\text{C}$.

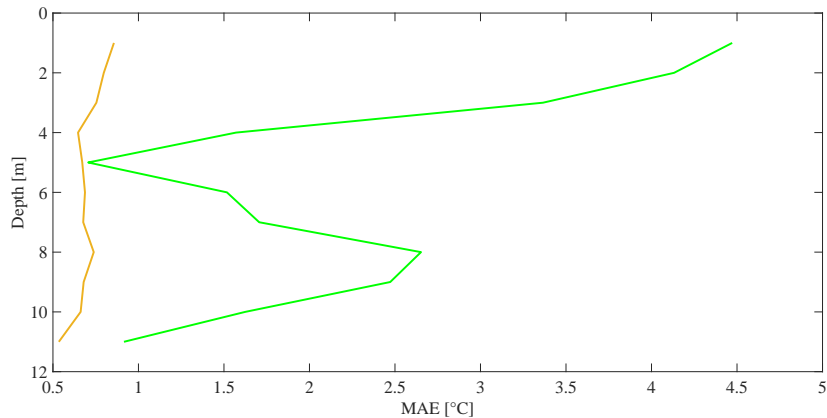


Figure 5.5: Mean absolute error (MAE) from the May to July 2018 period (orange line), and from December 2018 to February 2019 (green line), of the 17 m deep simulation of the Passaúna reservoir.

Differences between simulated and observed water temperatures could be related to several factors, such as the consideration of a fixed value for the light attenuation coefficient (K_w), despising its seasonal variability (Soares et al., 2019). The representation of the mixing

by the one-dimensional model is restricted to processes that act vertically, returning laterally averaged results, can also contribute to this effect, as well as analytical errors in the observations (Fenocchi et al., 2019). Goodness-of-fit metrics were nevertheless equivalent to published ones using GLM and similar 1D-hydrodynamic models, with results below 1.7 °C for the MAE and less than 2.3 °C for the RMSE.

Fenocchi et al. (2017), modeling a deep subalpine lake with different level settings and inlet and outlet flows, found a MAE in the range of 0.49 °C to 1.01 °C and RMSE between 0.87 °C to 1.49 °C with respect to temperature observations over the whole depth. Among these error indices, Read et al. (2014) used the RMSE, finding an error of 2.78 °C for 2368 study sites in Wisconsin, USA, applying an older version of GLM. This high error value compared to other studies was due to their simulations were conducted without an extensive calibration process, because of the large number of lakes in their study. Bueche et al. (2017) comment that the replication of the water temperature in their study can be considered to be more accurate, with an overall root mean square error of 0.65 °C and a mean error of 0.08 °C for the calibration period. For Weber et al. (2017), the calibrated stratification model run (1996-1999) showed a good agreement with observed water temperature profiles with a RMSE of 1.23 °C, but overestimated the summer surface temperatures to some extent. Ladwig et al. (2018) obtained an RMSE between 1.40 °C and 2.00 °C for the total water column for the calibrated and validated years (2009 - 2014). Bruce et al. (2018), when evaluating GLM performance in 32 lakes, found that the predicting of epilimnion temperatures was of similar magnitude to the full-profile temperatures (RMSE mean = 1.62 °C). For the hypolimnetic temperature simulations, average RMSE and NMAE values were relatively low, 1.31 °C and 0.14 °C respectively.

In the Brazil southeastern region, Lagoa da Pampulha (Belo Horizonte, Minas Gerais) was studied by Belico et al. (2017) with the GLM model. The model validation obtained the best results in the rainy season, with an annual RMSE of 1.14 °C. Soares et al. (2019) also applied GLM to a Minas Gerais reservoir (Serra Azul), modeling drought impacts on the lake's hydrodynamics. In the calibration period, the calculated RMSE was 1.33 °C and in the validation was 2.06 °C. Studies carried out in the region close to the Passaúna reservoir also showed errors in this values range, using other one-dimensional models. Männich (2013) applied a 1D model of vertical heat transport, developed by the author himself, at the Vossoroca lake, also located in the Curitiba Metropolitan Region (Paraná). Regarding the statistical parameters, found an average error of 0.49 °C and an average quadradite error of 0.42 °C, the error variance was 0.18 °C. Polli and Bleninger (2015) also studied the thermal evolution of the Vossoroca reservoir, developing a one-dimensional model to identify the seasonal behavior of the reservoir and critical periods (related to stratification and mixing). This model had an average error of 0.26 °C, a standard deviation of 1.42 °C and a mean square error of 1.45 °C. Table 5.1 summarizes the studies presenting the calibration MAE and/or RMSE of water temperature simulations applying 1D models.

Table 5.1: Studies presenting the calibration MAE and/or RMSE range of water temperature simulations applying 1D models.

Lake / reservoir	Model	Max. depth [m]	MAE [°C]	RMSE [°C]	Reference
Vossoroca (Brazil)	Developed by the author	17.0	0.49	0.42	Männich (2013)
2368 Wisconsin lakes (USA)	GLM	3.6 - 10.7	-	1.74 - 3.33	Read et al. (2014)
Vossoroca (Brazil)	Developed by the author	17.0	0.26	1.45	Polli and Bleninger (2015)
Pampulha (Brazil)	GLM	16.2	-	1.14	Belico et al. (2017)
Maggiore (Italy and Switzerland)	GLM	370.0	0.10 - 1.57	0.12 - 2.06	Fenocchi et al. (2017)
Ammersee (Germany)	GLM	83.7	0.01 - 0.69	0.19 - 1.81	Bueche et al. (2017)
Grosse Dhuen (Germany)	GLM	53.0	-	1.03 - 1.40	Weber et al. (2017)
32 lakes around the world	GLM	-	0.11	1.34	Bruce et al. (2018)
Tegel (Germany)	GLM	16.0	-	1.40 - 2.00	Ladwig et al. (2018)
Serra Azul (Brazil)	GLM	47.3	-	1.33 - 2.06	Soares et al. (2019)
Passaúna (Brazil)	GLM-AED	17.0	0.62 - 1.69	0.81 - 2.28	This study

5.1.3 Physical indices

The physical indices (Figure 5.6), calculated by the Lake Analyzer software, were plotted by comparing the results obtained with the thermistors data and the GLM-AED simulation data, for the depth of 17 m and 12 m. It is observed that the results with the observed data are similar to the modeled ones. The largest differences occurred for Schmidt Stability, which reproduced more accurately the errors of overestimation of summer epilimnetic temperatures. In Table 5.2 the MAE and RMSE of physical indices between the calculation by records measured and model configurations data are listed. Regarding the indices themselves, the results are in accordance with the literature, since, in the case of Schmidt Stability, higher values are observed in the warmer months, especially in the summer of 2019, indicating greater resistance to the waterbody mixture. It may also be noted day-night oscillations driven by alternating periods of heating and cooling. Brunt-Väisälä Frequency presents a similar pattern, with lower values in the coldest period, i.e., from mid-May to September 2018. This behavior also corresponds to the results for Wedderburn Number and Lake Number, which showed values below 1 mostly between these months, which denotes conditions of instability and, consequently, mixing in the water column.

Table 5.2: Error indices (MAE and RMSE) of physical indices of the Passaúna reservoir between the calculation by records measured and model data of the 17 m and 12 m deep simulations, from March 2018 to February 2019.

Index	MAE	RMSE	MAE	RMSE
	17 m deep	17 m deep	12 m deep	12 m deep
S_T [J mol $^{-2}$]	51.33	53.51	82.38	68.64
N^2 [s $^{-2}$]	1.39 e-3	1.48 e-3	1.89 e-3	1.94 e-3
W	17.31	16.93	34.22	36.27
L_N	8.64	7.35	17.54	12.302

The values of W and L_N were, predominantly, above 1, and the frequency with which this occurred was similar for the calculation made with the temperature observed values and with the modeled ones, varying from 90% to 99%. Table 5.3 lists these results in number of days, as well as for W and L_N less than 1 and the frequency of thermal gradients of different intensities ($\Delta T > 1$ °C, $\Delta T > 2$ °C and $\Delta T > 3$ °C). It is noted that the biggest difference between the surface and the reservoir bottom temperature, i.e. $\Delta T > 3$ °C, was also the one that had the

highest occurrence, from 33% (thermistors data) to 62% (simulation data 12 m). This means that between March 2018 and February 2019, the registration period for thermistors, conditions of thermal stability occurred with greater constancy. This analysis is verified by looking at Figure 5.7 with the temperature difference between the surface and the bottom. The figure also shows the depth of the thermocline, where it is observed that the thermocline shows oscillations in its depth value most of the time, maintaining certain stability in the coldest period, which corresponds to the season of complete mixing of the water column. In these months, from May to July 2018, the thermocline depth reached the highest values, which coincided with the reservoir maximum depth in each of the scenarios of calculating the physical indices.

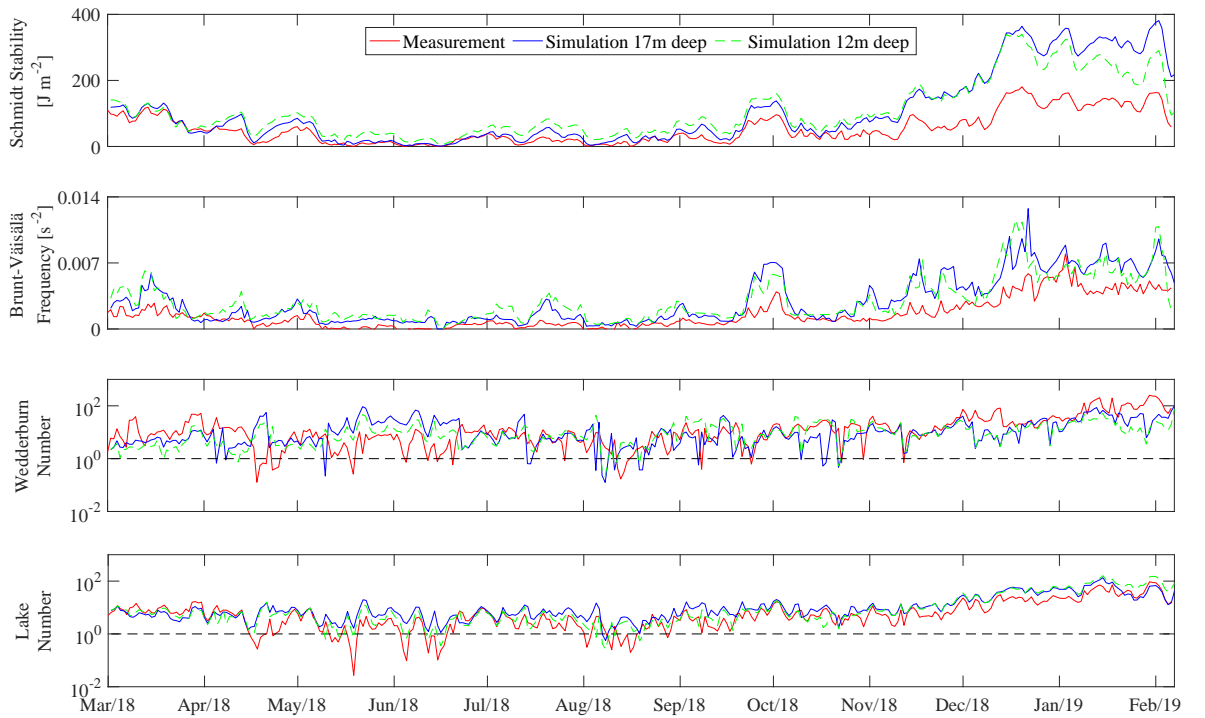


Figure 5.6: Physical indices of the Passaúna reservoir calculated with water temperature records measured by thermistors and model data of the 17 m and 12 m deep simulations, from March 2018 to February 2019.

Table 5.3: Number of days $W < 1$, $W > 1$, $L_N < 1$, $L_N > 1$, $\Delta T < 1^\circ\text{C}$, $\Delta T > 1^\circ\text{C}$, $\Delta T > 2^\circ\text{C}$ and $\Delta T > 3^\circ\text{C}$ of the Passaúna reservoir, from the physical indices calculated by records measured and model data of the 17 m and 12 m deep simulations, from March 2018 to February 2019.

Days	Measurement	Simulation (17 m deep)	Simulation (12 m deep)
$W < 1$	23	17	9
$W > 1$	320	326	334
$L_N < 1$	35	18	2
$L_N > 1$	308	325	341
$\Delta T < 1^\circ\text{C}$	91	29	13
$\Delta T > 1^\circ\text{C}$	83	73	59
$\Delta T > 2^\circ\text{C}$	55	55	59
$\Delta T > 3^\circ\text{C}$	114	186	212

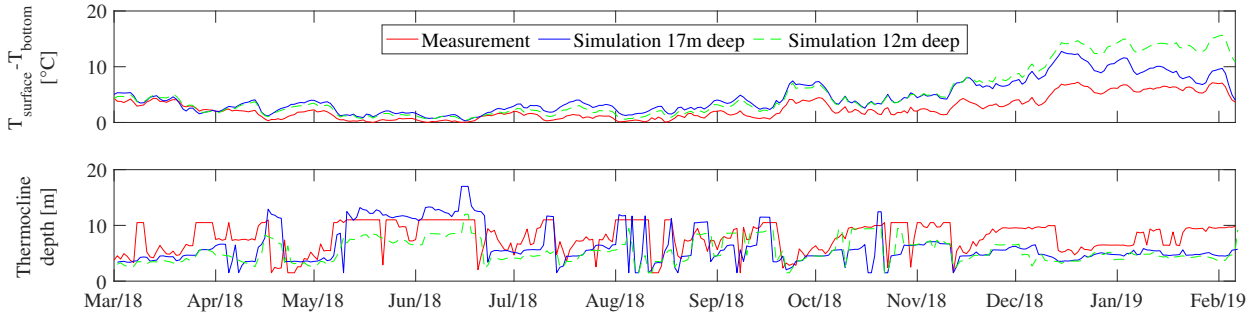


Figure 5.7: Surface and bottom temperature difference and thermocline depth of the Passaúna reservoir, from the physical indices calculated by records measured and model data of the 17 m and 12 m deep simulations, from March 2018 to February 2019.

5.2 ECOLOGICAL MODULE PERFORMANCE

5.2.1 Oxygen

The dissolved oxygen (DO) distribution in the water column, simulated in the configuration considering the reservoir total depth (17 m), is shown in Figure 5.8. It is observed that the model reproduced a strong DO gradient at the waterbody bottom, with values ranging from 0 to $7.9 \text{ mg O}_2 \text{ L}^{-1}$ and an average of $3.6 \text{ mg O}_2 \text{ L}^{-1}$ in the last layer, while (1 m) above the minimum value was $6.7 \text{ mg O}_2 \text{ L}^{-1}$, the maximum $8.8 \text{ mg O}_2 \text{ L}^{-1}$ and the average equal to $7.7 \text{ mg O}_2 \text{ L}^{-1}$. The DO decrease in the bottom is possibly associated with the sediment oxygen demand, resulting from the microbial activity of organic matter decomposition. In relation to the other layers, the GLM-AED resulted in very homogeneous values, not showing great differences between the epilimnion and hypolimnion, even in the periods corresponding to the thermal stratification. However, it is noticed that in the colder months, the DO values are slightly higher, since the oxygen solubility in water is inversely proportional to the temperature, that is, a higher concentration of DO dissolves in the water under colder conditions (Esteves, 2011).

Figures 5.9 and 5.10 below show the comparison between DO data measured by miniDOT and simulated by model for 17 m and 12 m deep, respectively, at surface (10 m above bed) and bottom (0.5 m above bed). The results for the surface layer were shown to be very smooth, without the representation, by the model, of the variations in concentration over time. While the sensor measurements recorded a range of values between 3.8 to $11.0 \text{ mg O}_2 \text{ L}^{-1}$, the model exhibited an average of $8.8 \pm 0.4 \text{ mg O}_2 \text{ L}^{-1}$ for the 17 m simulation and $8.7 \pm 0.6 \text{ mg O}_2 \text{ L}^{-1}$ for the 12 m. As for reservoir bottom concentrations, it is noted that the model was able to describe the variations measured by the Oxygen Logger, with the most synchronized ascents and descents in the case of the 17 m simulation, erring, however, in terms of magnitude. The measurements showed values from 0 to $8.8 \text{ mg O}_2 \text{ L}^{-1}$, with an average of $2.8 \text{ mg O}_2 \text{ L}^{-1}$; the configuration with 17 m was 0.3 to $8.7 \text{ mg O}_2 \text{ L}^{-1}$, an average of $4.4 \text{ mg O}_2 \text{ L}^{-1}$; and with 12 m was 1.3 to $8.6 \text{ mg O}_2 \text{ L}^{-1}$, an average of $4.5 \text{ mg O}_2 \text{ L}^{-1}$.

The correlation between the measured and simulated data is better captured in reservoir bottom, as already mentioned, as can be seen in the density scatterplot (right side) that the

dispersion between observed and modeled data is better distributed. For the surface, however, it appears that the model did not generate results across the spectrum of values measured by the sensor, so the points on the graph were concentrated in the upper right region of the area. For the 17 m simulation, the r at 0.5 m above bed was 50% greater than close to the surface; for the 12 m simulation, the correlation for the bottom was twice that for the 10 m above bed. As for the error indices (Table 5.4), however, the values were higher in the bottom, which means greater uncertainties in the modeled values for this layer. The highest value of MAE and RMSE was $2.65 \text{ mg O}_2 \text{ L}^{-1}$ and $3.00 \text{ mg O}_2 \text{ L}^{-1}$, respectively, for the reservoir bottom in the 12 m deep simulation; the lowest values were for this configuration also, on the surface (MAE equal to $1.19 \text{ mg O}_2 \text{ L}^{-1}$ and RMSE equal to $1.56 \text{ mg O}_2 \text{ L}^{-1}$). Bucak et al. (2018), in their modeling study of the effects of climatic and land use changes on phytoplankton and water quality of the largest Turkish freshwater lake (Lake Beyşehir), used the GLM and PCLake models. In terms of root mean square deviation, it presented only the result for the OD simulated by PCLake ($1.38 \text{ mg O}_2 \text{ L}^{-1}$), which is within the range of values obtained in the present work. The correlation coefficient found, described only for the GLM, was 0.82. Values of r above those calculated here were also displayed in Fennochi: 0.83 for the calibration step and 0.79 during validation (p -value < 0.001).

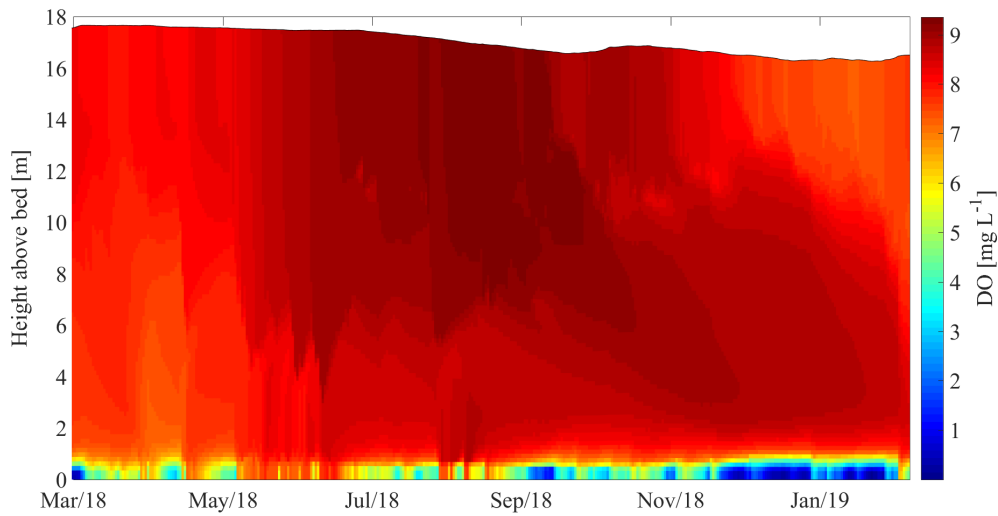


Figure 5.8: Contour plot of Passaúna reservoir dissolved oxygen (DO) in the 17 m deep simulation by GLM-AED, from March 2018 to February 2019.

Table 5.4: Error indices (MAE and RMSE) for Passaúna reservoir dissolved oxygen (DO) between measurements of the miniDOT and results obtained by GLM-AED model, from April 2018 to February 2019, at depths of 10 m and 0.5 m above bed.

Depth	MAE [mg O ₂ L ⁻¹]	RMSE [mg O ₂ L ⁻¹]	MAE [mg O ₂ L ⁻¹]	RMSE [mg O ₂ L ⁻¹]
	17 m deep	17 m deep	12 m deep	12 m deep
10 m above bed	1.16	1.47	1.19	1.56
0.5 m above bed	2.08	2.48	2.65	3.00

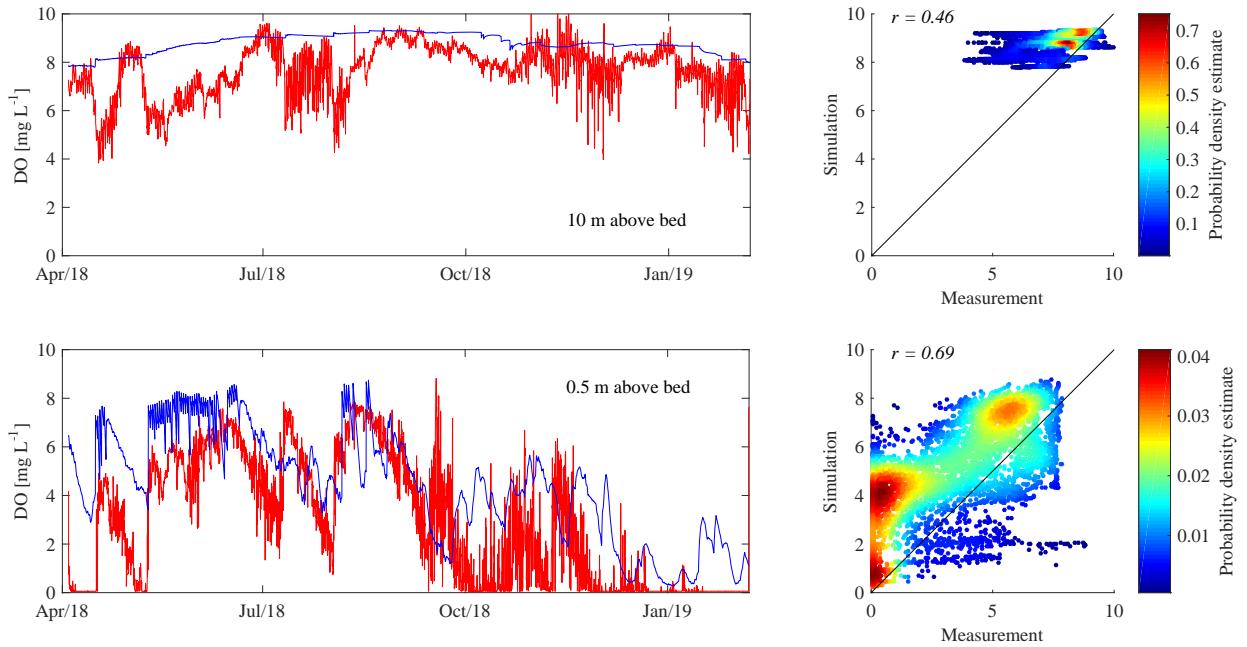


Figure 5.9: Comparison Passaúna reservoir dissolved oxygen (DO) between data measured by miniDOT (red line) and simulated by GLM-AED model (blue line; 17 m deep simulation), from April 2018 to February 2019, at depths of 10 m and 0.5 m above bed, along with the density scatterplot and correlation coefficient value (right side).

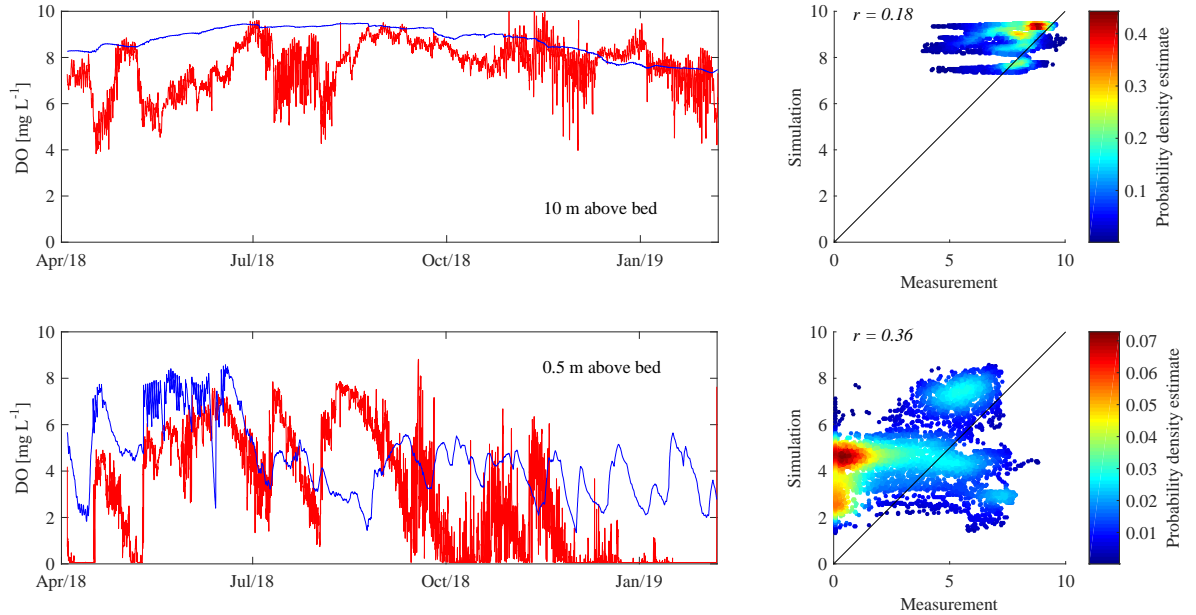


Figure 5.10: Comparison Passaúna reservoir dissolved oxygen (DO) between data measured by miniDOT (red line) and simulated by GLM-AED model (blue line; 12 m deep simulation), from April 2018 to February 2019, at depths of 10 m and 0.5 m above bed, along with the density scatterplot and correlation coefficient value (right side).

5.2.2 Nutrients (phosphorus and nitrogen)

Figures 5.11, 5.12, and 5.13 show the contour plot of the Passaúna reservoir nitrate (NO_3^-), ammonia (NH_4^+) and phosphate (PO_4^{3-}), simulated by GLM-AED in the 17 m deep configuration. NO_3^- showed a high gradient at the reservoir bottom, without showing concentrations in the

last layer, possibly due to the also DO absence in this region. Because the nitrification process does not occur in anaerobiosis, nitrate concentrations are reduced. This fact also explains the higher ammonia values (maximum 0.79 mg N L^{-1}) in the anaerobic hypolimnion, since in this condition the ammoniacal nitrogen oxidation happens basically through the anammox process, which occurs at low rates. In the other waterbody layers, NH_4^+ was quite uniform and with small concentrations (less than 0.10 mg N L^{-1}). This compound is quickly transformed into nitrite and nitrate after being released into the system by the organic matter decomposition (ammonification), which was responsible, probably, for the highest nitrate values (maximum of 0.59 mg N L^{-1}) in the water column. Close to the surface, nonetheless, values between 0.20 and 0.30 mg N L^{-1} were obtained, which may be due to the removal of much of the nitrate in this region by the plankton metabolic activity, especially phytoplankton in the epilimnion (Esteves, 2011). The phosphate showed a vertical distribution pattern similar to ammonia, with values in the order of $10^{-4} \text{ g P L}^{-1}$ in almost every profile, reaching a maximum of 0.05 mg P L^{-1} at the reservoir bottom.

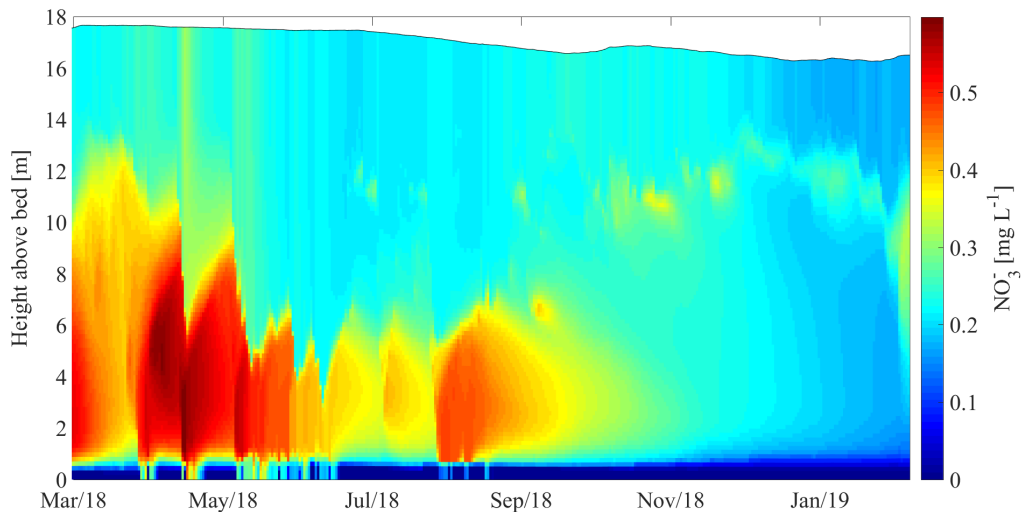


Figure 5.11: Contour plot of Passaúna reservoir nitrate (NO_3^-) in the 17 m deep simulation by GLM-AED, from March 2018 to February 2019.

Following, Figure 5.14 show the comparison between NO_3^- , NH_4^+ and PO_4^{3-} simulated results and data from laboratory analyzes of samples collected at a point close to Sanepar's water intake, under the MuDak project. In the nitrate case, there is also field data recorded by the Opus optical sensor, which shows a pattern of little variation in values (average of $0.22 \pm 0.05 \text{ mg N L}^{-1}$) over the period with measurements (March 2018 to February 2019), which was also reproduced by the model. The configuration simulated with the total reservoir depth showed values closer to the sensor, that is, an average of 0.22 mg N L^{-1} , a maximum of 0.31 mg N L^{-1} , and a minimum of 0.17 mg N L^{-1} . The simulation with a 12 m deep obtained an average of $0.31 \pm 0.04 \text{ mg N L}^{-1}$. The laboratory analyzes resulted in slightly more varied concentrations, from 0.03 to 0.38 mg N L^{-1} , notwithstanding, in terms of average (0.20 mg N L^{-1}).

The modeled NH_4^+ data proved to be practically constant during the analyzed period, with an average of 0.03 mg N L^{-1} in both simulations. The laboratory analyzes, however, showed values in higher scales, an average of 0.15 mg N L^{-1} , a maximum of 0.74 mg N L^{-1} , and a minimum of 0.01 mg N L^{-1} . The model results for phosphate, also shown in the figure, were not used as an analysis criterion in the calibration step since only one data ($0.0011 \text{ mg P L}^{-1}$) was obtained in the laboratory, the other field samples resulted in inconclusive values. The simulations in the two configurations were very similar, with their results (order of $10^{-4} \text{ g P L}^{-1}$) overlapping on the graph most of the time.

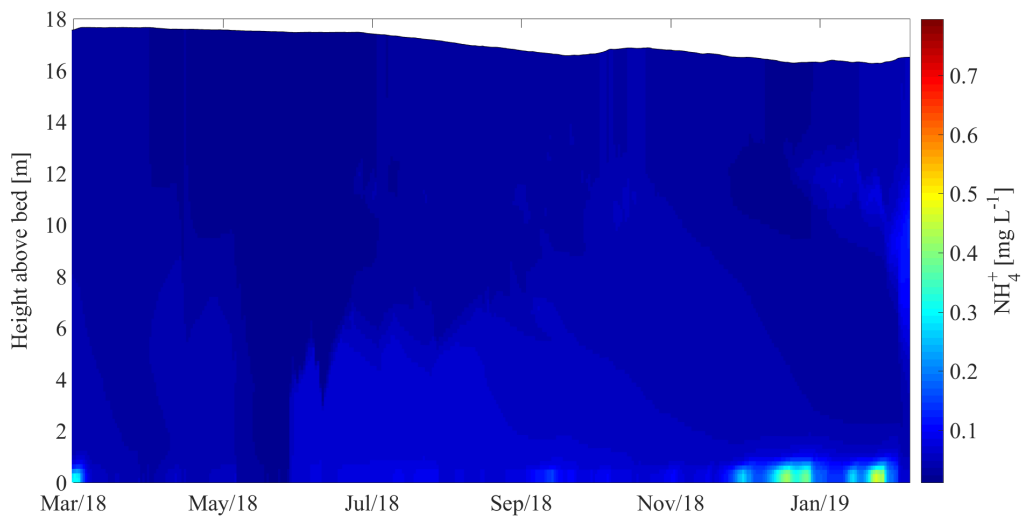


Figure 5.12: Contour plot of Passaúna reservoir ammonia (NH_4^+) in the 17 m deep simulation by GLM-AED, from March 2018 to February 2019

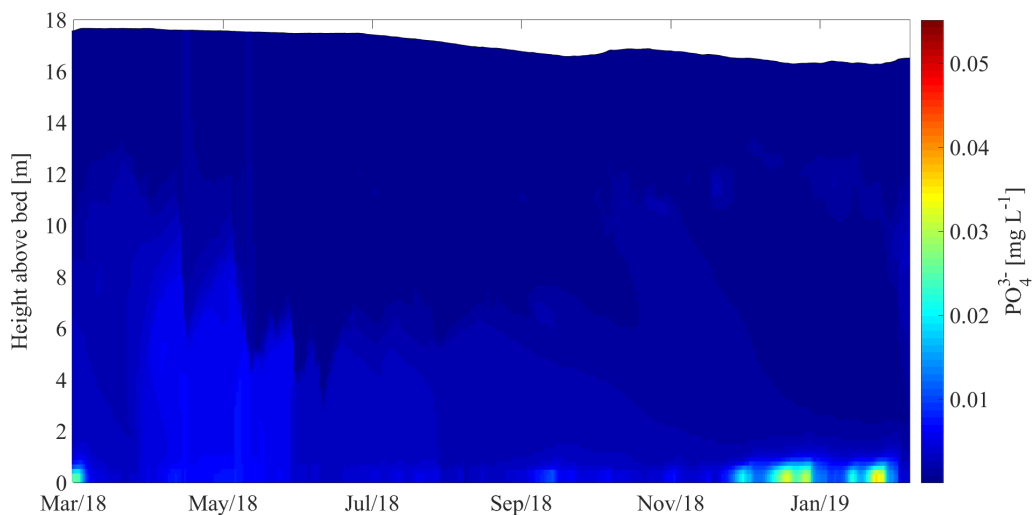


Figure 5.13: Contour plot of Passaúna reservoir phosphate (PO_4^{3-}) in the 17 m deep simulation by GLM-AED, from March 2018 to February 2019

The comparison of measured and modeled data of total nitrogen and phosphorus is shown in Figure 5.15, noting a few discrepancies between the results of the simulated configurations. The total nitrogen values obtained by the model showed a good agreement with most of the field data, with an average of 0.53 mg NL^{-1} for the 17 m deep simulation and 0.67 mg NL^{-1} for the 12 m. Three measurements carried out by Sanepar, however, were far from these values, but the same occurred in relation to the analyzes of the MuDak project (average of 0.55 mg NL^{-1} , maximum of 0.83 mg NL^{-1} and minimum of 0.37 mg NL^{-1}). Total phosphorus also showed a uniform pattern in the simulations, with an average value of 0.016 mg PL^{-1} for the 17 m configuration and 0.019 mg PL^{-1} for the consideration of 12 m deep. Thus, it demonstrated equivalence in relation to the order of magnitude of the measurements ($10^{-2} \text{ g PL}^{-1}$). Seasonal variations in concentrations were not captured by the model, so the correspondence between observed and modeled data in terms of magnitude and dynamics, in general, was verified.

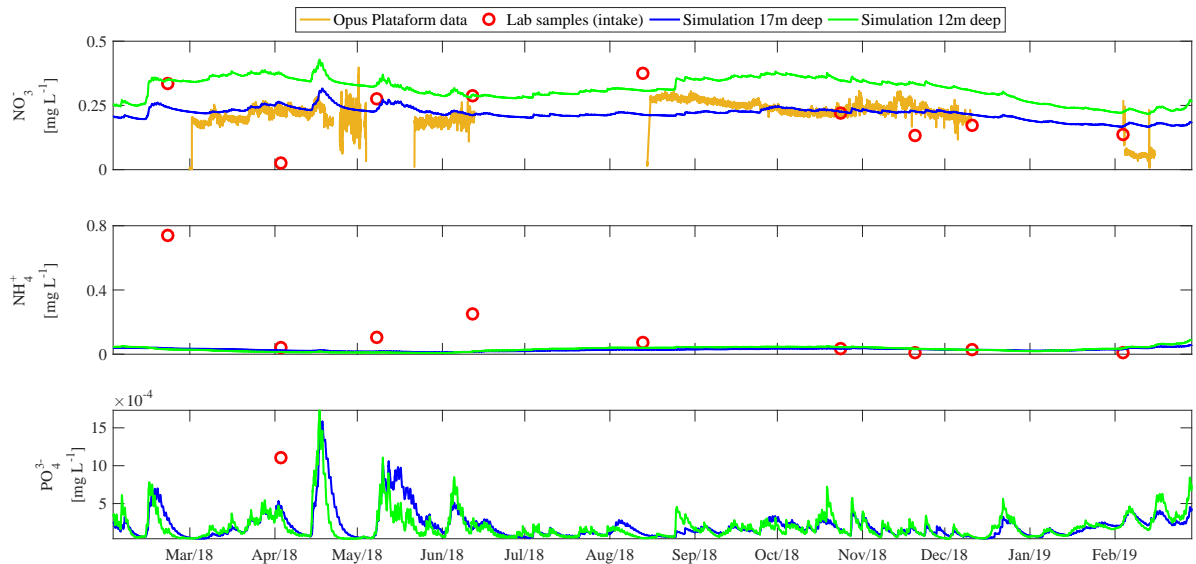


Figure 5.14: Comparison Passauna reservoir nitrate (NO_3^-), ammonia (NH_4^+) and phosphate (PO_4^{3-}) between data of MuDak laboratory analyzes referring to the intake region and results obtained by the GLM-AED model, along with NO_3^- records by the Opus optical sensor, from March 2018 to February 2019, at surface (up to 1 m deep).

The error metrics (MAE and RMSE) were calculated for the nitrate data obtained by the model in relation to the Opus sensor records (Table 5.5). The periods considered were the longest time intervals with continuous sensor recordings. It appears that the configuration with the total reservoir depth (17 m) showed errors about five times smaller than the simulation of 12 m. Nonetheless, the results for both simulations were significantly lower than the errors found in the Bucak et al. (2018) study, which reached a value of root mean square deviation equal to 16.39 mg NL^{-1} for NO_3^- simulated with GLM and 83.71 mg NL^{-1} with the PCLake model.

5.2.3 Chlorophyll-*a*

Regarding the phytoplankton module, only the results of chlorophyll-*a* were checked, a variable from which measured data had been available for the purposes of results evaluating.

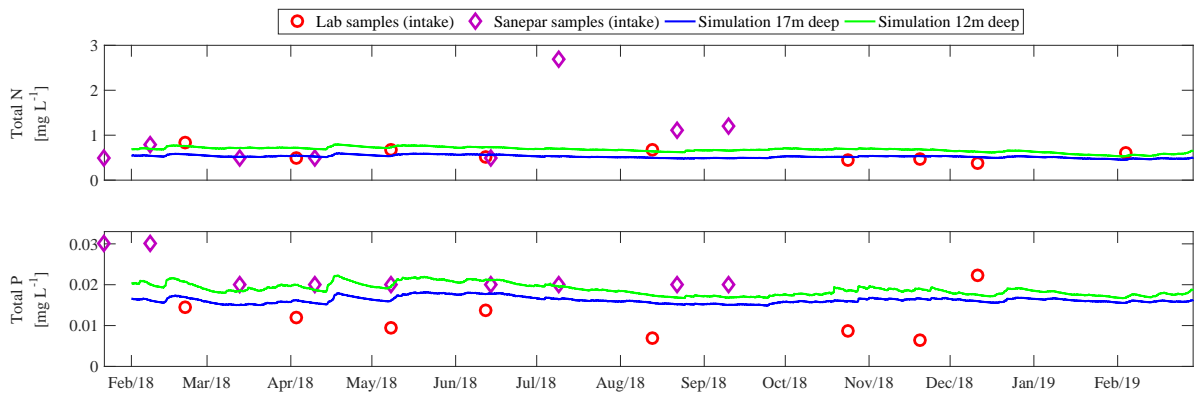


Figure 5.15: Comparison Passaúna reservoir total nitrogen and phosphorus between data of MuDak and Sanepar laboratory analyzes referring to the intake region and results obtained by the GLM-AED model, from February 2018 to February 2019, at surface (up to 1 m deep).

Table 5.5: Error indices (MAE and RMSE) for Passaúna reservoir nitrate (NO_3^-) between measurements of the Opus optical sensor and results obtained by the GLM-AED model.

Date	MAE [mg N L^{-1}] 17 m deep	RMSE [mg N L^{-1}] 17 m deep	MAE [mg N L^{-1}] 12 m deep	RMSE [mg N L^{-1}] 12 m deep
03/01/2018 - 04/19/2018	0.03	0.04	0.16	0.16
08/14/2018 - 12/04/2018	0.04	0.06	0.12	0.14

Figure 5.16 shows the distribution of chlorophyll-*a* in the reservoir vertical profile from 17 m simulation results. It is noticed that the concentrations occurred exclusively in the most superficial layers, where there is a predominance of solar radiation. The maximum values obtained by the model were approximately $10 \mu\text{g L}^{-1}$. In the colder months, concentrations were observed in deeper layers, probably due to the configuration of thermal instability in this period and, consequently, mixing in the water column of parameters related to water quality (OD and nutrients, for example).

Figure 5.17 shows the chlorophyll-*a* values obtained by the model in the most superficial reservoir layer in comparison to data measured from the samples collected in the field by the MuDak project, as well as the records of the NanoFlu optical sensor, both referring to the intake reservoir region. There is a better correspondence of the values for 17 m simulation, with an average of $5.9 \mu\text{g L}^{-1}$, a maximum of $9.7 \mu\text{g L}^{-1}$, and a minimum of $3.3 \mu\text{g L}^{-1}$. For the 12 m deep configuration, the values range from $5.5 \mu\text{g L}^{-1}$ to $17.2 \mu\text{g L}^{-1}$, with an average of $10.3 \mu\text{g L}^{-1}$. The results were, therefore, very similar to the measurements, which showed a variation of 1.9 to $8.1 \mu\text{g L}^{-1}$ in the laboratory analyzes, close to the sensor records (average of $6.7 \pm 2.1 \mu\text{g L}^{-1}$, maximum reaching $16.7 \mu\text{g L}^{-1}$ and minimum of zero).

Similar to the nitrate case, the MAE and RMSE error indices were also calculated for chlorophyll-*a*, considering the data from the NanoFlu sensor and the model results. It is noted in Table 5.6, as already commented, that the 17 m deep configuration had the best performance, with a maximum RMSE of $4.66 \mu\text{g L}^{-1}$ in the months of July to September 2018. Already the 12 m simulation showed a greater error (MAE = $6.98 \mu\text{g L}^{-1}$ and RMSE = $7.52 \mu\text{g L}^{-1}$) between

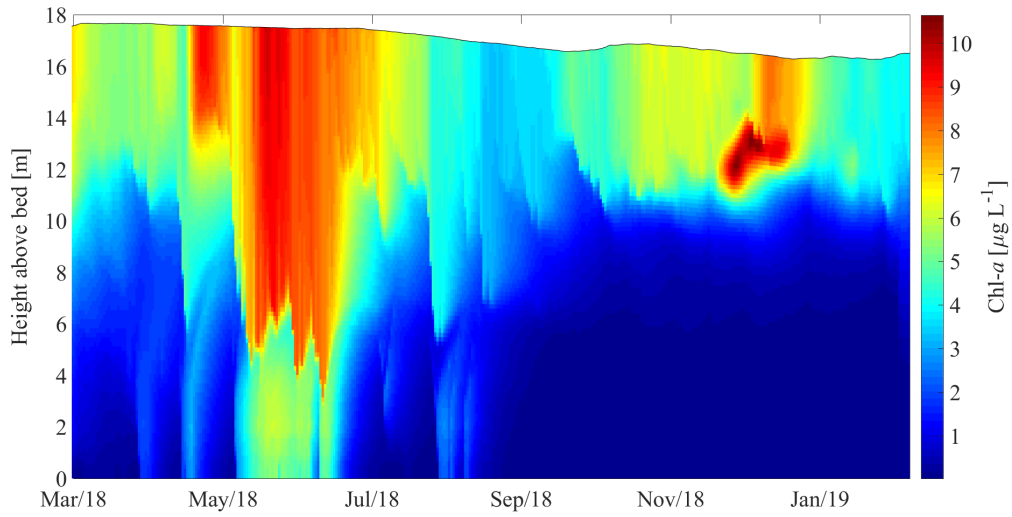


Figure 5.16: Contour plot of Passaúna reservoir chlorophyll-*a* in the 17 m deep simulation by GLM-AED, from March 2018 to February 2019

March to June 2018. The smallest errors found occurs for the 12 m deep configuration in February 2019. In general, the range of error index values covers the result obtained by Bucak et al. (2018) with the modeling using the GLM ($\text{RMSE} = 2.66 \mu\text{g L}^{-1}$). For PCLake, the RMSE obtained was even lower, $1.47 \mu\text{g L}^{-1}$ (Bucak et al., 2018).

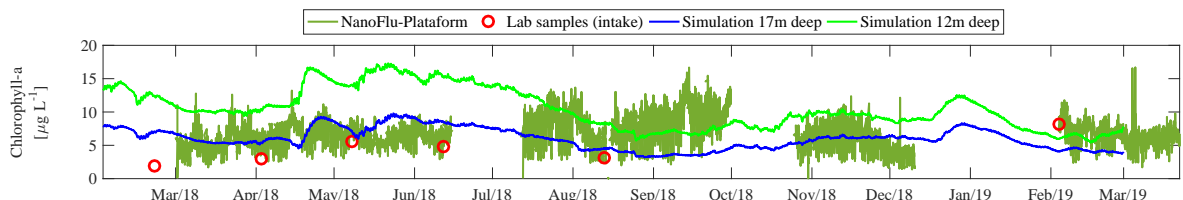


Figure 5.17: Comparison Passaúna reservoir chlorophyll-*a* between data of MuDak laboratory analyzes referring to the intake region and results obtained by the GLM-AED model, along with Chlorophyll-*a* records by the NanoFlu optical sensor, from March 2018 to February 2019, at surface (up to 1 m deep).

Table 5.6: Error indices (MAE and RMSE) for Passaúna reservoir chlorophyll-*a* between measurements of the NanoFlu optical sensor and results obtained by the GLM-AED model.

Date	MAE [$\mu\text{g L}^{-1}$] 17 m deep	RMSE [$\mu\text{g L}^{-1}$] 17 m deep	MAE [$\mu\text{g L}^{-1}$] 12 m deep	RMSE [$\mu\text{g L}^{-1}$] 12 m deep
03/01/2018 - 06/14/2018	1.74	2.13	6.98	7.52
07/12/2018 - 09/28/2018	4.01	4.66	2.63	3.24
10/25/2018 - 12/10/2018	1.64	1.96	3.81	4.15
02/04/2019 - 02/28/2019	3.05	3.33	1.46	1.84

5.2.4 Trophic State Index

The trophic level of Passaúna reservoir regarding the concentrations of total phosphorus and chlorophyll-*a* obtained by the model are shown in Figure 5.18, as well as the final trophic

state index (TSI), that is, calculated as the average of $TSI(TP)$ and $TSI(Chla)$ according to Lamparelli (2004). It is observed that only for the concentration of total phosphorus the reservoir trophic degree was classified as oligotrophic. In this case, for the 17 m deep simulation, the oligotrophic state was maintained throughout the analyzed period, but for the 12 m configuration, the trophic level changed to mesotrophic from January to July 2018 and October of that same year. For the chlorophyll- a values estimated by the model, the mesotrophic state was verified throughout entire the 17 m deep simulation. However, the waterbody proved to be undergoing eutrophication for the 12 m configuration in some months: December 2017 and 2018, January and February 2018, April to July 2018. The TSI also showed mesotrophic results in practically every simulation, only presenting conditions of lower primary productivity, that is, oligotrophic state, in August and September 2018 for the 17 m deep configuration.

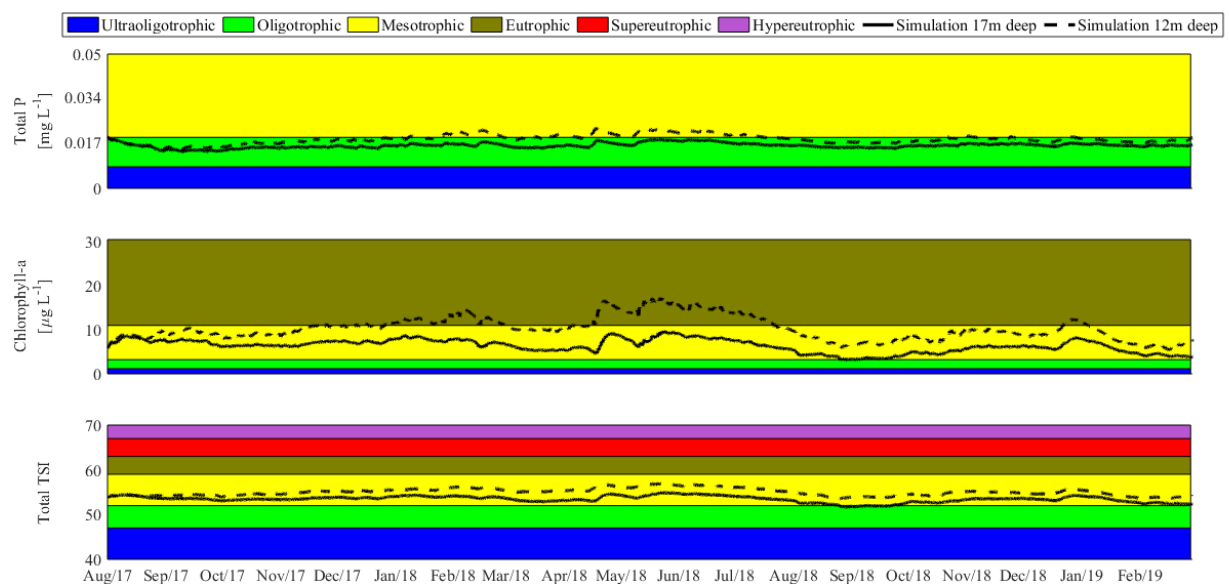


Figure 5.18: Trophic level of Passaúna reservoir regarding the concentrations of total phosphorus and chlorophyll- a obtained by GLM-AED model, and the final trophic state index (TSI), calculated according to Lamparelli (2004), from August 2017 to February 2019.

Barreto et al. (2019) also assessed the Passaúna reservoir trophic level, analyzing both spatial and temporal variability. For that, they used field data from different waterbody points over a hydrological year. The results showed that the intake region presented oligotrophic and mesotrophic conditions for total phosphorus and chlorophyll- a , and remained in the mesotrophic state by analyzing the mean TSI. From monitoring, they also observed that a small area upstream of the reservoir, called buffer, acts to cushion the loads carried by the inflows. As they verified little variation in the total phosphorus concentration over time at the most central points and close to the dam, they suggested the possibility that in these regions there is less impact of external conditions and greater influence of reservoir internal processes.

Continuous monitoring of a waterbody with measurements at different sample points is not always possible in practice, due to the necessary investment. The use of models that consider the longitudinal dimension, 2D or 3D, is also not very viable in some circumstances. They usually

require extensive calibration, with many parameters, and do not allow the simulation of various management scenarios as quickly as a 1D model. Thus, although the 1DV (one-dimensional vertical) modeling used in this study does not provide a spatial analysis of the waterbody water quality, it was still found to be a very useful tool. The simulation of the GLM-AED model reproduced the predominant Passaúna reservoir trophic state and how quickly your results are generated, in a few minutes at most, allows the simulation of different scenarios even over long periods. Thus, several prognoses can be made, varying the nutrients load entering the reservoir, to assist in the decision making of the present in terms of waterbody management.

6 CONCLUSIONS

The present application of GLM-AED (General Lake Model – Aquatic EcoDynamics) to Passaúna reservoir, from August 2017 to February 2019, aimed to evaluate the performance of the one-dimensional coupled model in reproducing the physical, chemical, and biological processes of this subtropical water supply reservoir. In order to obtain all the information needed in the modeling, it was necessary to use data from different monitoring stations, which required the verification of the compatibility of the station records (meteorological) with the correlation calculation. It was also faced with the need to correct failures in the historical series, as well as the use of data adjusted by other models, in the case of hydrological records. To make up for the lack of water quality data, interpolations and extrapolations were performed with the calculation, first, of the input loads, and then obtain the values in concentration. This premise was adopted intending to achieve a reasonable estimate of the conditions of each tributary, considering their flow rates separately. All the mentioned procedures demonstrate the effort required, by the modeler, to represent the dynamics of the studied aquatic ecosystem in the most reliable way possible.

A defiance faced in hydrodynamic and ecological modeling is the values attribution of parameter, especially when dealing with a subtropical aquatic ecosystem. Most of the experimental studies, carried out to define the values range of several parameters, were developed in temperate water bodies, which present different patterns from the ecosystems located adjacent to the tropics (Fragoso Jr, 2008). Carrying out a thorough calibration, which requires different approaches, is also essential to obtain a model satisfactory performance. Depending on the availability of field data for comparison with the model results, it is possible to fit the parameters with intend to adjust the order of magnitude of the variables under analysis and / or their dynamics. In the particular case of the present study, there was a set of spatial (water column) and temporal data measured by thermistors installed in the reservoir, which was very valuable for the temperature calibration. In this stage, there was a strong influence of the entrainment associated with plunging inflows, since the model results presented great variations with the value change of the river inflow slope parameter. The light attenuation coefficient also had a significant effect on the results, but it was decided to define it according to the consolidated calculation in the literature (Poole and Atkins, 1929) from field data. In the ecological module, in short, it was necessary to adjust the rates of nitrification and denitrification, as well as of processes related to particulate organic phosphorus (decomposition and sedimentation), phytoplankton growth, the fraction of metabolic loss that is true respiration, and the carbon to chlorophyll ratio.

Another modeling challenge verified was the reservoir depth definition to be used, since 1DV (one-dimensional vertical) models represent the waterbody as horizontally homogeneous layers. Was chose to simulate one configuration considering the reservoir total depth (17 m) and

another using the approximate depth of the intake region (12 m), as it is the place where the field measurements, used in the comparison of the modeled results, were made. In this regard, the results showed, in general, better performance in the simulation with 17 m deep. It was observed that with this methodology the model was able to reproduce the reservoir water balance more adequately, which influenced the results of the waterbody thermal profile. It was noticed that the model started to lose quality in the temperature results due to the uncertainties in the water balance input information, since problems were detected in both in the same period. Despite this, the model was able to represent the stratification phenology, also verified by the physical indices calculation, which demonstrated greater instability in the coldest period, with the occurrence of mixing between the layers. The error metrics between the temperature model results and the thermistors records are in accordance with values found in literature, since the mean absolute error (MAE) was below 1.7 °C and the root mean square error (RMSE) less than 2.3 °C.

Regarding dissolved oxygen, the model showed a very homogeneous distribution pattern in the water column. The dynamics were better reproduced in the bottom layer, which exhibited a higher correlation coefficient. However, MAE and RMSE were lower for the region close to the surface, indicating greater agreement of the values in terms of the order of magnitude. As for chemical substances (nitrogen and phosphorus) and chlorophyll-*a*, due to the restriction of the measured data, adjustment of the order of magnitude was prioritized. Even for parameters with continuous sensor records (nitrate and chlorophyll-*a*), little correlation was found in comparison to laboratory analyzes, that is, without enough information to represent the dynamics of the variables in the reservoir. Although the model results were validated only for the layer close to the surface, as it was in this region that field data were available, an important analysis of the reservoir water quality could be performed with the classification of its trophic state. The total phosphorus concentrations resulted in the waterbody oligotrophic state in almost the entire simulated period. For chlorophyll-*a* and for the final trophic state index, there was a predominance of mesotrophic conditions. Such results correspond to the Passaúna reservoir trophic level verified in another study with data from field collections.

The 1DV (one-dimensional vertical) modeling used in this study does not provide a spatial analysis of the waterbody, that is, it is not able to reproduce the longitudinal gradients of the interest variables. In spite of that, it presents as advantages in relation to 2D and 3D models the possibility of studies of different scenarios and long periods of simulation, with low computational cost and minimum calibration requirements. The GLM-AED, specifically, proved to be a suitable model for making forecasts of the Passaúna reservoir, since it presented satisfactory results, with responses to driving factors. It is noteworthy, however, that the modeling implemented in the present work is an initial study. As next steps, it would be interesting to carry out the automatic calibration of the hydrodynamic module, besides considering the seasonal variability of the light attenuation coefficient, and perform the simulation of the phytoplanktonic species characteristic of the study area. Other suggestions for future research are the effect verification of the sensitivity of the calibration of the atmospheric parameters, as well as the

simulation of different scenarios altering the nutrient load, in order to observe the phytoplankton response. It also stands out that in the current moment of water crisis in Paraná, studies focusing on the knowledge of drought impacts on the hydrodynamics and ecosystem of the waterbody as a whole are extremely relevant.

REFERENCES

- ANA (2018). *Relatório de segurança de barragens 2017*. ANA, Brasília, Brazil.
- Andreoli, C. V. and Carneiro, C. (2005). *Gestão integrada de mananciais de abastecimento eutrofizados*. Sanepar / Finep, Curitiba, Brazil.
- Andreoli, C. V., Hoppen, C., Pegorini, E. S., and Dalarmi, O. A. (2003). Crise da água e os mananciais de abastecimento: a disponibilidade de água na região metropolitana de Curitiba. In Andreoli, C. O., editor, *Mananciais de abastecimento: planejamento e gestão. Estudo de caso do Altíssimo Iguaçu*, page 494. Sanepar/Finep, Curitiba, Brazil.
- Araucária, P. M. (2003). *Perfil Municipal*. Secretaria Municipal de Planejamento SMPL, Departamento de Gestão do Conhecimento, Brazil.
- Ayala, A. I., Cortés, A., Fleenor, W. E., and Rueda, F. J. (2014). Seasonal scale modeling of river inflows in stratified reservoirs: Structural vs. parametric uncertainty in inflow mixing. *Environ. Modell. Softw.*, 60:84–98.
- Barbosa, C. C., Minoti, R. T., and Gomes, L. N. L. (2015). Análise de sensibilidade e otimização da calibração do modelo GLM aplicado ao lago Paranoá, Brasília DF. In *XXI Simpósio Brasileiro de Recursos Hídricos*, pages 1–8, Brasília, Brazil.
- Barbosa, L. G., Barbosa, F. A. R., and Bicudo, C. E. M. (2012). Inter-annual chemical stratification in Brazilian natural lakes: meromixis and hypolimnetic memory. *Acta Limnologica Brasiliensis*, 24:127–139.
- Barreto, N. P., Gurski, L. K. K., Almeida, E. C. d. O., de Souza, C. F., Dec, L. P., do Prado, L. L., Hilgert, S., Kishi, R., de Souza, D. C., and Knapik, H. G. (2019). Variabilidade espacial e temporal dos níveis de trofa no Reservatório do Passaúna - PR. In *XXIII Simpósio Brasileiro de Recursos Hídricos*, pages 1–10, Foz do Iguaçu, Brazil.
- Belico, J. C. B., Silva, T., Giani, A., Figueiredo, C., Ambrózio, L., and Nascimento, N. (2017). Impacto de eventos chuvosos na dinâmica físico-química e biológica em reservatórios urbanos. Estudo de caso: lagoa da Pampulha. In *XXII Simpósio Brasileiro de Recursos Hídricos*, pages 1–8, Florianópolis, Brazil.
- Bhagowati, B. and Ahamad, K. U. (2019). A review on lake eutrophication dynamics and recent developments in lake modeling. *Ecohydrology & Hydrobiology*, 19:155–166.
- Bird, R. E. (1984). A simple, solar spectral model for direct-normal and diffuse horizontal irradiance. *Sol. Energy*, 32:461–471.

- Bruce, L. C., Frassl, M. A., Arhonditsis, G. B., Gal, G., Hamilton, D. P., Hanson, P. C., Hetherington, A. L., Melack, J. M., Read, J. S., Rinke, K., Rigosi, A., Trolle, D., Winslow, L., Adrian, R., Ayala, A. I., Bocaniov, S. A., Boehrer, B., Boon, C., Brookes, J. D., Bueche, T., Busch, B. D., Copetti, D., Cort, A., Eytö, E. D., Elliott, J. A., Gallina, N., Gilboa, Y., Guyennon, N., Huang, L., Kerimoglu, O., Lenters, J. D., Macintyre, S., Makler-pick, V., McBride, C. G., Moreira, S., Ozkundakci, D., Rusak, J. A., Samal, N. R., Pilotti, M., Rueda, F. J., Schmid, M., Shatwell, T., Snorthheim, C., Valerio, G., Linden, L. V. D., Vetter, M., Vinçon-leite, B., Wang, J., Weber, M., Wickramaratne, C., Woolway, R. I., Yao, H., and Hipsey, M. R. (2018). A multi-lake comparative analysis of the General Lake Model (GLM): Stress-testing across a global observatory network. *Environmental Modelling & Software*, 102:274–291.
- Bruce, L. C., Hamilton, D., Imberger, J., Gal, G., Gophen, M., Zohary, T., and Hambright, K. D. (2006). A numerical simulation of the role of zooplankton in C, N and P cycling in Lake Kinneret, Israel. *Ecological Modelling*, 193:412–436.
- Bucak, T., Trolle, D., Tav, Ü. N., Çak, A., Özgen, A., Jeppesen, E., and Beklio, M. (2018). Modeling the effects of climatic and land use changes on phytoplankton and water quality of the largest Turkish freshwater lake: Lake Beyşehir. *Science of the Total Environment*, 621:802–816.
- Bueche, T., Hamilton, D. P., and Vetter, M. (2017). Using the General Lake Model (GLM) to simulate water temperatures and ice cover of a medium-sized lake : a case study of Lake Ammersee, Germany. *Environ Earth Sci*, 76(461).
- Carlson, R. E. (1977). A trophic state index for lakes. *Limnology and Oceanography*, 22(2):361–369.
- Carneiro, C., Kelderman, P., and Irvine, K. (2016). Assessment of phosphorus sediment–water exchange through water and mass budget in Passaúna Reservoir (Paraná State, Brazil). *Environmental Earth Sciences*, 75:564–577.
- Castro, C. O., Loureiro, O. C. S., Santos, A. V., Silva, J., and Rauen, W. B. (2017). Water sustainability assessment for the region of Curitiba. *International Journal of Sustainable Building Technology and Urban Development*, 8:184–194.
- CETESB, editor (2018). *Qualidade das águas interiores no estado de São Paulo*. São Paulo, Brazil.
- COALIAR. (2013). *Resolution n° 04/2013. Approves the proposal to update the framing of surface waterbodies in the domain of the Paraná State, in the coverage area of the Committee of the Alto Iguaçu Basin and Upper Ribeira Affluents*. Rapporteurs: Ingrid Illich Muller and Ricardo Lamberti de Faria. Committee of the Alto Iguaçu Basin and Upper Ribeira Affluents, Curitiba (Brazil), July 11, 2013.

- Cohen, J. (1988). *Statistical power analysis for the behavioral sciences*. Routledge, New York, USA, second edition.
- COMECA (2017). *Região Metropolitana de Curitiba*. Revista da Região Metropolitana de Curitiba, Curitiba, Brazil.
- CONAMA. (2005). *Resolution n° 357/2005. Provides for the classification and environmental guidelines for the framing of surface waterbodies, as well as establishing the conditions and standards for effluents discharge*. Rapporteur: Marina Silva. Federal Official Gazette, Brasilia (Brazil), March 18, 2005.
- Costa, R. M. P., Alcantara, J. K. A., and Rauen, W. B. (2015). Diagnóstico da qualidade da água do reservatório do rio Passaúna. In *Encontro de Pesquisa e Iniciação Científica da Universidade Positivo - EPIC 2015*, pages 1–2, Brazil.
- Cunha, C. L. N., Carneiro, C., Gobbi, E. F., and Andreoli, C. V. (2011). *Eutrofização em Reservatórios: Gestão Preventiva. Estudo Interdisciplinar na Bacia do Rio Verde, PR*. UFPR, Curitiba, Brazil.
- Dancey, C. and Reidy, J. (2006). *Estatística sem matemática para psicologia: usando SPSS para Windows*. Porto Alegre.
- Dias, L. N. (1997). *Estudo integrado da bacia hidrográfica do reservatório Passaúna (Araucária-Paraná-Brasil), considerando a interrelação da ocupação dos solos com a qualidade das águas*. Master in hydraulics and sanitation, São Carlos School of Engineering, University of São Paulo.
- Dodds, W. K. (2006). Eutrophication and trophic state in rivers and streams. *Limnol. Oceanogr.*, 51:671–680.
- Esteves, F. A. (2011). *Fundamentos de limnologia*. Interciência / Finep, Rio de Janeiro, Brazil, 3 edition.
- Fadel, A., Sharaf, N., Siblini, M., Slim, K., and Kobaissi, A. (2019). A simple modelling approach to simulate the effect of different climate scenarios on toxic cyanobacterial bloom in a eutrophic reservoir. *Ecohydrology & Hydrobiology*, 19:359–369.
- Fenocchi, A., Rogora, M., Morabitob, G., Marchetto, A., Sibilla, S., and Dresti, C. (2019). Applicability of a one-dimensional coupled ecological-hydrodynamic numerical model to future projections in a very deep large lake (Lake Maggiore, Northern Italy / Southern Switzerland). *Ecological Modelling*, 392:38–51.
- Fenocchi, A., Rogora, M., Sibilla, S., Ciampittiello, M., and Dresti, C. (2018). Forecasting the evolution in the mixing regime of a deep subalpine lake under climate change scenarios

- through numerical modelling (Lake Maggiore, Northern Italy / Southern Switzerland). *Climate Dynamics*, 51:3521–3536.
- Fenocchi, A., Rogora, M., Sibilla, S., and Dresti, C. (2017). Limnologica Relevance of inflows on the thermodynamic structure and on the modeling of a deep subalpine lake (Lake Maggiore , Northern. *Limnologica*, 63:42–56.
- Fernandes, T. S. (2018). *Avaliação da aplicação do modelo hidrodinâmico GLM em duas regiões limnologicamente distintas do lago Paranoá - DF*. Monograph in civil and environmental engineering, Faculty of Technology, University of Brasilia.
- Fischer, H. B., List, E. J., Koh, R. C. Y., Imberger, J., and Brooks, N. H. (1979). *Mixing in Inland and Coastal Waters*. Academic Press Inc., New York, USA.
- Folke, C., Carpenter, S., Walker, B., Scheffer, M., Elmqvist, T., Gunderson, L., and Holling, C. S. (2004). Regime Shifts , Resilience , and Biodiversity in Ecosystem Management. *Annu. Rev. Ecol. Evol. Syst.*, 35:557–581.
- Fragoso Jr, C. R. (2008). Modelagem de reservatórios em zonas tropicais: parâmetros brasileiros. In *I Encontro Nacional de Hidroinformática*, Fortaleza.
- Fuchs, S., Hilgert, S., Sotiri, K., Wagner, A., Ishikawa, M., Kern, J., Jirka, S., Klassen, I., Krumm, J., Malewski, C., Rohr, H., and Pakzad, K. (2019). Sustainable management of reservoirs - defining minimum data needs and model complexity. In *GRoW- Water as a Global Resource*, Frankfurt, Germany. Status Seminar 2019.
- Gal, G., Hipsey, M. R., Parparov, A., Wagner, U., Makler, V., and Zohary, T. (2009). Implementation of ecological modeling as an effective management and investigation tool: Lake Kinneret as a case study. *Ecol. Model.*, 220:1697–1718.
- Godoy, R. F. B. (2017). *Dinâmica da qualidade da água em reservatório de abastecimento público: estudo de caso do Passaúna - PR*. Master in engineering of water resources and environmental, Federal University of Paraná.
- Hamilton, D. P. and Schladow, S. G. (1997). Water quality in lakes and reservoirs. *Part I Model description, Ecol. Model.*, 96:91–110.
- Hipsey, M. R., Bruce, L. C., Boon, C., Busch, B., Carey, C. C., Hamilton, D. P., Hanson, P. C., Read, J. S., Sousa, E. D., Weber, M., and Winslow, L. A. (2019). A General Lake Model (GLM 3.0) for linking with high-frequency sensor data from the Global Lake Ecological Observatory Network (GLEON). *Geosci. Model Dev*, 12:473–523.
- Hipsey, M. R., Bruce, L. C., and Hamilton, D. P. (2013). *Aquatic Ecodynamics (AED) Model Library Science Manual*. The University of Western Australia.

- Huang, L., Wang, J., Zhu, L., Ju, J., and Daut, G. (2017). The Warming of Large Lakes on the Tibetan Plateau: Evidence From a Lake Model Simulation of Nam Co, China, During 1979 - 2012. *Journal of Geophysical Research: Atmospheres*, 122:95–107.
- IAP (2017). *Qualidade das águas dos reservatórios do estado do Paraná*. Paraná, Brazil.
- Idso, S. B. (1973). On the concept of lake stability. *Limnology and Oceanography*, 18:681–683.
- Imberger, J., Patterson, J., Hebbert, B., and Loh, I. (1978). Dynamics of reservoir of medium size. *J. Hydraul. Eng.-ASCE*, 104:725–743.
- Imberger, J. and Patterson, J. C. (1981). A dynamic reservoir simulation model-DYRESM:5. In Fischer, H. B., editor, *Transport Models for Inland and Coastal Waters*, pages 310–361. Academic Press, New York, USA.
- Imberger, J. and Patterson, J. C. (1990). Physical limnology. *Advances in Applied Mechanics*, 27:303–475.
- Ishii, I. H. (1987). *Contribuição ao estudo do ciclo do carbono na represa de três marias, MG*. Master in ecology and natural resources, Federal University of São Carlos.
- Kern, J. and Schenk, A. (2019). A multi-modal system for monitoring of water quality – setup and first results from Passaúná reservoir. In *XIX Simpósio Brasileiro de Sensoriamento Remoto*, Santos, Brazil.
- Kern, J., Schenk, A., and Hinz, S. (2018a). Radiometric calibration of a UAV-mounted hyperspectral snapshot camera with focus on uniform spectral sampling. In *9th Workshop on Hyperspectral Image and Signal Processing: Evolution in Remote Sensing (WHISPERS)*.
- Kern, J., Schenk, A., and Hinz, S. (2018b). UAS-based hyper-spectral imaging for estimation of water quality parameters in reservoirs. In *Poster presentation, EGU General Assembly*.
- Krumm, J. and Haag, I. (2019a). Multikriterielle Analyse eines Wasserhaushaltsmodells unter Berücksichtigung der Unsicherheit der Datengrundlage. In *Forum für Hydrologie und Wasserbewirtschaftung, Heft 41.19*. Forum für Hydrologie und Wasserbewirtschaftung, Heft 41.19.
- Krumm, J. and Haag, I. (2019b). Simulation des Wasserhaushalts für die Einzugsgebiete der Trinkwassertalsperren Große Dhünn (NRW) und Passaúna (Paraná, Brasilien). In *Vortrag beim Internationalen LARSIM-Anwenderworkshop 2019 am 19./20*, Wiesbaden. Vortrag beim Internationalen LARSIM-Anwenderworkshop 2019 am 19./20.
- Krumm, J., Haag, I., and N., W. (2019). Adaption des Wasserhaushaltsmodells LARSIM zur Anwendung bei veränderter Datenlage und unter subtropischen Bedingungen am Beispiel des

- Passaúna (Brasilien). In *Forum für Hydrologie und Wasserbewirtschaftung, Heft 41.19.* Forum für Hydrologie und Wasserbewirtschaftung, Heft 41.19.
- Ladwig, R., Furusato, E., Kirillin, G., Hinkelmann, R., and Hupfer, M. (2018). Climate Change Demands Adaptive Management of Urban Lakes: Model-Based Assessment of Management Scenarios for Lake Tegel (Berlin, Germany). *Water*, 186:1–23.
- Lamparelli, M. C. (2004). *Grau de trofia em corpos d'água do Estado de São Paulo: Avaliação dos métodos de monitoramento.* D. sc. in science in the area of the terrestrial and aquatic ecosystem, University of São Paulo.
- Li, J. X. and Liao, W. G. (2002). Discussion on the synthetic adjustive guidelines for the prevention and cure of eutrophication. *Prot. Water Resour.*, 2:4–5.
- Männich, M. (2013). *Estimativa de emissões de gases de efeito estufa em reservatórios e lagos – contribuições para o monitoramento e modelagem 1d - vertical.* D. sc. in engineering of water resources and environmental, Federal University of Paraná.
- Marcon, L. (2018). *High temporal resolution measurement of ebullition in a subtropical reservoir.* Master in engineering of water resources and environmental, Federal University of Paraná.
- Marcon, L., Bleninger, T., Männich, M., and Hilgert, S. (2019). High-frequency measurements of gas ebullition in a Brazilian subtropical reservoir — identification of relevant triggers and seasonal patterns. *Environmental Monitoring and Assessment*, 191:357.
- Marcon, L., Bleninger, T. B., and Mannich, M. (2017). Monitoramento contínuo de ebulação de gases em um reservatório subtropical. In *XXII Simpósio Brasileiro de Recursos Hídricos*, pages 1–8, Florianópolis, Brazil.
- Menshutkin, V. V., Rukhovets, L. A., and Filatov, N. N. (2014). Ecosystem Modeling of Freshwater Lakes (Review): 2. Models of Freshwater Lake's Ecosystem. *Water Resources*, 41:32–45.
- MuDak-WRM (2019). *Multidisciplinary Data Acquisition as Key for a Globally Applicable Water Resource Management. Unpublished data from research project partners.* Project coordinated by Dr.-Ing Stephan Fuchs and Dr.-Ing. Tobias Bleninger.
- Mueller, H., Hamilton, D. P., and Doole, G. J. (2016). Evaluating services and damage costs of degradation of a major lake ecosystem. *Ecosystem Services*, 22:370–380.
- Odum, E. P. (1971). *Fundamentals of Ecology.* W. B-Saunders Company, Philadelphia – London – Toronto, 3 edition.
- Polli, B. A. (2018). *Modeling of heat transport in lakes: spatial and temporal characterization.* D. sc. in engineering of water resources and environmental, Federal University of Paraná.

- Polli, B. A. and Bleninger, T. (2015). Modelagem do transporte de calor no reservatório vassouroca. In *XXII Simpósio Brasileiro de Recursos Hídricos*, pages 1–8, Florianópolis, Brazil.
- Poole, H. H. and Atkins, W. R. G. (1929). Photo-eletric measurements of submarine ilumination throughout the year. *J. Mar. Biol. Assoc. U.K.*, 16:297– 394.
- Porto, R. L., Branco, S. M., Cleary, R. W., Coimbra, R. M., Eiger, S., Luca, S. J., Nogueira, V. P. Q., and Porto, M. F. A. (1991). *Hidrologia ambiental*. Universidade de São Paulo: Associação Brasileira de Recursos Hídricos, São Paulo, Brazil.
- Rauen, W. B., Ferraresi, A. C., Maranho, L., Oliveira, E., Costa, R., Alcantara, J., and Dziedzic, M. (2018). Index-based and compliance assessment of water quality for a Brazilian subtropical reservoir. *Eng Sanit Ambient*, 23:841–848.
- Read, J. S., Hamilton, D. P., Jones, I. D., Muraoka, K., Winslow, L. A., Kroiss, R., Wu, C. H., and Gaiser, E. (2011). Derivation of lake mixing and stratification indices from high-resolution lake buoy data. *Environmental Modelling & Software*, 26:1325–1336.
- Read, J. S., Winslow, L. A., Hansen, G. J. A., Hoek, J. V. D., Hanson, P. C., Bruce, L. C., and Markfort, C. D. (2014). Simulating 2368 temperate lakes reveals weak coherence in stratification phenology. *Ecological Modelling*, 291:142–150.
- Rosman, P. C. C. (2019). *Referência Técnica do SISBAHIA*. Available at: <<http://www.sisbahia.coppe.ufrj.br/>>. Access in: July 1, 2019.
- Salgado, M. S. K. and Rauen, W. B. (2014). Coleta e análise de sedimentos do reservatório do Passaúna. In *Encontro de Pesquisa e Iniciação Científica da Universidade Positivo - EPIC 2014*, pages 1–2, Brazil.
- SANEPAR (2013). *Plano Diretor SAIC: Sistema de Abastecimento de Água Integrado de Curitiba e Região Metropolitana*. Sanepar, Curitiba, Brazil.
- Sauniti, R. M., Fernandes, L. A., and Bittencourt, A. V. L. (2004). Estudo do assoreamento do reservatório da barragem do rio Passaúna - Curitiba - PR. *Boletim Paranaense de Geociências*, 54:65–82.
- Sherman, F. S., Imberger, J., and Corcos, G. M. (1978). Turbulence and mixing in stably stratified waters. *Annu. Rev. Fluid Mech.*, 10:267–288.
- Silva, T., Vinçon-leite, B., Lemaire, B., Poague, K., and Nascimento, N. (2015). Urban stormwater runoff impacts on the ecosystem of a tropical lake. In *E-proceedings of the 36th IAHR World Congress*, Netherlands.
- Siqueira, A. C. (2014). *Avaliação do assoreamento do reservatório de abastecimento de água do rio Passaúna*. Final paper, Positivo University.

- Smaha, N. and Gobbi, M. F. (2003). Implementação de um modelo para simular a eutrofização do reservatório do Passaúna - Curitiba - PR. *RBRH – Revista Brasileira de Recursos Hídricos*, 8:59–69.
- Soares, L. M. V., Silva, T. F. d. G., Vinçon-Leite, B., Eleutério, J. C., de Lima, L. C., and Nascimento, N. d. O. (2019). Modelling drought impacts on the hydrodynamics of a tropical water supply reservoir. *Inland Waters*, 9(4):422–437.
- Sotiri, K. (2016). *Investigation of urban mass fluxes to river systems through the use of reservoirs as validation points*. Master in water and river basin management, Karlsruhe Institute of Technology.
- Sotiri, K., Hilgert, S., and Fuchs, S. (2019). Sediment classification in a Brazilian reservoir: Pros and cons of parametric low frequencies. *Journal of Advances in Oceanography and Limnology (in press)*.
- Spigel, R. H., Imberger, J., and Rayner, K. N. (1986). Modeling the diurnal mixed layer. *Limnol. Oceanogr.*, 31:533–556.
- Tamanini, M. S. A. (2008). *Diagnóstico físico-ambiental para a determinação da fragilidade potencial e emergente da bacia do baixo curso do rio Passaúna em Araucária - Paraná*. Master in geography, Federal University of Paraná.
- Thomann, R. V. and Mueller, J. A. (1987). *Principles of surface water quality modeling and control*. Harper Collins Publishers, USA.
- Thompson, R. and Imberger, J. (1980). Response of a numerical model of a stratified lake to wind stress. In *In: Proc. 2nd Int. Symp. Stratified Flows*, volume 1, pages 562–570, Trondheim.
- Toledo Jr., A. P. (1990). *Informe preliminar sobre os estudos para a obtenção de um índice para a avaliação do estado trófico de reservatórios de regiões quentes tropicais*. CETESB - Companhia de Tecnologia de Saneamento Ambiental, São Paulo, Brazil.
- Toledo Jr., A. P., Talarico, M., Chinez, S. J., and Agudo, E. G. (1983). Aplicação de modelos simplificados para a avaliação do processo da eutrofização em lagos e reservatórios tropicais. In *12º Congresso Brasileiro de Engenharia Sanitária*, Camboriú, Brazil. Associação Brasileira de Engenharia Sanitária.
- Trolle, D., Hamilton, D. P., Hipsey, M. R., Bolding, K., Bruggeman, J., Mooij, W. M., Janse, J. H., Nielsen, A., Jeppesen, E., Elliott, J. A., Makler-Pick, V., Petzoldt, T., Rinke, K., Flindt, M. R., Arhonditsis, G. B., Gal, G., Bjerring, R., Tominaga, K., Hoen, J., Downing, A. S., Marques, D. M., Hanson, C. R. F. J., Søndergaard, M., and Hanson, P. C. (2012). A community-based framework for aquatic ecosystem models. *Hydrobiologia*, 683:25–34.

- Tundisi, J. G. and Tundisi, T. M. (2008). *Limnologia*. Oficina de Textos, São Paulo, Brazil, 1 edition.
- Veiga, B. V. and Dziedzic, M. (2010). Estimating nutrient loads in the Passaúna reservoir with FLUX. *Water International*, 35:210–222.
- Vinçon-leite, B. and Casenave, C. (2019). Modelling eutrophication in lake ecosystems: A review. *Science of the Total Environment*, 651:2985–3001.
- Von Sperling, M. (1996). *Introdução à qualidade das águas e ao tratamento de esgotos*. DESA / UFMG, Belo Horizonte, Brazil.
- Von Sperling, M. (1999). *Morfologia de lagos e represas*. DESA / UFMG, Belo Horizonte, Brazil.
- Von Sperling, M. (2014). *Estudos e modelagem da qualidade da água de rios*. UFMG, Belo Horizonte, Brazil, 2 edition.
- Wagner, A., Hilgert, S., Kattenborn, T., and Fuchs, S. (2018). Proximal VIS-NIR Spectrometry to Retrieve Substance Concentrations in Surface Waters Using Partial Least Squares Modelling. In *New Technologies in Water Sector*, pages 194–201, Zagreb, Croatia. 10th Eastern European Young Water Professionals Conference IWA YWP.
- Wagner, A., Hilgert, S., Kishi T., R., Drummond, S., Kiemle, L., Nickel, J. P., Sotiri, K., and Fuchs, S. (2019). Flow-proportional large volume composite sampling to assess substance fluxes. In *Oral Presentation, Geophysical Research Abstracts*. EGU General Assembly 2019.
- Weber, M., Rinke, K., Hipsey, M. R., and Boehrer, B. (2017). Optimizing withdrawal from drinking water reservoirs to reduce downstream temperature pollution and reservoir hypoxia. *Journal of Environmental Management*, 197:96–105.
- Weinstock, J. (1981). Vertical turbulence diffusivity for weak or strong stable stratification. *J. Geophys. Res.*, 86:9925–9928.
- Wosiacki, L. (2017). *Mapping of suspended solid plume using Acoustic Doppler Current Profiler applied to a reservoir inflow*. Master in engineering of water resources and environmental, Federal University of Paraná.
- Wu, J. (1973). Wind induced entrainment across a stable density interface. *J. Fluid Mech.*, 61:275–278.
- Wuest, A. and Lorke, A. (2009). Small-Scale Turbulence and Mixing: Energy Fluxes in Stratified Lakes. In Likens, G. E., editor, *Encyclopedia of Inland Waters*, pages 628–635. Academic Press, Oxford.

- Xavier, C. F. (2005). *Avaliação da influência do uso e ocupação do solo e de características geomorfológicas sobre a qualidade das águas de dois reservatórios da região metropolitana de Curitiba - Paraná*. Master in soils, Federal University of Paraná.
- Yao, H., Samal, N. R., Joehnk, K. D., Fang, X., Bruce, L. C., Pierson, D. C., Rusak, J. A., and James, A. (2014). Comparing ice and temperature simulations by four dynamic lake models in Harp Lake: past performance and future predictions. *Hydrological Processes*, 28:4587–4601.
- Yeates, P. S. and Imberger, J. (2003). Pseudo two-dimensional simulations of internal and boundary fluxes in stratified lakes and reservoirs. *International Journal of River Basin Research*, 1:1–23.
- Zarebska, Z. (2016). *Small scale sediment analysis in a Brazilian reservoir*. Master, Karlsruhe Institute of Technology.

APPENDIX A – METEOROLOGICAL DATA COMPARISON

In Figure A.1 are plotted the meteorological data (air temperature, shortwave radiation, relative humidity, and wind speed) from May 19, 2018, to February 28, 2019, obtained by Tecpar (CTB-60 solarimetric station) and Sanepar monitoring stations, both close to the Passaúna reservoir. The objective is to show that the data similarity validates, in a certain way, the use of the records of the 2 stations, complementing each other, in the model input file. The other graphs (Figures A.2, A.3, A.4, and A.5) show the density scatterplot of the data from these stations, with Pearson's correlation coefficient (r). It is observed that, according to the literature, the result for all variables presented a correlation considered strong, that is, above 0.7 (Cohen, 1988; Dancey and Reidy, 2006).

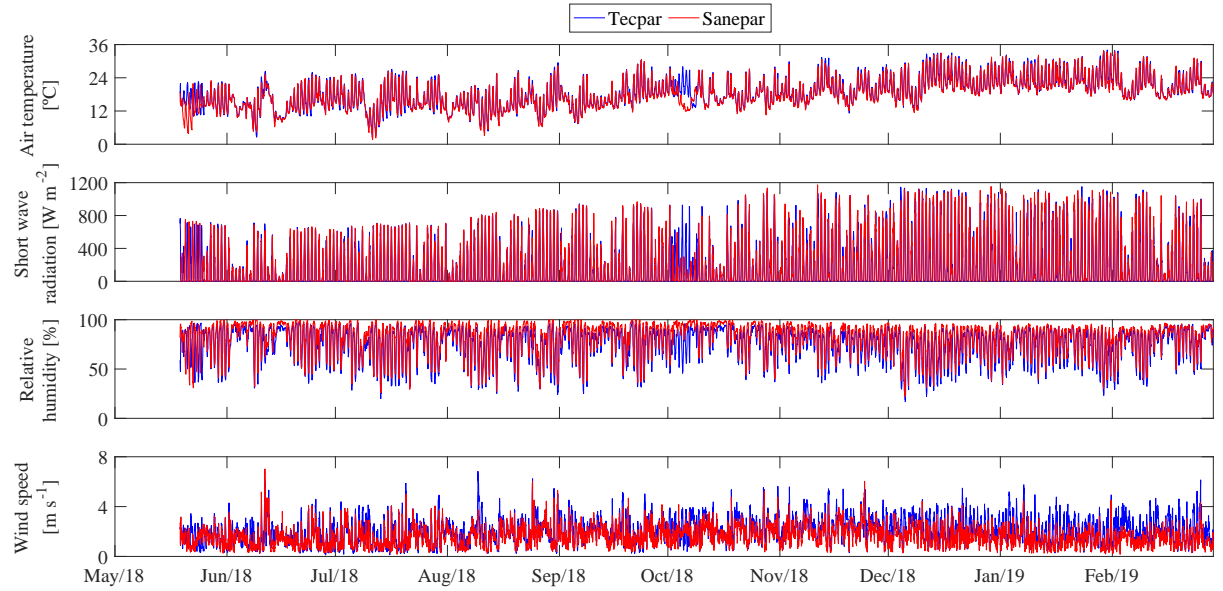


Figure A.1: Comparison of the meteorological data from Tecpar and Sanepar monitoring stations close to the Passaúna reservoir, from May 19, 2018, to February 28, 2019.

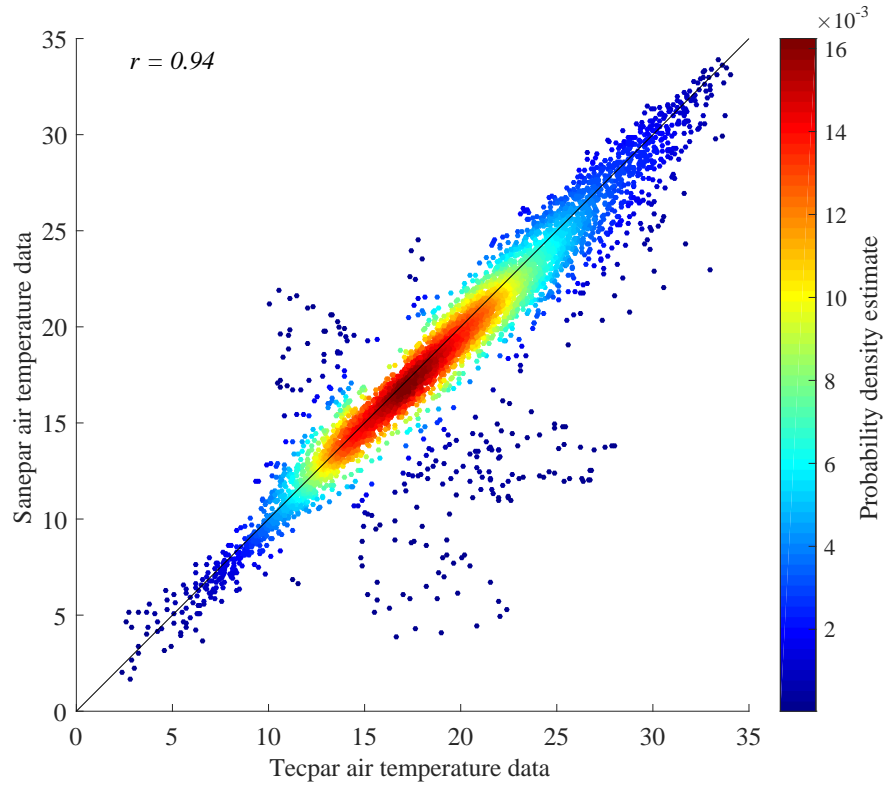


Figure A.2: Density scatterplot of the Tecpar and Sanepar monitoring stations data of air temperature, from May 19, 2018, to February 28, 2019, with Pearson's correlation coefficient (r).

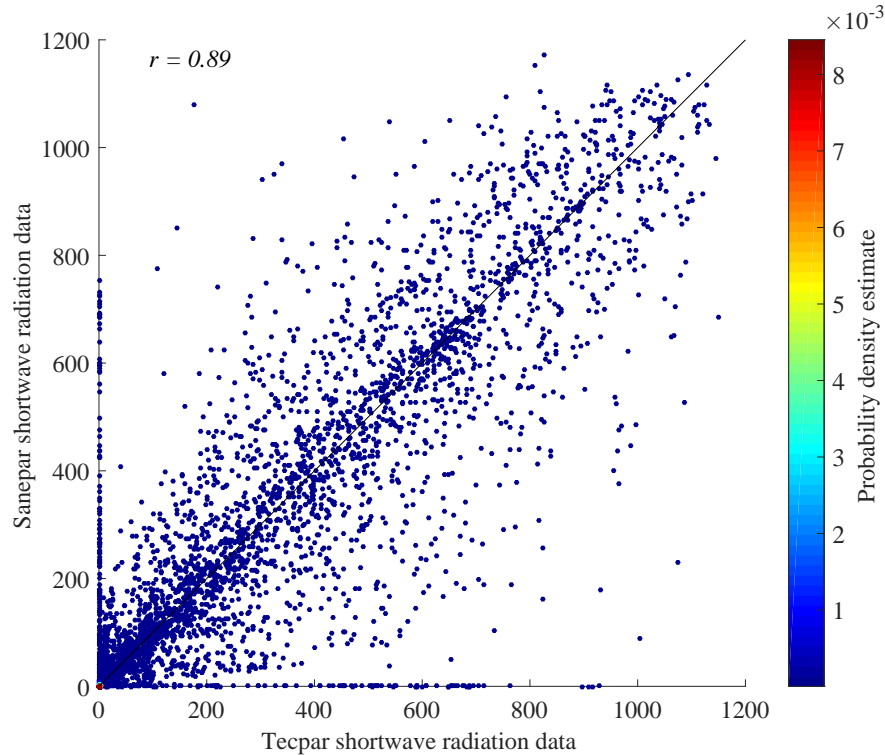


Figure A.3: Density scatterplot of the Tecpar and Sanepar monitoring stations data of shortwave radiation, from May 19, 2018, to February 28, 2019, with Pearson's correlation coefficient (r).

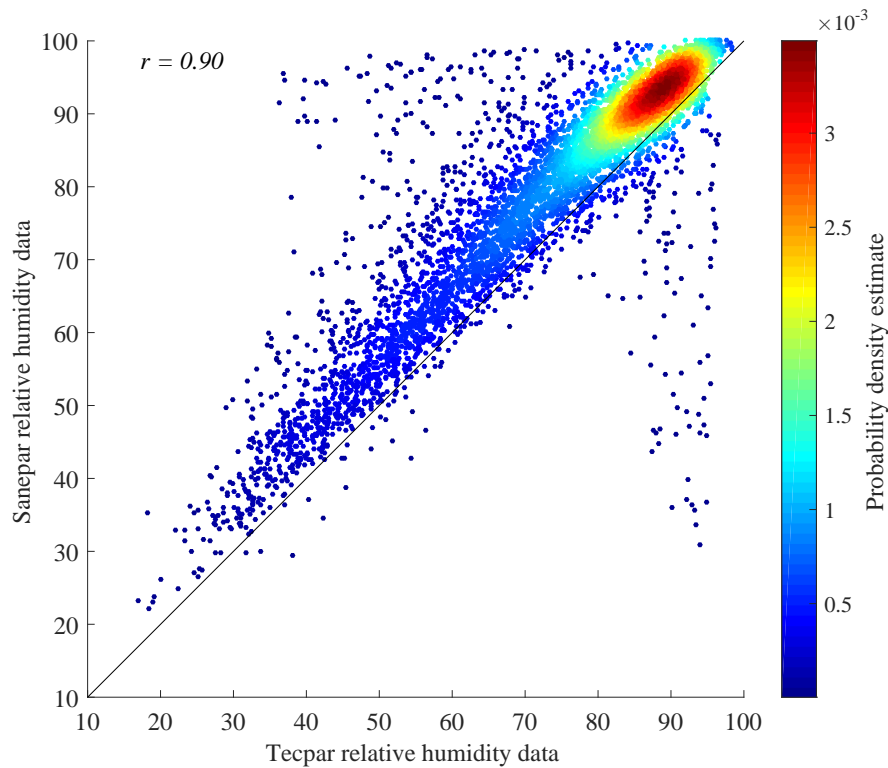


Figure A.4: Density scatterplot of the Tecpar and Sanepar monitoring stations data of relative humidity, from May 19, 2018, to February 28, 2019, with Pearson's correlation coefficient (r).

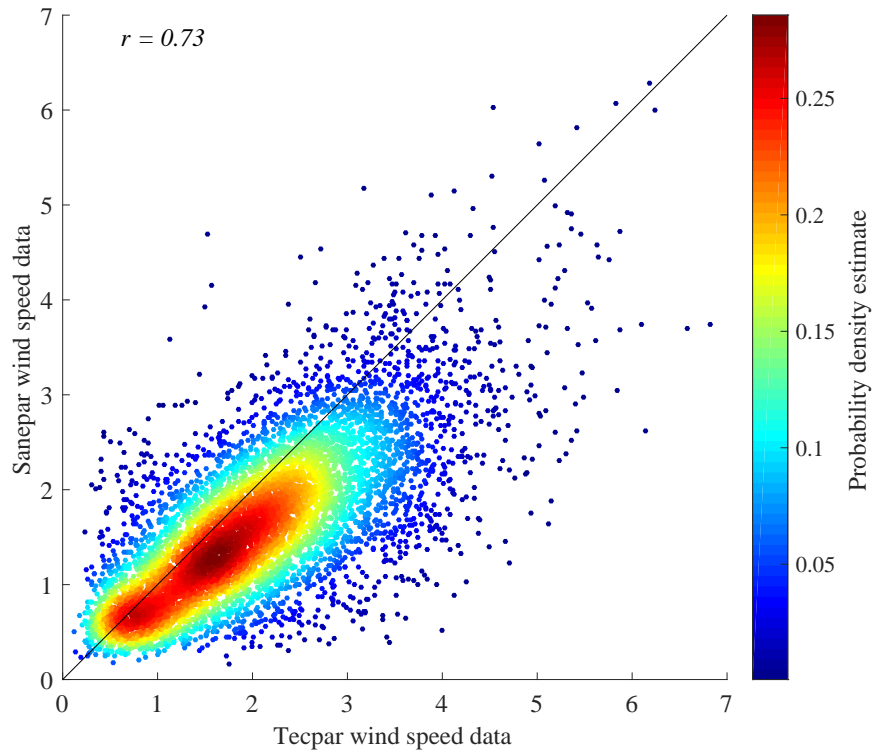


Figure A.5: Density scatterplot of the Tecpar and Sanepar monitoring stations data of wind speed, from May 19, 2018, to February 28, 2019, with Pearson's correlation coefficient (r).